

SCIENCE OF TSUNAMI HAZARDS

Journal of Tsunami Society International

Volume 30

Number 4

2011

OBSERVATION OF TSUNAMI RADIATION AT TOHOKU BY REMOTE SENSING 223

Frank C. Lin - *Dept. of Mathematics and Computer Science, University of Maryland Eastern Shore Princess Anne, MD., USA.*

Weiwei Zhu - *Dept. of Mathematics and Computer Science, University of Maryland Eastern Shore, Princess Anne, MD., USA.*

Kingkarn Sookhanaphibarn - *Intelligent Computer Entertainment Laboratory, Dept. of Human and Computer Intelligence, Ritsumeikan University Kusatsu, Shiga, JAPAN*

TOWARD INDONESIAN TSUNAMI EARLY WARNING SYSTEM BY USING RAPID RUPTURE DURATIONS CALCULATION 233

Madlazim - *Physics Department, Faculty of Mathematics and Sciences, Surabaya State University (UNESA) Jl. Ketintang, Surabaya, INDONESIA*

TSUNAMI WAVE LOADING ON A BRIDGE DECK WITH PERFORATIONS 244

P. Lukkunaprasit¹, T.L. Lau², A. Ruangrassamee³ and T. Ohmachi⁴

¹*Professor, Dept. of Civil Engineering, Chulalongkorn University, Bangkok, THAILAND*

²*Graduate Student, Dept. of Civil Engineering, Chulalongkorn University, Bangkok, THAILAND*

³*Assistant Professor, Dept. of Civil Engineering, Chulalongkorn University, Bangkok, THAILAND*

⁴*Professor, Dept. of Built Environment, Tokyo Institute of Technology, Yokohama, JAPAN*

THE EARTHQUAKE AND TSUNAMI OF JULY 21, 365 AD IN THE EASTERN MEDITERRANEAN SEA - Review of Impact on the Ancient World - Assessment of Recurrence and Future Impact. 253

George Pararas-Carayannis - *Tsunami Society International, Honolulu, Hawaii, USA*

WWW.TSUNAMISOCIETY.ORG

TSUNAMI SOCIETY INTERNATIONAL, 1741 Ala Moana Blvd. #70, Honolulu, HI 96815, USA.

SCIENCE OF TSUNAMI HAZARDS is a CERTIFIED OPEN ACCESS Journal included in the prestigious international academic journal database DOAJ, maintained by the University of Lund in Sweden with the support of the European Union. SCIENCE OF TSUNAMI HAZARDS is also preserved, archived and disseminated by the National Library, The Hague, NETHERLANDS, the Library of Congress, Washington D.C., USA, the Electronic Library of Los Alamos, National Laboratory, New Mexico, USA, the EBSCO Publishing databases and ELSEVIER Publishing in Amsterdam. The vast dissemination gives the journal additional global exposure and readership in 90% of the academic institutions worldwide, including nation-wide access to databases in more than 70 countries.

OBJECTIVE: Tsunami Society International publishes this interdisciplinary journal to increase and disseminate knowledge about tsunamis and their hazards.

DISCLAIMER: Although the articles in SCIENCE OF TSUNAMI HAZARDS have been technically reviewed by peers, Tsunami Society International is not responsible for the veracity of any statement, opinion or consequences.

EDITORIAL STAFF

Dr. George Pararas-Carayannis, Editor
<mailto:drgeorgepc@yahoo.com>

EDITORIAL BOARD

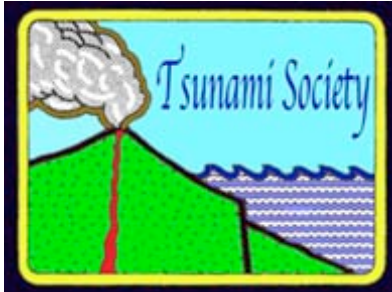
Dr. Charles MADER, Mader Consulting Co., Colorado, New Mexico, Hawaii, USA
Dr. Hermann FRITZ, Georgia Institute of Technology, USA
Prof. George CURTIS, University of Hawaii -Hilo, USA
Dr. Tad S. MURTY, University of Ottawa, CANADA
Dr. Zygmunt KOWALIK, University of Alaska, USA
Dr. Galen GISLER, NORWAY
Prof. Kam Tim CHAU, Hong Kong Polytechnic University, HONG KONG
Dr. Jochen BUNDSCHUH, (ICE) COSTA RICA, Royal Institute of Technology, SWEDEN
Dr. Yurii SHOKIN, Novosibirsk, RUSSIAN FEDERATION

TSUNAMI SOCIETY INTERNATIONAL, OFFICERS

Dr. George Pararas-Carayannis, President;
Dr. Tad Murty, Vice President;
Dr. Carolyn Forbes, Secretary/Treasurer.

Submit manuscripts of research papers, notes or letters to the Editor. If a research paper is accepted for publication the author(s) must submit a scan-ready manuscript, a Doc, TeX or a PDF file in the journal format. Issues of the journal are published electronically in PDF format. There is a minimal publication fee for authors who are members of Tsunami Society International for three years and slightly higher for non-members. Tsunami Society International members are notified by e-mail when a new issue is available. Permission to use figures, tables and brief excerpts from this journal in scientific and educational works is granted provided that the source is acknowledged.

Recent and all past journal issues are available at: <http://www.TsunamiSociety.org> CD-ROMs of past volumes may be purchased by contacting Tsunami Society International at postmaster@tsunamisociety.org Issues of the journal from 1982 thru 2005 are also available in PDF format at the Los Alamos National Laboratory Library <http://epubs.lanl.gov/tsunami/>



SCIENCE OF TSUNAMI HAZARDS

Journal of Tsunami Society International

Volume 30

Number 4

2011

OBSERVATION OF TSUNAMI RADIATION AT TOHOKU BY REMOTE SENSING

Frank C. Lin^{1*}, Weiwei Zhu^{1**}, Kingkarn Sookhanaphibarn²

¹Dept. of Mathematics and Computer Science
University of Maryland Eastern Shore
Princess Anne, MD. 21853, U.S.A.

²Intelligent Computer Entertainment Laboratory
Dept. of Human and Computer Intelligence
Ritsumeikan University
1-1-1 Noji Higashi, Kusatsu, Shiga, 525-8577, Japan

ABSTRACT

We present *prima facie* evidence that upon the onset of the Tohoku tsunami of Mar. 11, 2011 infrared radiation was emitted by the tsunami and was detected by the Japanese satellite MTSAT-IR1, in agreement with our earlier findings for the Great Sumatra Tsunami of 2004. Implications for a worldwide Tsunami Early Warning System are discussed.

Keywords: *Tsunami, Tsunami Radiation, Tsunami Signal, Tsunami Early Warning System, Tohoku*

*Corresponding author. Email: linbfrank@gmail.com. Tel/Fax: +662 612 4705. **wzhu@umes.edu. #kingkarn@ice.ci.ritsumei.ac.jp.

1. INTRODUCTION

In previous communications (Na Nakornphanom et al. 2007; Lin et al. 2010; Lin and Sookahanaphibarn 2011) we have provided clear evidence that at the *birth* of a tsunami, as the cold water is lifted to the surface of the ocean, the tsunami *emits an infrared radiation of 11 ± 0.5 microns*, which being in the thermal range can be detected by satellites. We have shown that this radiation is captured by the infrared sensors of the Chinese Meteorological Satellite FY-2C, which is geostationary at Lon 105°E and Lat 0°N, as well as by the NOAA V5 Pathfinder satellite. We have investigated seven earthquake locations in the Indian Ocean on Dec. 26, 2004 including the Main Event at Banda Aceh. We found that of these seven earthquakes there were five that emitted the telltale tsunami signal whereas in two cases no radiation was detected, indicating that these respective earthquakes, though of comparable magnitude, did not spawn a tsunami. This *Sachverhalt* has obviously important implications for the reliability of tsunami early warning systems, which we shall discuss subsequently. Noise such as cloud or heat emanating from landmass has been accounted for.

In this paper we shall apply the same methodology to the Tohoku tsunami of Mar. 11, 2011. The tsunami radiation has been, as expected, captured by the MTSAT-IR1 satellite of the Japan Meteorological Society. The present work confirms the validity of our previous approach in a different geophysical context and for several new events. Some speculative suggestions for possible predictions of future events based on the pattern of foreshocks are considered.

The Tohoku events that we investigate in this paper are listed in the Table below, together with their attributes:

Table 1: Tohoku Earthquake Events and Attributes.

Event	Me	Time UTC	Latitude in degrees	Latitude in pixels	Longitude in degrees	Longitude in pixels	Signal at Epicenter, S in pixels	M _t Eq.1
Main-shock	9.0	05:46	38.297N	38	142.372E	142	255	7.99
Foreshock	7.2	02:45	38.424N	145	142.636E	186	197	7.62
Aftershock-1	7.1	14:32	38.253N	145	141.640E	181	161	7.33
Aftershock-2	6.6	08:16	37.007N	261	140:477E	207	none	

2. THE MAIN EVENT

On Friday, March 11, 2011 at 05:46:24 UTC (02:46:24 p.m. local time) at the location 38.297°N and 142.372°E at the depth of 30 km and at a distance of 129 km East of Sendai, Honshu, Japan an earthquake of magnitude 9.0 occurred. According to the Jet Propulsion Laboratory of Caltech (Caltech 2011), the coast of northeast Japan moved eastward up to 4 meters and the coastline generally subsided up to 1.1 meters. This is due to the fault at the subduction zone between the Pacific and the North American plates. The Pacific plate moved westwards descending beneath Japan. The slip was

approximately 300 km long and 150 km wide. At least 15,703 people were killed and at least 332,395 buildings destroyed or damaged by the earthquake and tsunami along the entire east coast of Honshu. The tsunami runup height was 37.88 m at Miyako. The economic loss in Japan is estimated to be more than 300 billion U.S. dollars. In addition, several reactors were damaged at Fukushima and leaked radiation, posing a health hazard. Both life and property damages were sustained in other parts of the world.

Evidently, the Early Warning System in Japan was inadequate to cope with a disaster of this magnitude. Our proposal of detecting the *birth* of tsunamis by remote sensing could possibly enhance the warning system and save life and property in future.

The following cropped satellite image was recorded by the MTSAT-IT1 on 2011-03-11 at 06:30 UTC at latitude 38.322°N. According to our previous work, the tsunami radiation should be visible in the infrared domain, provided that the cool water from the bottom of the ocean has reached the ocean surface (Lin et al. 2010).

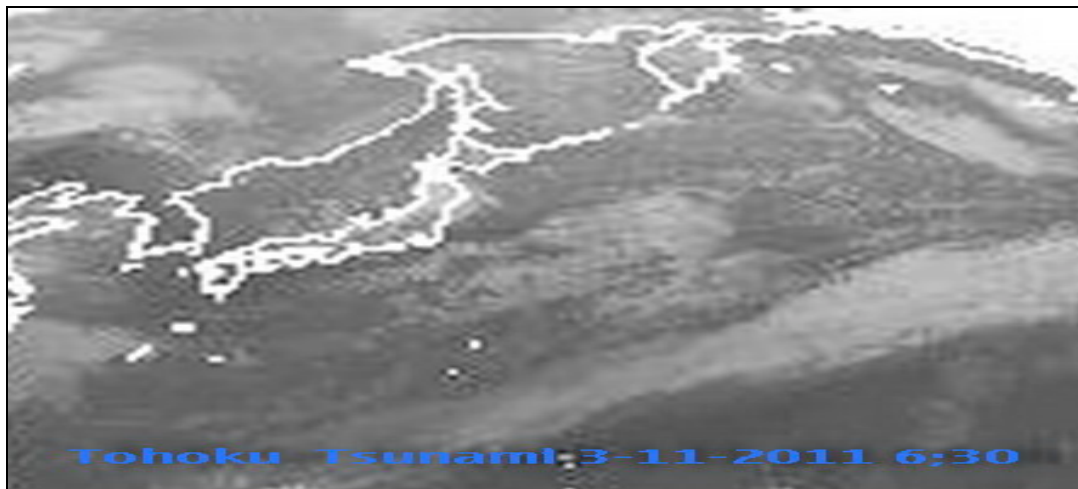


Fig.1: Satellite Image of the Main Event for the Tohoku Tsunami of 2011-03-11

In Fig.2 we show the Signal Diagram for the aforementioned latitude and we discern indeed a spike at the location of the undersea earthquake corresponding to the thermal emission detected by the satellite. This confirms the validity of our procedure previously applied to the Great Sumatra Tsunami in the Indian Ocean, albeit for a high latitude event, where the water temperature is significantly lower. An arrow points to the tsunami signal.

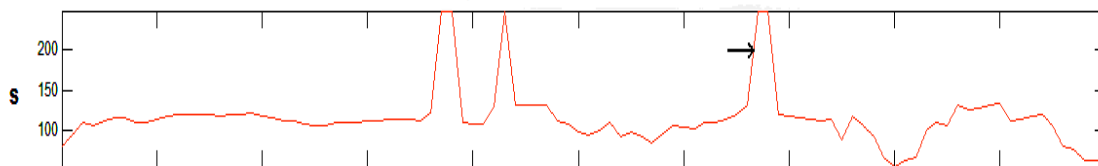


Fig.2: Signal Diagram of Tohoku Main Event of 2011-3-11

The Wavelet Diagram for this event is shown in Fig.3. Again, an arrow points to the tsunami signal. As before, the Haar mother-wavelet is selected.

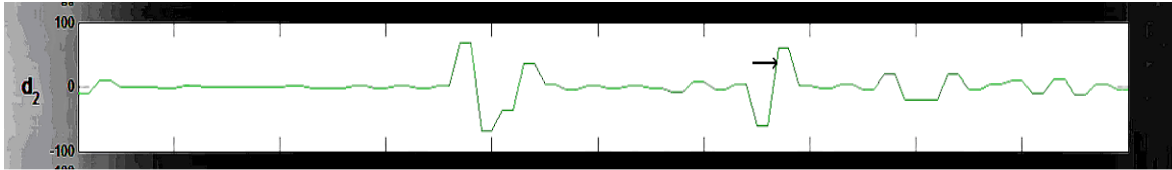


Fig.3: Wavelet Diagram of Tohoku Main Event of 2011-3-11

Regarding the horizontal scale, all Signal Diagrams encompass 500 pixels between notches and all Wavelet Diagrams span 200 pixels between notches unless otherwise labeled. For the vertical scale, the range of Signal Diagrams is from 0 to 250, and the range for Wavelet Diagrams is from -100 to +100 unless otherwise labeled

3. FORESHOCKS AND AFTERSHOCKS

The Main Event was preceded by numerous foreshocks and followed by hundreds of aftershocks. On March 9, 2011, at 02:45 UTC a foreshock of magnitude 7.2 occurred at latitude 38.424°N and longitude 142.836°E at the depth of 32 km. We examined the satellite image for 03:32 UTC at this latitude. Fig. 4 shows the corresponding Signal Diagram.

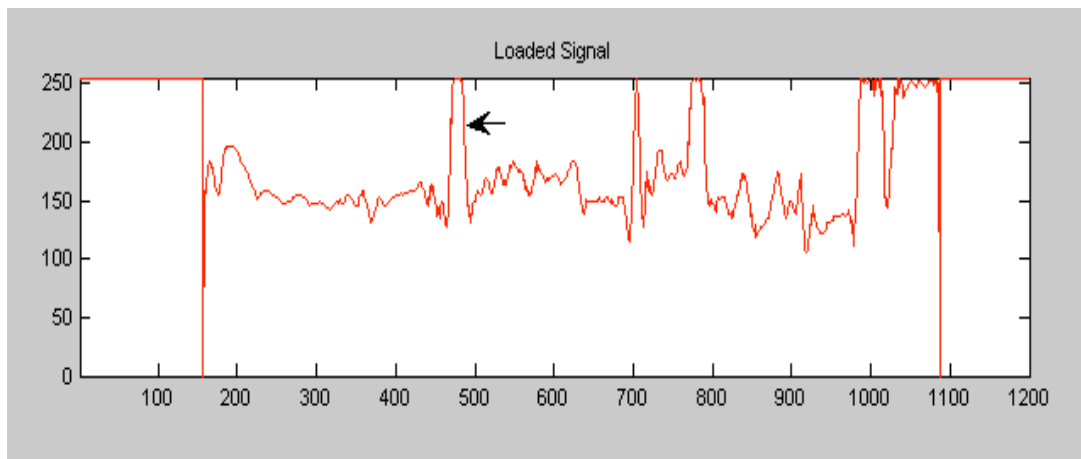


Fig. 4: Signal Diagram of Tohoku Foreshock of 2011-3-9

It is seen that at the location of the undersea earthquake, a distinct tsunami signal is found indicating that the cool ocean water from the bottom has reached the surface and thus was detected by the satellite. An arrow again points to the tsunami signal. This is the first time that this

phenomenon has been associated with a foreshock. Since 1973, there were 9 earthquakes on the Japan trench with $M_e \geq 7$. This suggests that the Main Event could possibly have been predicted if all significant foreshocks were taken into account, by e.g. using a Neural Network (Lin and Mohamed 1999; Lin et al. 2002). The corresponding Wavelet Diagram, where an arrow points to the Tsunami Signal, is shown in Fig 5 below:

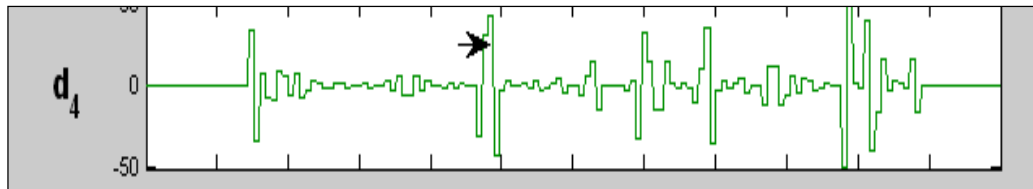


Fig.5: Wavelet Diagram of Tohoku Foreshock of 2011-3-9

There were 4 major aftershocks after the Main Event: On Mar. 11 at 06:15 UTC a magnitude 7.9 aftershock occurred at 36.27°N and 141.14°E; at 06:25 UTC on the same day, a magnitude 7.7 aftershock occurred at 38.05°N and 144.59°E; on Apr. 7, 2011 at 14:32 UTC a magnitude 7.1 aftershock occurred at 38.253°N and 141.640°E; and on Apr. 11, 2011 at 08:16 UTC a magnitude 6.6 aftershock occurred at 37.007 °N and 140.477°E. We shall call the last two Aftershock-1 and Aftershock-2. The satellite images were recorded at 15:33 UTC and 08:32 UTC respectively.

We obtained for Aftershock-1 the following Signal and Wavelet diagrams.

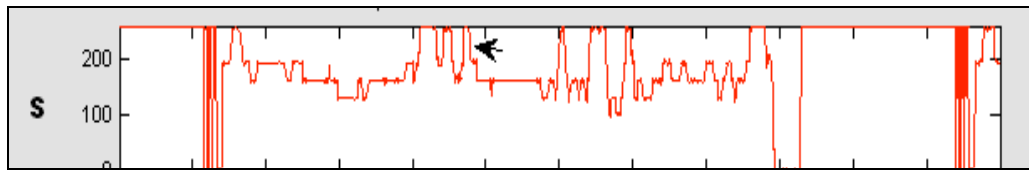


Fig.6: Signal Diagram of Tohoku Aftershock-1

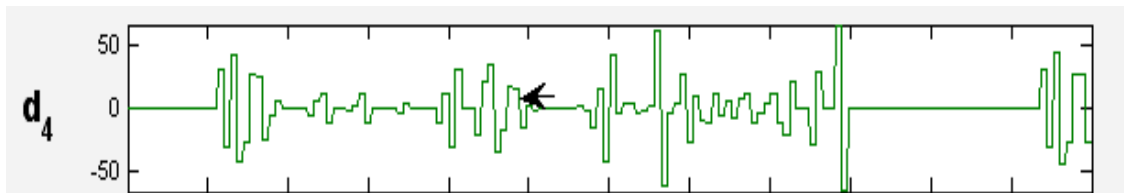


Fig.7: Wavelet Diagram for Tohoku Aftershock-1

An arrow points to the tsunami signal for Aftershock-1. Although the cold water has reached the ocean surface, it did not cause widespread damage. The propagation of tsunamis in infrared space is the subject of future research.

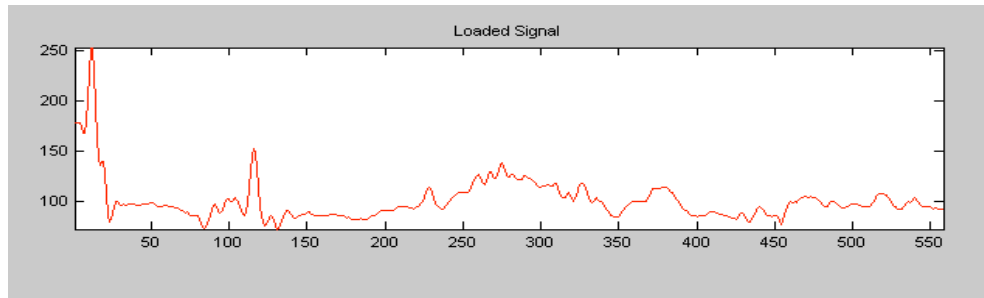


Fig.8: Signal Diagram for Tohoku Aftershock-2

Aftershock-2 is an interesting case in that no tsunami signal is discernible at longitude 140.477°E or pixel value 207 (see Fig. 8). This is probably due to the fact that the satellite image was taken only sixteen minutes after the earthquake was detected. This may not have provided adequate time for sufficient quantity of cold water to reach the ocean surface in order to trigger the tsunami signal. Alternately, and perhaps more likely, the cold water may not have breached the ocean surface at all, as some cases in the Indian Ocean that we have investigated (Lin et al. 2010). The thermodynamic and hydrodynamic mechanism by which the cold water is lifted to the ocean surface has yet to be elucidated.

IV. Tsunami Magnitude

We define the Tsunami Magnitude *in infrared space*, in analogy to the definition of Iida et al. (1967) in visible space, as follows:

$$M_t = \log_2 S \quad (1)$$

where

M_t = Tsunami Magnitude,

S = Tsunami Signal (Pixel brightness at the epicenter. See Table 1 for numerical values obtained directly from the satellite images).

Similarly, the Tsunami Intensity can be defined as:

$$I_t = \log_2 (\sqrt{2} * S) \quad (2)$$

In visible space (Rastogi and Jaiswal 2006) S is the estimated maximum run up height of the wave. This measure has been suggested based on the effect and damage caused by the tsunami. The velocity of a tsunami in the open ocean is given by

$$V = (dg)^{1/2} \quad (3)$$

where d is the ocean depth and g the acceleration of gravity.

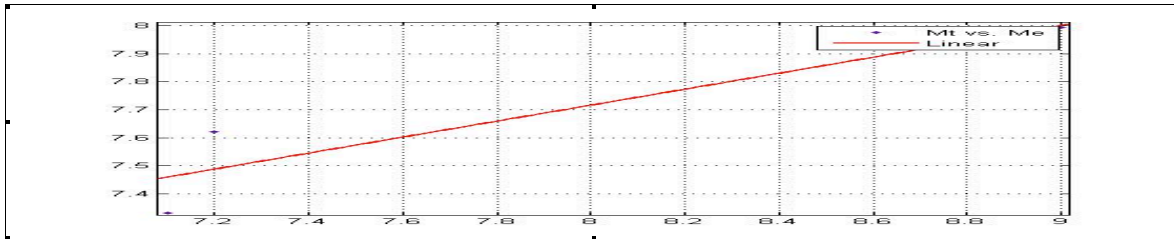


Fig.9: Earthquake Magnitude versus Tsunami Magnitude

Using the data from Table 1, a linear interpolation of Tsunami Magnitude versus Earthquake Magnitude is given in Fig. 9. We have shown in (Lin and Sookhanaphibarn 2011) that all tsunami representations must be linear. In general, the tsunami magnitudes are 10% less than those of the Indian Ocean (Lin et al. 2010). This is probably due to the greater temperature gradient of the latter.

5. EARLY WARNING BY REMOTE SENSING (REMOTE)

At the onset of a tsunami event, the cold water is lifted up to the surface. The tsunami burst is therefore characterized by a temperature gradient. Meteorological satellites such as the Chinese FY-2C, recording between the wavelengths 10.5 and 12.5 μm , is able to detect this temperature gradient.

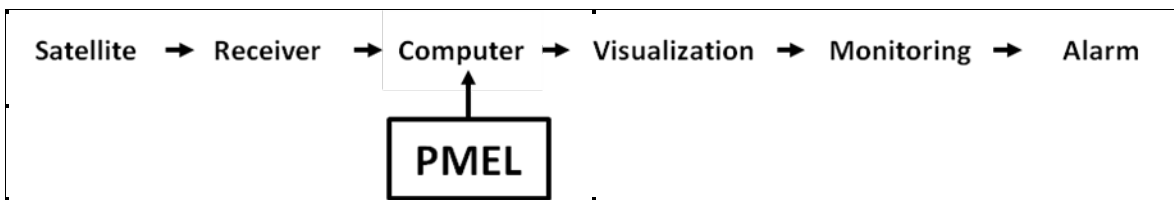


Fig.10: Early warning system

Our method consists of using an antenna and receiver to capture the tsunami radiation in infrared domain. A PC producing visualizations that we have shown in the figures in this paper processes this signal. At the same time undersea earthquake activities are collected in real time from watchdogs such as PMEL (Fig. 10). The visualization will then confirm or refute the birth of a tsunami associated with this earthquake, such that a warning can be instantly and automatically issued.

6. COMPARISON WITH DART

Present methods such as “The Deep-ocean Assessment and Reporting of Tsunami” (DART) to detect tsunamis measure aquatic pressure changes due to submarine earthquakes. The DART system functions as follows: Pressure sensors are placed at the ocean bottom near the earthquake zone. An acoustic modem transducer encodes the data into sound waves. A communications buoy processes the information and sends it by radio waves to a weather satellite (GOES). Computers at ground station calculate tsunami’s starting point, speed and arrival times.

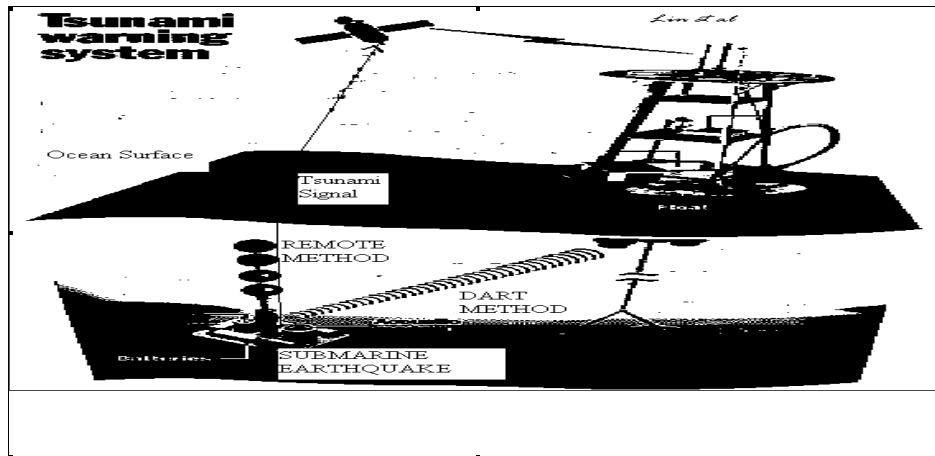


Fig.11: DART vs. REMOTE

The above Figure (Fig.11) shows the *modus operandi* of the two systems. We shall consider the following discussion points in comparing the DART and REMOTE methods: 1) Time Delay, 2) Cost, 3) Reliability and 4) Availability.

1) Time Delay: For the DART System, the earthquake is registered by an underwater pressure gauge, which forwards this information acoustically to a buoy at the surface of the ocean. Since the signal travels at the speed of sound over hundreds of kilometers, a time lapse is incurred. In the Mentawai tsunami of 2010, for instance, it took one hour for the information to reach the first buoy and another hour to reach the second buoy. *This time lapse is critical for the effectiveness of Early Warning.* An hour also lapsed between the Tohoku Main Event and when the tsunami reached the Fukushima nuclear plant.

In our REMOTE system, as soon as the cold water reaches the surface of the ocean, an infrared radiation (called the Tsunami Signal) is emitted which travels to the satellite at the speed of light, i.e. instantaneously. No time delay is thereby incurred.

2) Cost: An individual buoy costs over one million dollars to put in place. Its maintenance is generally beyond the financial capability of poorer nations. Many buoys are needed to adequately protect an extended coastline. In the REMOTE system, just one setup is sufficient to protect a country, provided that it has access to a weather satellite. The initial cost is less than a hundreds of that of a buoy and the maintenance cost is minimal.

3) Reliability: The pressure changes as measured by DART may not trigger a tsunami, and consequently the present method yields high rates of false positive alarms. According to reports from NOAA and others (Gonzalez 1999), approximately 75% of all warnings issued since 1948 have been false. The REMOTE method will broadcast a warning if and only if the cold water has reached the surface of the ocean and is thus more reliable.

4) Availability: At present, some 39 buoys have been implemented, mostly along the Pacific Rim. Large segments of the earth, such as the Indian Ocean, the Mediterranean Ocean and South America are not yet safeguarded.

7. CONCLUSION

We have made the remarkable finding that as the cold water from the bottom of the ocean is lifted up to the ocean surface by a submarine earthquake it emits an infrared radiation centered around 11 microns which can be detected by a satellite. We used this tool to investigate tsunami events of Dec. 26, 2004 in the Indian Ocean (Lin et al. 2010) and of Mar. 11, 2011 in the Tohoku region. It is found that each event will either send out this tsunami signal signifying the birth of a tsunami, or no signal is sent in which case no Tsunami Warning should be issued. There is therefore no false positives or false negatives. In comparison to DART, it is ascertained that this system, called REMOTE, has essentially no time delay, is orders of magnitude less expensive, unambiguous and can be easily made available to the world thereby substantially improving and augmenting the saving of life and property.

REFERENCES

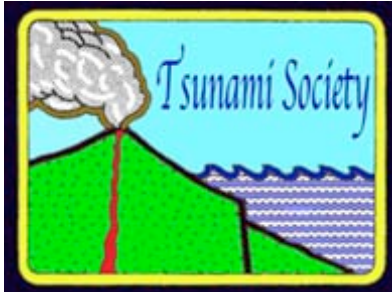
- Caltech (2011): <ftp://sideshow.jpl.nasa.gov/pub/usrs/ARIA>. See also <http://earthquake.usgs.gov/earthquakes/eqinthenews/2011/usc0001xgp/> (2011).
- Elborn, S. and F.C.Lin (1992), Analysis & Prediction of Earthquakes for Southern California Using A Neural Network. *Geologia Applicata e Idrogeologia* Vol.xxvii, pp.111-121, Bari, Italy.
- Gonzalez, F. (1999), TSUNAMI!, *Scientific American*, 280, 56-65
- Iida, K, Cox D. and Pararas-Carayannis G. (1967), Preliminary Catalog of Tsunamis Occurring in the Pacific Ocean. Hawaii Institute of Geophysics, Honolulu, HI, August (Rept. HIG- 67-10)
- Lin, F.C. and I. Panikkar (1995), Study of Seismic Activity in Central Asia Applying A Parallel Distributed Paradigm. Proceedings of the 1995 International Geoscience & Remote Sensing Symposium, Firenze, Italy, July 10-14
- Lin, F.C. Lin and I.E. Mohamed (1999), Predicting Seismic Aftershocks Using a Neural Network. Proceedings of the International Geoscience & Remote Sensing Symposium (IGARSS '99), Hamburg, Germany
- Lin, F.C., N. Elhassan, A. Hassan and A. Yousif (2002), Forecast of Seismic Aftershocks using a Neural Network. Proceedings of the 9th International Conference on Neural Information Processing, Singapore

Lin, F.C., K. Na Nakornphanom, K. Sookhanaphibarn, and C. Lursinsap (2010), A New Paradigm for Detecting Tsunamis by Remote Sensing. *Int. Journal of Geoinformatics*, 6(1), 19-30.

Lin, F.C. and K. Sookhanaphibarn (2011), Representation of Tsunamis in Generalized Hyperspace. *Proceedings of the IEEE International Geoscience and Remote Sensing Symposium (IGARSS'11)*, Sendai/Vancouver, July 21, 2011. pp. 4355-4358

Na Nakornphanom, K., Frank C. Lin and C. Lursinsap (2007), Tsunami Detection and Early Warning by TIR Remote Sensing. *Proceedings of The Third Shanghai International Symposium on Nonlinear Sciences and Applications*, June 6-10

Rastogi, B.K. and Jaiswal, R.K. (2006), A Catalog of Tsunamis in the Indian Ocean, *Science of Tsunami Hazards*, 25(3), p. 128.



SCIENCE OF TSUNAMI HAZARDS

Journal of Tsunami Society International

Volume 30

Number 4

2011

TOWARD INDONESIAN TSUNAMI EARLY WARNING SYSTEM BY USING RAPID RUPTURE DURATIONS CALCULATION

Madlazim

Physics Department, Faculty of Mathematics and Sciences, Surabaya State University
(UNESA) Jl. Ketintang, Surabaya 60231, Indonesia.

e-mail: m_lazim@physics.its.ac.id

ABSTRACT

Indonesia has an Indonesian Tsunami Early Warning System (Ina-TEWS) since 2008. The Ina-TEWS has used automatic processing on hypocenter; M_{wp} , M_w (mB) and M_j . If earthquake occurred in Ocean, depth < 70 km and magnitude > 7 , then Ina-TEWS announce early warning that the earthquake can generate tsunami. However, the announcement of the Ina-TEWS is still not accuracy. Purpose of this study is to estimate earthquake rupture duration of large Indonesia earthquakes that occurred in Indian Ocean, Java, Timor Sea, Banda Sea, Arafura Sea and Pacific Ocean using a direct procedure and software developed Lomax and Michelini for rapid assessment of earthquake tsunami potential by deriving two simple measures from vertical component broadband P-wave velocity record. The first is the high-frequency apparent rupture duration, T_{dur} which may be related to can be related to the critical parameters rupture length (L), depth (z), and shear modulus (μ). The second is a confirmation of the earlier finding by Lomax and Michelini, namely that the rupture duration has a stronger influence to generate tsunami than M_w and Depth. We analyzed at least 510 vertical seismogram recorded by GEOFON-IA and IRIS-DMC networks. Our analysis shows that the seismic potency, LWD, which is more obviously related to capability to generate a tsunami than former. The larger T_{dur} the larger is the seismic potency LWD because T_{dur} is proportional to L/v_r (with v_r – rupture velocity). We also suggest that tsunami potential is not directly related to the faulting type of source and for events that have rupture duration greater than 50 s, the earthquakes generated tsunami. With available real-time seismogram data, rapid calculation, rupture duration discriminant can be completed within 3 to 8 min after the P-onset.

Key words: Rupture duration; Tsunami early warning; Body wave; Earthquake dynamics.

Science of Tsunami Hazards, Vol. 30, No. 4, page 233 (2011)

1. INTRODUCTION

Indonesia is surrounded by the Indo-Australian and Philippine Sea tectonic plates, which subduct beneath the Eurasian plate, with five big islands and several peninsulas. Indonesia has experienced thousands of earthquakes and hundreds of tsunamis over the past four hundred years [1]. Sumatra and Java are two of the most vulnerable islands to tsunami impact since they are located directly in front of the Indo-Australian plate [2,3,4]. Papua, Sulawesi, Sumbawa, Flores and Sumba are other islands that also have been experiencing several earthquake and tsunamis, although not as frequently as Sumatra and Java. Fig. 1 shows the epicenters of earthquakes that have occurred in the region.

The Indonesian islands along the Great Sunda Arc are particularly susceptible to earthquake and tsunami hazards. According to the Harvard Centroid-Moment-Tensor Catalog (<http://www.globalcmt.org>), more than 30 earthquakes with magnitude 7 or greater occurred during the last 30 years along the Sunda subduction zone [5]. The largest event with a magnitude $M_w=9.3$ was the Sumatra-Andaman earthquake of 26 December 2004 which had a rupture of over 1100 km [6,7,8] and generated a catastrophic, ocean-wide tsunami. Also during the last decades, devastating earthquakes and tsunamis occurred near the islands of Sumba and Sumbawa at the southeastern part of the Sunda subduction zone. The largest were the $M_w = 8.3$ Sumba earthquake of 1977, the East Java Earthquake ($M_w = 7.8$) of 1994 and the $M_w = 7.7$ Pangandaran earthquake in 2006 [5]. Most recent was the $M_w = 7.4$ Metawai earthquake and tsunami of 25 October 2010.

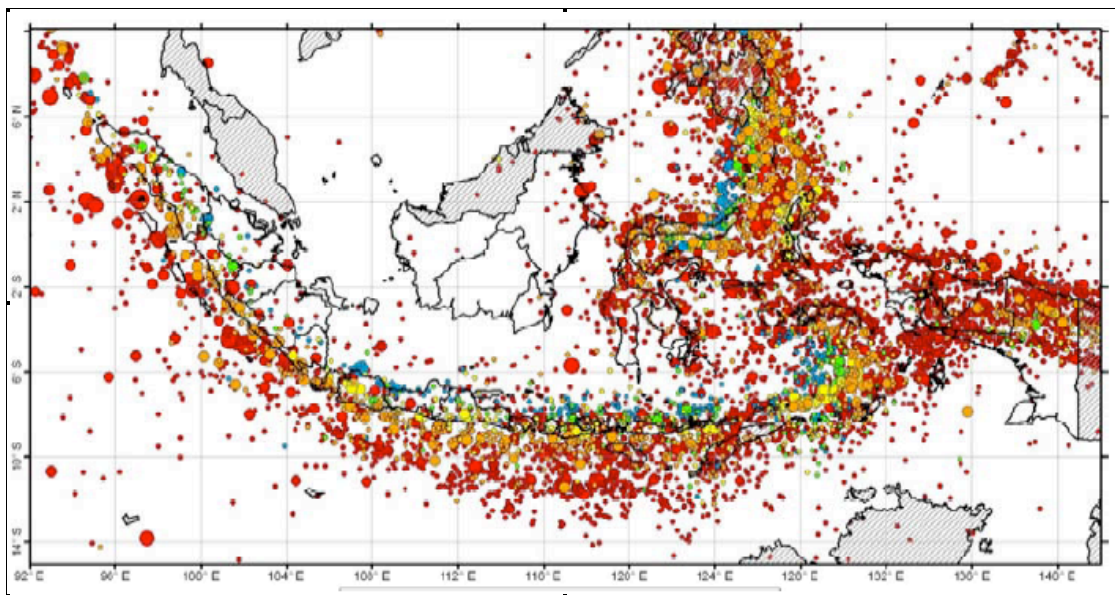


Fig. 1. Epicenters Indonesia earthquake occurred in range 1900 -2009 for magnitude > 5 [9].

The development of Ina-TEWS is being carried out by the Indonesian Government with support of donor countries (Germany, China, Japan, USA, and France) and international organizations (UNESCO, UNDP, UNOCHA, ISDR etc.). Preliminary operation begun in mid-2005 and Ina-TEWS was finally launched in November 2008. Indonesia was characterized as the riskiest country because

of its proximity to tsunami generation regions of the Indian tectonic plate. Thus, the country developed a national system, namely, “The Indonesian Tsunami Early Warning System” (Ina-TEWS). Operational components of Ina-TEWS include monitoring, processing, and telecommunication systems. The monitoring system includes land monitoring of seismic observations (160 broadband seismometers, 500 accelerometers) and GPS observation (40 units), sea surface monitoring with Buoys (22) and 80 tide gauges. BMKG (the Meteorological and Geophysics Agency), is the organization responsible for operating the National Operational Centre, which collects and processes all seismic data, determines earthquake locations, analyzes whether an earthquake is potentially tsunamigenic, issues earthquake information and tsunami warnings and integrates other observation data for confirmation or subsequent cancellation of the warning [8].

Ina-TEWS integrates all monitoring information coming from seismic, GPS, buoy and tide gauges, as well as the modeling system - taken from the tsunami database and geospatial data. The system provides recommendations to the officer-on-duty when the level of warning warrants it and the time that such warning should be issued. Currently, the decision on whether an event is tsunamigenic is based on earthquake parameters such as magnitude, location and depth. Sometimes, the decision requires support from various detailed information sources, tsunami modeling and related data in the DSS system. DSS consists of information retrieval system. Additionally received data and information become a decision bonus, which is shared in the dissemination network. Overview of all the information on data and maps give assistance to the operator in selecting the kind of information that should be disseminated for a certain area [10]. The decision can be wrong if the earthquake parameters are not accurate.

Failures in warning for tsunamis have occurred in Indonesia because earthquake parameters - such as magnitude, location and depth estimates of the Ina-TEWS - were not accurate. For example, BMKG announced that the Mentawai earthquake of October 25, 2010 presented no tsunami threat and cancelled the warning about one hour after the earthquake’s origin time when, in fact, a tsunami had been generated. This Mentawai tsunami left 270 people with significant injuries and 142 with minor injuries. Also, there was considerable damage on the Mentawai Islands, where 6 out of 27 coastal villages that were destroyed and 517 homes were either ruined or carried away by the tsunami.

The present study provides an analysis of seismic data of large Indonesian earthquakes as recorded by the vertical components of seismographs, for the purpose of providing a more accurate, rapid and direct procedure in assessing tsunami potential by estimating a quake’s rupture duration (T_{dur}). Additionally, the study analyzes the relation of rupture duration versus the centroid moment tensor magnitude (M_w) and the earthquakes’ focal depth.

2. DATA AND METHOD

Analysis was performed on at least 510 seismograms of fifty-one events which had epicenters in the Indian Ocean, Java, Timor Sea, Banda Sea, Arafura Sea and the Pacific Ocean, which satisfied the following criteria: (1) had faulting geometry with thrust, strike-slip or normal (2) had moment magnitude (M_w) between 6.7 and 9.0, and (3) had availability of at least ten high-quality teleseismic digital P-wave recordings with good azimuthal coverage and high signal to noise ratio for each event. Rupture duration was obtained for each event by using data of 10 vertical broadband teleseismic [11,12,13], P-wave data (2° – 30°). We used a direct procedure [11,12,13] to

estimate quake rupture duration. The procedure was used to assess tsunami potential by estimating rupture duration (T_{dur}) with a measure of delay time of 90% rms amplitude $T_{0.9}$, delay time of 80% rms amplitude $T_{0.8}$, delay time of 50% rms amplitude $T_{0.5}$ and delay time of 20% rms amplitude $T_{0.2}$. These parameters are simple to measure on observed P-wave seismograms and can be correlated to critical parameters of rupture length (L), width (W), slip (D) and focal depth - also needed for assessing tsunami potential. This direct, period-duration procedure gives improved identification of recent earthquakes which produced large or destructive tsunamis, relative to the use of Moment Magnitude (M_w)[14].

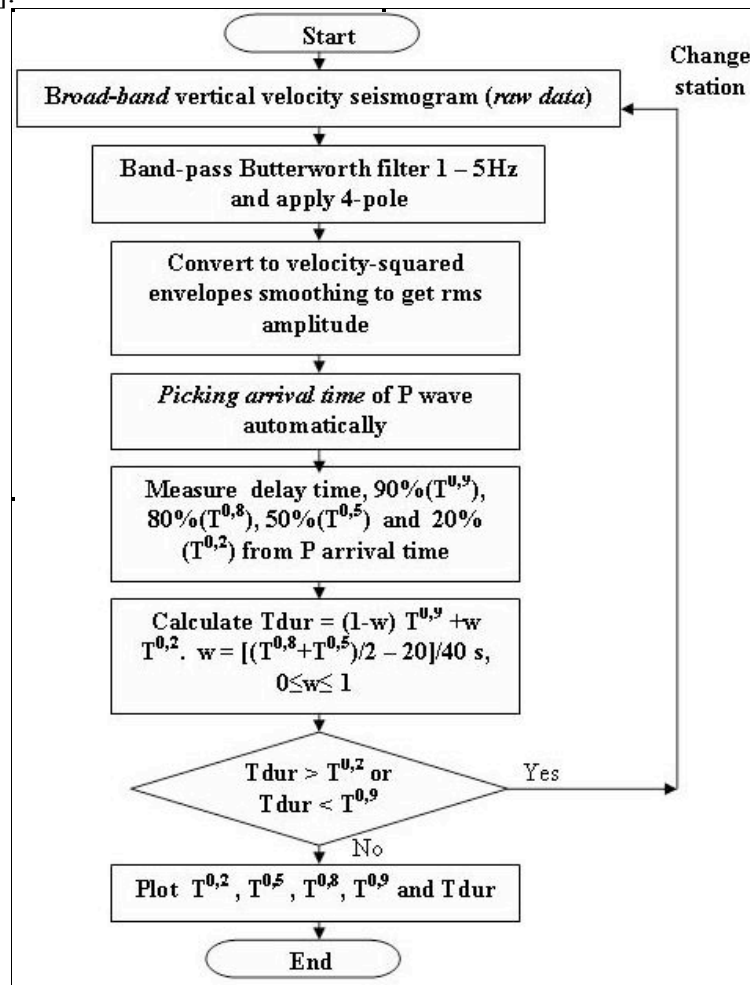
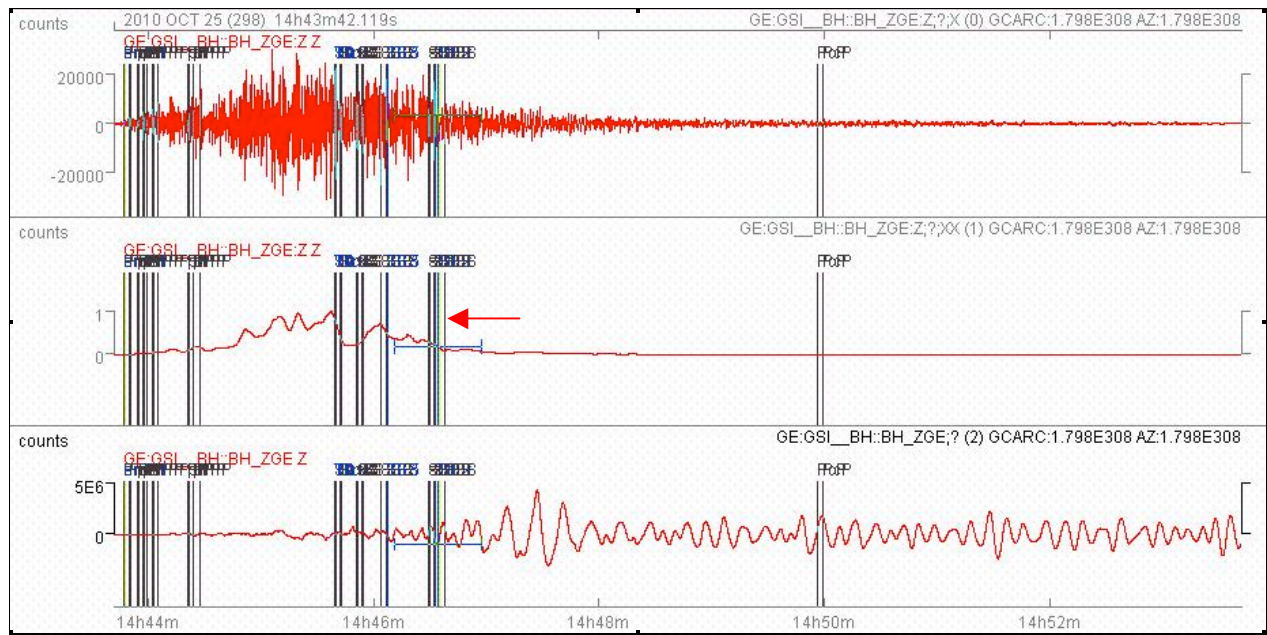
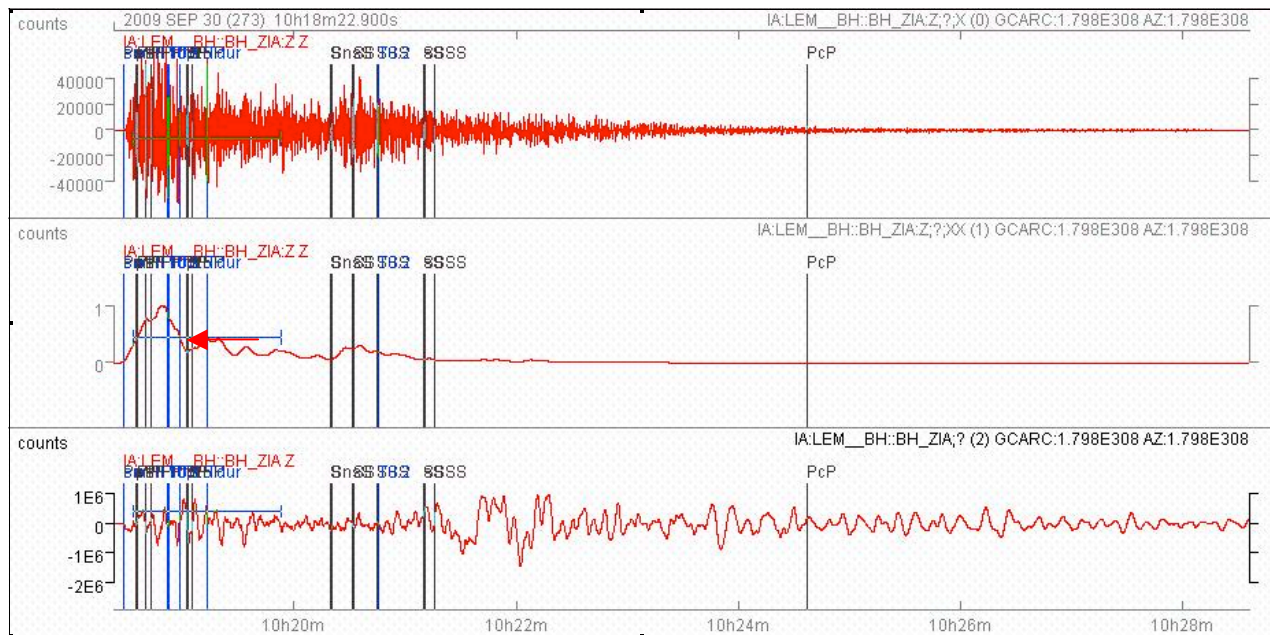


Fig. 2. Direct procedure to calculate rupture duration

For each event the vertical seismograms recorded by stations of the GEOFON-IA and IRIS-DMC networks were used, at different distances and azimuths and then calculated the average rupture duration to get a better estimate. As discriminants for tsunami potential, we first consider the rupture duration, “ T_{dur} ” calculated from the envelope decay of squared, high-frequency, HF; 1–5 Hz bandpass [14,15] of P-wave seismograms at teleseismic distance [11,12,13]. Fig. 2 is a flow chart which outlines the procedure. An example of the analysis of rupture duration processing is illustrated by Fig. 3.



Top



Bottom

Fig. 3. Single-station, period-duration processing examples for (Top) 2010 October 25, M_w 7.8, $T_{dur} = 119$ s, Mentawai, Indonesia tsunami earthquake, station GE.GSI at 5.366° , and (Bottom) period-duration processing examples for September 30, 2009, Padang non-tsunami earthquake (M_w 7.6, $T_{dur} = 25$ s, station IA.LEM at 9.433° , Butterworth-filtered HF seismogram (trace 0), smoothed, velocity squared envelope (trace 1) showing raw, broadband velocity seismogram (trace 2). Automatic P pick; $T_{0,9}$, $T_{0,8}$, $5T_{0,5}$ and $T_{0,2}$ are delay time from P arrival time; “ T_{dur} ” is rupture duration (red arrow).

3. RESULTS AND DISCUSSION

In order to analyze the relationship between rupture duration, centroid moment tensor magnitude (M_w) and focal depth, rupture durations were estimated by using data provided by the Global CMT catalogue (<http://www.globalcmt.org>) on moment magnitudes and focal depths. Based on the analysis, it became clear that rupture duration increases when the centroid moment tensor magnitude also increases (Fig. 4a). Thus, the results of the present study were in good agreement with those of Bilek and Lay (1999). Figures 4a and 4b illustrate that for earthquakes that have moment magnitude (M_w) greater than 7 and focal depth less than 70 km, no tsunami is generated if the rupture duration is less than 50 seconds. Table 1 provides estimates of rupture duration for large earthquakes occurring in the Indonesian region. Also, table 1 illustrates that tsunami potentials do not only depend on earthquake magnitude and focal depth. All of the earthquakes occurring in the ocean with magnitudes $M_w > 7$ and depths < 70 km (Ina-TEWS' criteria), did not generate tsunamis. As shown by Table 1, centroid moment tensor magnitude (M_w) is found to be a good discriminant for many, past, tsunamigenic earthquakes, but not for all. It was determined that rupture durations have effects which are greater than those of other discriminants (M_w , focal depth and type of faulting). Most of the earthquakes that generated tsunamis have rupture duration greater than 50 seconds. These results are also in agreement with those obtained by other studies (Okal, 1988)[16]; Geist and Yoshioka 1996)[17] and Lomax and Michelini, 2011). There is a higher probability of tsunami generation when the earthquake rupture duration (T_{dur}) is longer and the rupture length is greater. Also, the rupture duration gives more information on tsunami impact, M_o/μ , depth and size than M_w and other currently used discriminants. Figure 4a and 4b illustrate more information of the effect of rupture duration on tsunami generation. The longer the rupture duration, the shallower is the source of the earthquake. For rupture durations greater than 50 seconds, focal depth less than 50 km, and moment magnitudes $M_w > 7$, the rupture length is longer, because " T_{dur} " is proportional to L and greater M_o/μ , which is also proportional to L . So, with rupture duration information more can be known of the four parameters.

The local earthquake of January 1, 1996 represents an anomaly, since the rupture duration was 33 seconds (Table 1 on shadow row), yet it generated a local tsunami [4,18]. This anomalous phenomenon explains the issuance of false warnings from greater events with short duration but which have a high-frequency P signal. The 1996 event may have been one of those associated with fast ruptures, higher than normal stress drop, shorter length (L), but larger D .

Table 1. Assessment of tsunami potential in Indonesia using rupture duration estimation

Global CMT Catalog							Author	NGDC /TL/BMKG			
Origin Time	Lat. (°)	Long. (°)	Depth (km)	M _w	Fault type	Region	T _{dur} (s)	H _{max} (m)	NR	TP	
19910704 1143150	-8.02	124.73	17	6.7	Tr	Flores	19			nT	
19921212 0529499	-8.34	122.49	20	7.7	Tr	Flores	78	26.20	26	T	
19921220 2053006	-6.60	130.52	70	7.2	OT	Banda sea	39			nT	
19940215 1707517	-5.15	104.27	16	6.8	SS	S Sumatra	21			nT	
19940602 1817340	-11.03	113.04	15	7.7	Tr	Banyuwangi	130	13.90	24	T	
19941008 2144135	-1.19	127.87	15	6.8	SS	Halmahera	13			nT	
19950127 2016521	-4.43	134.45	22	6.8	N	Papua	36	NA	1	nT	
19950213 1504304	-1.31	127.57	15	6.7	SS	Halmahera	11			nT	
19950319 2353218	-4.18	135.10	19	6.8	SS	Papua	21			nT	
19950514 1133286	-8.60	125.26	16	6.9	N	Flores	53	4.00	1	T	
19951108 0714260	2.00	94.77	29	6.9	Tr	N Sumatra	21			nT	
19960101 0805100	0.74	119.93	15	7.9	Tr	Sulawesi	33	3.43	16	T	
19960217 0559305	-0.89	136.95	33	8.2	Tr	Papua	114	7.68	162	T	
19981109 0538486	-6.94	128.95	25	7.0	Tr	Banda sea	37			nT	
19981129 1410451	-2.03	125.00	16	7.7	SS	Ceram sea	55	2.70	1	T	
20000504 0421334	-1.29	123.59	19	7.5	SS	Sulawesi	96	5.00	1	T	
20000604 1628465	-4.73	101.94	43	7.9	Tr	Bengkulu	43			nT	
20001025 0932321	-7.28	105.43	46	6.8	Tr	Sunda Strait	17			nT	
20010116 1325143	-4.38	101.42	20	6.8	Tr	S Sumatra	23			nT	
20010213 1928451	-5.40	102.36	21	7.3	Tr	S Sumatra	28			nT	
20021010 1050419	-1.79	134.30	15	7.5	SS	Papua	134	3.00	1	T	
20021102 0126259	2.65	95.99	23	7.2	Tr	N Sumatra	33			nT	
20030526 1923385	2.61	128.88	34	6.9	Tr	Halmahera	15			nT	
20040128 2215340	-3.11	127.30	17	6.6	OS	Seram sea	13			nT	
20040205 2105128	-3.62	135.53	13	7.0	OS	Papua	36			nT	
20040207 0242437	-4.03	134.78	12	7.3	SS	Papua	68	NA	NA	T	
20040725 1435254	-2.68	104.38	600	7.3	N	S Sumatra	8			nT	
20041111 2126580	-7.87	125.12	17	7.5	Tr	Alor sea	76	2.00	NA	T	
20041226 0101900	3.09	94.26	29	9.0	Tr	Aceh	460	50.90	999	T	
20050302 1042169	-6.54	129.99	196	7.1	OS	Banda sea	9			nT	
20050328 1610315	1.67	97.07	26	8.6	Tr	Nias	112	3.00	17	T	
20050410 1029178	-1.68	99.54	12	6.7	Tr	Nias	37	0.40	1	nT	
20050514 0505246	0.42	98.24	39	6.7	Tr	Nias	21			nT	
20050519 015525	1.88	96.74	12	6.8	Tr	Nias	13			nT	
20050705 015263	1.56	96.93	16	6.6	Tr	Nias	29			nT	
20060127 165948	-5.61	128.20	397	7.6	N	Banda sea	8			nT	
20060314 0657375	-3.35	127.31	13	6.7	N	Seram sea	117			T	
20060516 1528312	0.01	96.98	14	6.8	N	Nias	12			nT	
20060717 0819287	-9.25	107.41	34	7.6	Tr	Tasikmalaya	170	10.00	196	T	
20070912 2349037	-2.46	100.13	43	7.9	Tr	S Sumatra	168	NA	NA	T	
20070912 1111156	-3.78	100.99	17	8.5	Tr	S Sumatra	174	5.00	47	T	
20070913 0335369	-2.31	99.39	22	7.0	Tr	S Sumatra	25			nT	
20080220 0808454	2.69	95.98	15	7.3	Tr	Simelue	45			nT	
20080225 0836424	-2.66	99.95	14	7.2	Tr	S Sumatra	37	0.12	1	nT	
20090103 1944090	-0.38	132.83	15	7.7	Tr	Papua	30	NA	NA	nT	
20090526 1923385	2.61	128.88	34	6.9	Tr	Halmahera	36			nT	
20090816 0738286	-1.56	99.45	12	6.7	Tr	S Sumatra	34	0.18	1	nT	
20090902 0755075	-8.12	107.33	53	7.0	Tr	Tasikmalaya	13			nT	
20090930 1016092	-0.79	99.67	78	7.6	Tr	Padang	27	0.27	1	nT	
20100406 2215191	2.07	96.74	18	7.8	Tr	N Sumatra	116	0.44	6	T	
20101025 1442222	-3.71	99.32	12	7.8	Tr	Mentawai	136	7.00	22	T	

T:Tsunami; nT:non-Tsunami; T_{dur}: rupture duration; Tr: thrust; SS:strike-slip; N:Normal : OT: oblique] thrust; OS: oblique strike slip faulting; H_{max}: [maximum water height](http://www.ngdc.noaa.gov/hazard/); NR: number of runups; NGDC: National Geophysical Data Centre (<http://www.ngdc.noaa.gov/hazard/>); TL, Tsunami Laboratory (<http://tsun.sccc.ru/nh/tsunami.php>); NA:not available data; TP:Tsunami potensial. Definition: tsunami occurred if (1) H_{max} ≥ 0,5 m and NR more then one times.

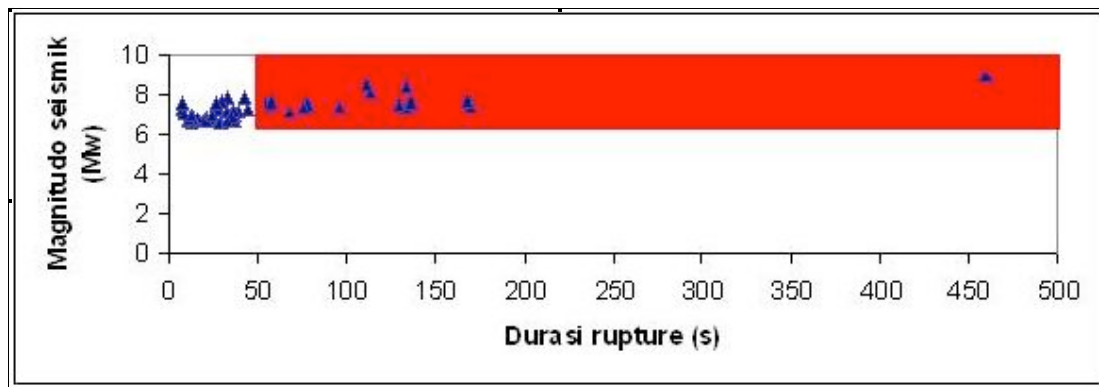


Fig. 4 (a) The relation between magnitude (Mw) and rupture duration, red zone is tsunami potential.

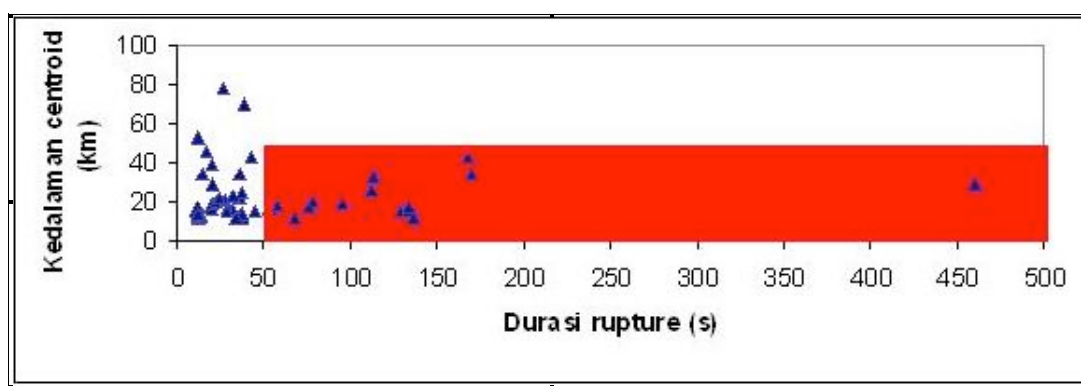


Fig. 4 (b) The relation between source depth and rupture duration, red zone is tsunami potential

Out of 51 earthquakes shown in Table 1 with Mw between 6.7 and 9.0, sixteen (or 31%) had rupture duration, $T_{dur} > 50$ s, and all sixteen (100%) produced a tsunami. By contrast, from 35 earthquakes with $T_{dur} < 50$ s only one (or 2.8%) produced a tsunami and 25% of the earthquakes had strike-slip faulting, while 75% earthquakes of the total of 51 have reverse faulting and generated tsunamis. This determination indicates that earthquake rupture duration has a stronger influence in generating tsunami than Mw and focal depth. Many earthquakes have Mw greater and shallower than others, but such earthquakes did not generate tsunamis. For example, the June 4, 2000 earthquake had magnitude ($M_w = 7.9$) greater than that of the February 7, 2004 ($M_w = 7.3$) (Table 1). However, the average rupture duration of the June 4, 2000 earthquake was 43 seconds which was shorter than that of the February 7, 2004, which was 68 seconds. Apparently, the shear modulus of the source of the June 4, 2000 earthquake was greater than that of the February 7, 2004. Therefore, the ratio of seismic moment (M_0) to shear modulus, μ ($M_0/\mu = LWD$) for the June 4, 2000 earthquake is smaller than the ratio of M_0 to μ (M_0/μ) of the February 7, 2004 event. Consequently, the length of rupture caused by June 4, 2000 earthquake was shorter than the rupture length of the February 7, 2004 earthquake. The smaller ratio of M_0 to μ , the shorter is the rupture length and the shorter is the rupture duration as well [19]. These results are good agreement with the results of Bilek and Lay (1999) [21] which showed strong trends of decreasing normalized source duration with increasing depth below the sea floor and that the estimated shear modulus of the seismogenic zone increases over depth ranging from 5–50 km.

Of the events that had rupture duration greater than 50 seconds, four events involved strike-slip faulting (Table 1, with darker shadow) and nine involved thrust faulting. All such events generated tsunamis. Based on the analysis, it is suggested that the tsunami potential is not directly related to the faulting mechanism of an earthquake. These results are a good agreement with Lomax and Michelini (2011). Many of the earthquakes have thrust, normal, or strike-slip faulting with rupture duration less than 50 seconds and these events did not generate tsunamis.

Most of the earthquakes indicated a trend of decreasing rupture duration with increasing depth below the seafloor (Fig. 4b). This finding is also in good agreement with the results of Bilek and Lay (1999). All of the events that have rupture duration greater than 50 seconds, had shallow depths (≤ 50 km) and generated tsunamis. However, as previously stated, not all shallow earthquakes generated tsunamis if the rupture duration was less than 50 seconds.

The performance of Ina-TEWS needs to be evaluated against a set of parameters preset by the international community. These parameters are considered crucial in evaluating tsunamigenic earthquakes and in disseminating correctly tsunami advisories to civil defense administrators and the general public – and thus minimize false warnings and unnecessary panic. One of the most critical aspects of a tsunami warning system is to be able to estimate earthquake parameters with reasonable accuracy in the shortest possible time. Earthquake location and magnitude are the two critical parameters to be estimated, so that the right scenario for evaluation can be chosen [21].

As primary discriminants in evaluating tsunami potentials, the Ina-TEWS uses the centroid-moment tensor magnitude M_w , representing the seismic potency LWD, which is estimated through an indirect, inversion procedure. The estimated M_w and the implied LWD value vary with the depth of faulting, assumed earth model and other factors and is only available within a period of 30 minutes or more after an earthquake. The use of more direct procedures for hazard assessment, when available, could avoid these problems and help in a more effective early warning (Lomax and Michelini, 2011).

4. CONCLUSIONS

Examination of the rupture duration of large earthquakes occurring in the ocean in the Indonesian region, illustrates the need for rapid and accurate information about the potential of tsunami generation. Analysis of rupture durations for fifty-one events using the direct procedure, determined that of the 51 earthquakes in Table 1 with moment magnitude M_w between 6.7 and 9.0, sixteen (or 31%) had rupture duration, $T_{dur} > 50$ seconds and all sixteen generated tsunamis. Of the thirty five of the earthquakes which had rupture duration $T_{dur} < 50$ seconds, only one (2,8%) generated a tsunami. Only 75% of the fifty-one earthquakes were associated with reverse faulting generated tsunamis. This means that earthquake rupture duration can be used as a discriminant for more accurate and rapid tsunami warning. Earthquakes that have a strike-slip fault type can also generate a tsunami, when the average rupture duration is greater than 50 seconds. The present analysis and results suggest that tsunami potential is not directly related to the faulting mechanism of an earthquake. With available real-time seismographic data, a rapid calculation of the direct, rupture duration discriminant can be completed within 3-8 min after the P wave arrival and thus help in issuing more effective and reliable early tsunami warning. It is recommended that rupture duration should be included as a primary discriminant for Ina-TEWS operations.

Acknowledgments

The GEOFON and BMKG-IA network (<http://webdc.eu>) and IRIS DMC (<http://ww.iris.edu>) provided access to waveforms used in this study; we thank all those who install, operate and maintain seismic stations worldwide. The Global CMT Catalog (<http://www.globalcmt.org/MTsearch.html>) provided access to CMT data used in this study; we thank all those who install, operate and maintain worldwide. Furthermore, I thank Prof. Anthony Lomax who gave us guidance in understanding the rupture duration calculation and in applying SeisGram2k software to estimate it (<http://alomax.free.fr/software.html>). Our discussions with him were beneficial. I thank Dr. George Pararas-Carayannis for editing certain sections to make what I wrote clearer for reading.

REFERENCES

1. Aydan, O., 2008. Seismic and tsunami hazard potential in Indonesia with a spacial emphasis on Sumatra island, Journal of The School of Marine Science and Technology, Tokai University, 6 (3), 19-38.
2. Madlazim, Bagus Jaya Santosa, Jonathan M. Lees and Widya Utama, 2010. Earthquake Source Parameters at Sumatran Fault Zone: Identification of the Activated Fault Plane, Cent. Eur. J. Geosci.,2(4),2010.DOI:10.2478/v10085-010-0016-5.
3. Madlazim, 2011. CMT, Fault Plane and Rupture Duration for Earthquakes in Sumatra and Possibility of its Implementation for Tsunami Early Warning System, PhD Program of Technology Sepuluh Nopember Institute (ITS) Surabaya. Dissertation.
4. Baeda, A. Y., 2011. Seismic and Tsunami Hazard Potential in Sulawesi Island, Indonesia, Journal of International Development and Cooperation, Vol. 17, No. 1, 2011, pp. 17-30.
5. Brune, S., Babeyko, A.Y., Ladage, S., and Sobolev, S. V., 2010. Landslide tsunami hazard in the Indonesian Sunda Arc, Nat. Hazards Earth Syst. Sci., 10, 589–604.
6. Kruger, F. and Ohrnberger, M., 2005. Tracking the rupture of the Mw 9.3 Sumatra earthquake over 1150 km at teleseismic distance, Nature, 435, 937–939, doi:10.1038/nature03696.
7. Lay, T., Kanamori, H., Ammon, C. J., Nettles, M., Ward, S. N., Aster, R. C., Beck, S. L., Bilek, S. L., Brudzinski, M. R., Butler, R., DeShon, H. R., Ekstrom, G., Satake, K. and Sipkin, S., 2005. The great Sumatra- Andaman earthquake of 26 December 2004, Science, 308, 1127–1133.
8. Ishii, M., Shearer, P. M., Houston, H., and Vidale, J. E., 2005. Extent, duration and speed of the 2004 Sumatra-Andaman earthquake imaged by the Hi-Net array, Nature, 435, 933–936, 2005.
9. Irsyam, M., Sengara, W., Aldiarnar, F., Widiyantoro, S., Triyoso, W., Hilman, D., Kertapati, E., Meilano, I., Suhardjono, Asrurifak, M., Ridwan, M., 2010. Ringkasan Hasil Studi Tim Revisi Peta Gempa Indonesia 2010, Bandung.
10. Pribadi, S., 2008. Indonesia Tsunami Early Warning System for Disaster Mitigation,

الندوة الدولية عن إدارة الكوارث

11. Lomax, A., Michelini, A. & Piatanesi, A., 2007. An energy-duration procedure for rapid determination of earthquake magnitude and tsunamigenic potential, *Geophys. J. Int.*, 170, 1195–1209, doi:10.1111/j.1365-246X.2007.03469.x.
12. Lomax, A. & Michelini, A., 2009a. Mwpd: a duration-amplitude procedure for rapid determination of earthquake magnitude and tsunamigenic potential from P waveforms, *Geophys. J. Int.*, 176, 200–214, doi:10.1111/j.1365-246X.2008.03974.x.
13. Lomax, A. & Michelini, A., 2009b. Tsunami early warning using earthquake rupture duration, *Geophys. Res. Lett.*, 36, L09306, doi:10.1029/2009GL037223.
14. Lomax, A. and A. Michelini, 2011. Tsunami early warning using earthquake rupture duration and P-wave dominant period: the importance of length and depth of faulting, *Geophys. J. Int.* 185, 283-291, doi: 10.1111/j.1365-246X.2010.04916.x.
15. Hara, T., 2007. Measurement of the duration of high-frequency energy radiation and its application to determination of the magnitudes of large shallow earthquakes, *Earth Planets Space*, 59, 227–231.
16. Okal, E.A., 1988. Seismic parameters controlling far-field tsunami amplitudes: a review, *Nat. Hazards*, 1, 67–96.
17. Geist, E. and Yoshioka, S., 1996. Source Parameters Controlling the Generation and Propagation of Potential Local Tsunamis, *Natural Hazards* 13: 151-177.
18. Gomez, J.M., Madariaga, R., Walpersdorf, A., and Chalard, E., 2000. The 1996 Earthquakes in Sulawesi, Indonesia, *Bull. Seism. Soc. Am.*, 90, 3, pp. 739–751.
19. Bilek, S. L. and Lay, T., 1999. Rigidity variations with depth along interplate megathrust faults in subduction zones, *NATURE*, Vol. 400, 29 July 1999, www.nature.com.
20. Geist, E.L. & Bilek, S.L., 2001. Effect of depth-dependent shear modulus on tsunami generation along subduction zones, *Geophys. Res. Lett.*, 28, 1315–1318, doi:10.1029/2000GL012385.
21. Nakamura, Y., 1988. On the urgent earthquake detection and alarm system (UrEDAS), in *Proc. of the 9th World Conference on Earthquake Engineering*, Tokyo-Kyoto, Japan.



TSUNAMI WAVE LOADING ON A BRIDGE DECK WITH PERFORATIONS

P. Lukkunaprasit¹, T.L. Lau², A. Ruangrassamee³ and T. Ohmachi⁴¹Professor, Dept. of Civil Engineering, Chulalongkorn University, Bangkok, Thailand²Graduate Student, Dept. of Civil Engineering, Chulalongkorn University, Bangkok, Thailand³Assistant Professor, Dept. of Civil Engineering, Chulalongkorn University, Bangkok, Thailand⁴Professor, Dept. of Built Environment, Tokyo Institute of Technology, Yokohama, Japan

Email: lpanitan@chula.ac.th, celau@eng.usm.my, Anat.R@eng.chula.ac.th, ohmachi@enveng.titech.ac.jp

ABSTRACT

Tsunamis have damaged bridges to various extents in the 2004 Indian Ocean Tsunami. This paper reports an experimental investigation of the effect of perforations in the girders and parapets on the horizontal tsunami loads. The results reveal that the maximum pressures impinging on the front face of the pier and deck are 4.5 and 3 times the hydrostatic pressure at 80mm nominal wave heights. The percentage of force reduction of the bridge deck with 10% perforated girders and 60% perforated parapets is found to be close to the percentage of perforation area in the deck. However, it is also noted that perforations in the bridge deck can substantially reduce the tsunami forces acting on it throughout the force time history. Thus, less damage to the bridge is anticipated for the bridge deck with perforations in girders and parapets.

Keywords: Tsunami, bridge deck, experiment, perforation, loading, pressure

1. INTRODUCTION

Evidences of partial to total collapse of bridges and extensively displaced bridge decks in the 2004 Indian Ocean tsunami (Unjoh, 2005; Sheth et al., 2006; and Ballantyne, 2006; Maheshwari et al., 2006; Scawthorn et al., 2006; Lukkunaprasit and Ruangrassamee, 2008) have prompted investigation of bridge performance under tsunami forces. The design of bridges to prevent these failures has not been thoroughly explored and the provision of an effective countermeasure remains an important issue. As bridges are an important lifeline structure which needs to achieve immediate occupancy performance after a disastrous event, the tsunami loading on bridges has to be investigated in view of the paucity of related established studies.

The experimental studies of tsunami forces on bridges have been conducted by Kataoka et al. (2006), Shoji and Mori (2006) and Iemura et al. (2007) recently. The latter study investigated the wave action on an I-girder bridge deck which was located on a dry bed while the others modeled the box type bridge decks which were placed on a wet bed at certain height of still-water. Shoji and Mori (2006) located the bridge deck on abutments whereas Kataoka et al. (2006) and Iemura et al. (2007) simplified the models by neglecting the bridge piers (personal communication with the authors). No pressure or force measurements were recorded by Shoji and Mori (2006). Kataoka et al. (2006) found that the slowly-varying drag force on the bridge deck which followed the impulsive force, averaged over a 0.5 s duration, can be well predicted with wave height-dependent formula stipulated by the Japan Port and Harbour Association (JPHA, 1999). On the other hand, drag force with drag coefficient of 1.1 is proposed for estimating tsunami forces on the bridge deck by Iemura et al. (2007) in which the maximum forces and maximum flow velocity were found to occur practically at the same time.

The wave propagation on shore and the wave-structure interaction are complex, which in turn has resulted in the inadequacy of the theoretical approach for tsunami force estimation for bridges using the current state of the art. Therefore, wave flume experiments were conducted with the purposes to investigate the actions of wave on a bridge system and thus to assess the effectiveness of perforation in bridge girders and parapets in reducing the tsunami-induced forces on the bridge. The present study investigated two configurations of bridge decks, one was the common bridge deck with solid girder and parapets (hereafter referred to as solid bridge deck) and the other one was the proposed bridge deck with perforated girders and parapets (hereafter defined as perforated bridge deck).

2. EXPERIMENTAL SETUP

A 1/100 single column bridge bent scale model with six I-girders and parapets was tested in a 40m long with 1m × 1m cross section wave flume (Figure 1). Two bridge configurations were investigated as shown in Figure 2, viz. the original prototype configuration typical in Thailand with solid girders and parapets, and the modified one with 10% and 60% perforation in its girders and parapets, respectively. The details of the bridge deck are given in Table 1. Tsunami waves were simulated by an abrupt release of a predetermined quantity of water from an elevated tank. The

severely hit Phuket Beach in Thailand with 0.5 degree slope was adopted as the typical beach profile. The solitary-like tsunami waves broke into bores, propagated as surges on dry bed (as described by Camfield (1994)) and impinged on the bridge model which was installed at downstream of the wave flume. The force was measured by a high frequency load cell mounted at the base of the model while the pressure was obtained from pressure gauges which were installed on the front face of the base of the pier (P1) and the front (P2f) and back (P2b) faces of the mid-span of the front bridge girder. Two nominal wave heights of 65mm and 80mm were performed. The nominal wave height is defined as the maximum flow depth at the bridge site in the absence of the model.

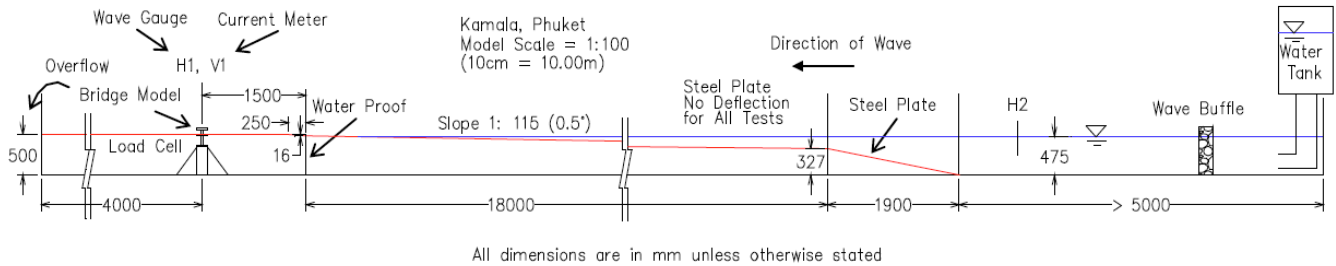


Figure 1 Test setup

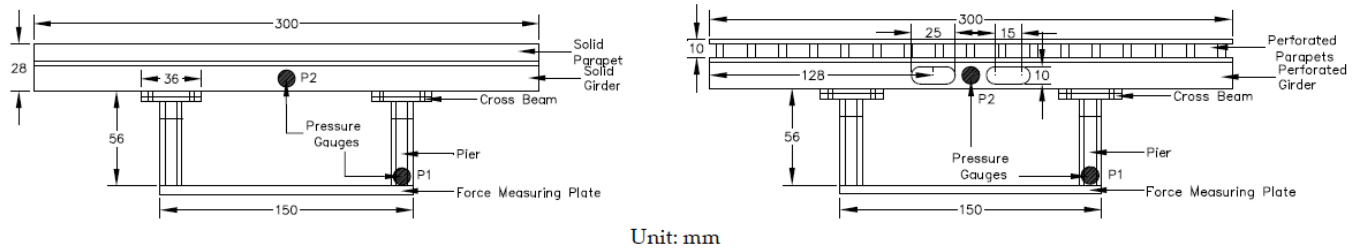


Figure 2 Solid deck (left) and perforated deck (right) models

Table 1 Details of bridge deck

Deck models	Solid	Perforated
Vertical projection area of each girder	4500mm ²	4500mm ²
Vertical projection area of each parapet	3000mm ²	3000mm ²
Vertical projection area of the slab	900mm ²	900mm ²
Perforation area (percentage) in girders	0mm ² (0)	450mm ² (10)
Perforation area (percentage) in parapets	0mm ² (0)	1800mm ² (60)

3. RESULTS AND DISCUSSION

Figure 3 shows the snapshots indicating the sequence of the generated tsunami flow striking the bridge model (highlighted in dotted lines in the figure for clear presentation) at 80mm nominal wave height. Two length scales with the length interval of 1cm were attached on the side wall of the flume. The wave propagates from the right side to the left side of the model. Prior to the installation of the bridge model, the wave height and flow velocity at the location of the model (as denoted as H1 and V1 in Figure 1) were measured and these values were correlated with the wave height at a reference point (H2 in Figure 1) located at the upstream of the wave flume. During the execution of the tests, the wave height at H2 was only recorded in order to minimize the interference of the flow regime adjacent to the model due to the installation of measuring instruments.

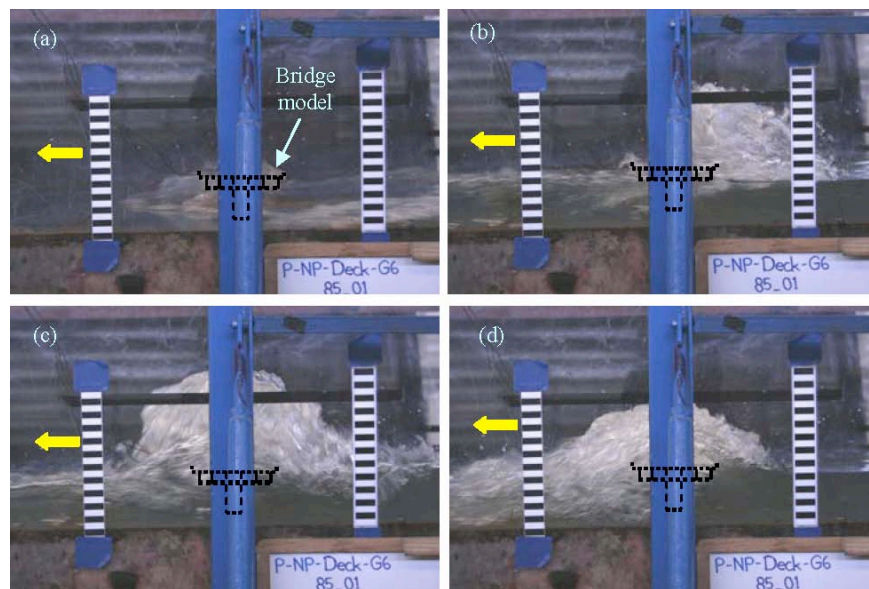


Figure 3 Sequence of the wave attacking the bridge model at 80mm nominal wave height

Figure 4 illustrates the recorded time histories of wave height (H1), flow velocity (V1), total force (on the piers and deck) and pressures for the 65mm and 80mm nominal wave heights. Table 2 summarizes the results of wave heights, forces on the bridge deck and pressures at the front and back faces of the front girder normalized with the maximum wave heights at H1. At the wave front, the surge travels with shallow wave height but with the maximum flow velocity as depicted in Figure 4a. The wave strikes the bottoms of the bridge piers initially and splashes upward to the soffit of the cross beam. The pressure at the base of the pier attains a maximum value up to almost 4.5 times the hydrostatic pressure (see Figure 4c and Table 2). At this instant, no pressure reading is recorded at the front and back faces of the front girder as shown in Figures 4d and 4e, respectively. Thus, the resulting force, depicted as the first peak of the force time history in Figure 4b, is essentially the wave force acting on the piers only.

Thereafter the wave height increases but the flow velocity decreases. When the wave reaches the

girders, it splashes up (Figure 3b), collapses on the deck (Figure 3c) and then overtops the deck (Figure 3d). The upward splashes of two and three times the incoming wave heights are observed at the 65mm and 80mm nominal wave heights, respectively. This produces the highest force in the second peak of the time history. The pressure gauges at the front girder start registering the readings (Figures 4d and 4e). It is found that the front face pressure on the front girder varies in the same trend with the recorded force. The maximum pressures at the front face girder are in the range of 1.7 to 2.2 times (for 65mm nominal wave height) and 2.2 to 3 times (for 80mm nominal wave height) the hydrostatic pressure. However, the maximum pressures at the back face of the front girder are slightly less than the hydrostatic pressure for both nominal wave heights.

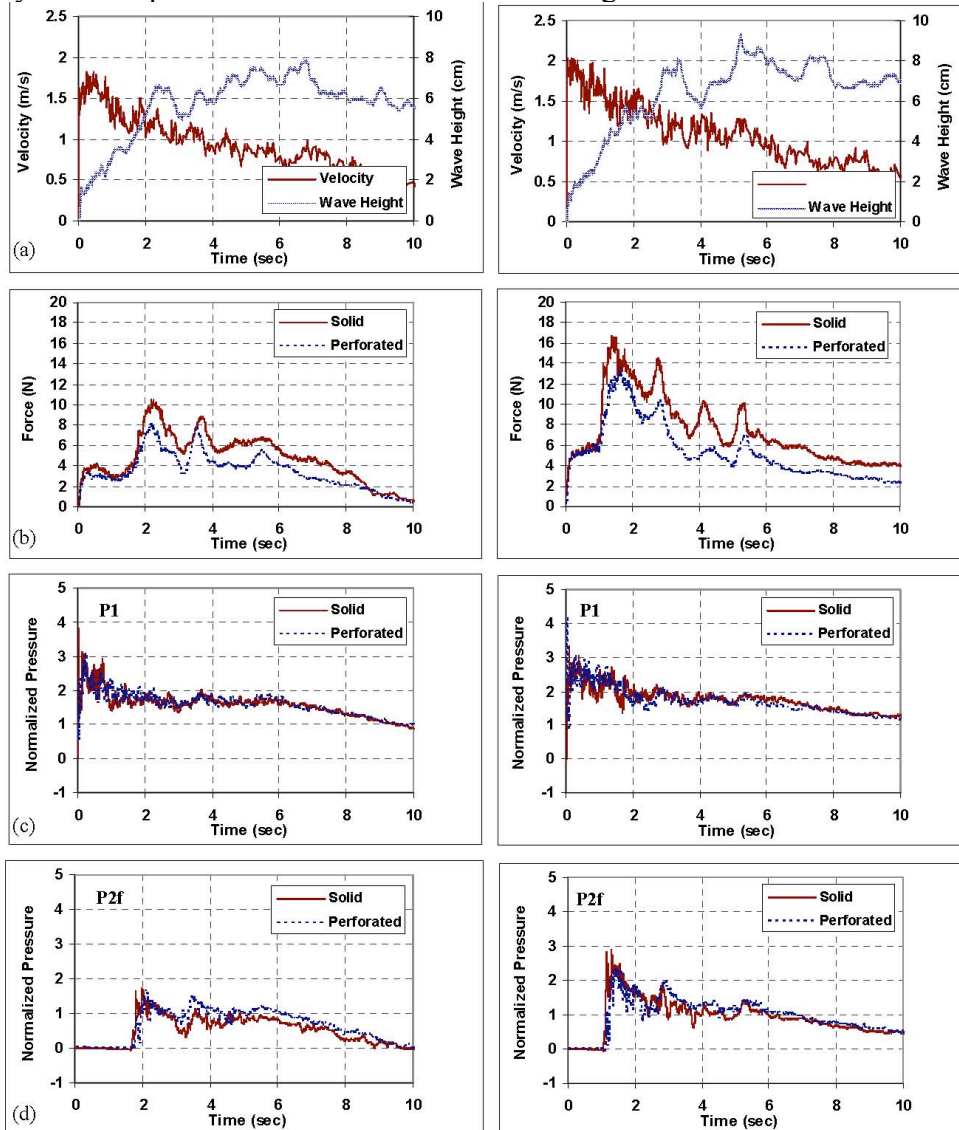


Figure 4 Correlation among (a) wave height and flow velocity, (b) total wave force and (c-e) pressures on the bridge model with solid deck and perforated deck at 65mm (left) and 80mm (right) nominal wave heights

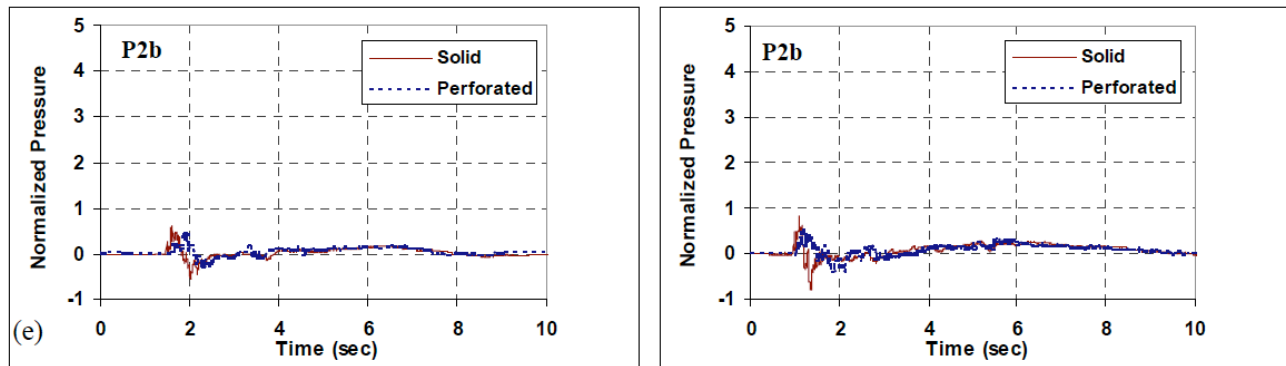


Figure 4(Cont'd) Correlation among wave height, flow velocity, total wave force and pressures on the bridge model with solid deck and perforated deck at 65mm (left) and 80mm (right) nominal wave heights

Table 2 Summary of results

Test	Deck model	Maximum wave height (cm)	Peak force on the deck (N)	<u>Perforated</u> solid	Normalized peak pressure at the base of the pier	Normalized peak pressure at the mid-span of the front girder (front face)
1	Solid	6.58	9.4		4.3	1.7
2	Solid	6.62	8.8		3.4	1.9
3	Solid	6.80	8.6		3.8	1.7
			Mean= 8.9	-	3.8	1.8
4	Perforated	6.78	7.2		4.1	2.2
5	Perforated	6.71	6.3		3.5	1.7
6	Perforated	6.80	6.5		3.1	1.7
			Mean= 6.7	0.75	3.6	1.9
7	Solid	8.32	12.4		3.5	2.7
8	Solid	8.34	12.5		4.4	2.9
9	Solid	8.41	13.0		3.0	3.0
			Mean=12.6	-	3.6	2.9
10	Perforated	8.02	9.4		3.3	2.4
11	Perforated	8.23	8.8		3.2	2.2
12	Perforated	8.18	8.7		4.2	2.4
			Mean= 9.0	0.71	3.6	2.3

The second peak forces, which are the highest forces in the time histories, are picked up as the maximum forces that impinge on the deck (Table 2) after subtraction of the forces acting on the piers from the stand alone pier model. The force time histories on the bridge deck are presented in Figure 5.

The wave force at 80mm nominal height increases to its peak more rapidly than the one at 65mm nominal height. Substantial reduction in forces has been witnessed in the perforated bridge deck. Unfortunately, the difference of pressure distribution in solid and perforated decks cannot be clearly distinguished due to the limited pressure measurement along the deck. However, higher fluctuation in the pressure record of the perforated deck is detected at 80mm nominal wave height (Figure 4d).

In general, bridge deck with perforations in the girders and parapets can reduce the forces at the peak and throughout the whole time history at both the considered nominal wave heights. Based on the summary in Table 2, the peak force reductions of 25% and 29% are obtained for 65mm and 80mm nominal wave heights, respectively. The peak force reductions are close to the area reduction of the entire vertical projection area of the deck, which is 27%. This seems to be simply caused by the reduction of the attacked area of the deck. However, substantial reductions are gained as far as the whole time histories are concerned. The mean forces exerting on the bridge with perforations, which are the time average of the areas below the force time history, are determined to be 33% and 39% lower than the values in solid deck bridge at 65mm and 80mm nominal wave heights, respectively.

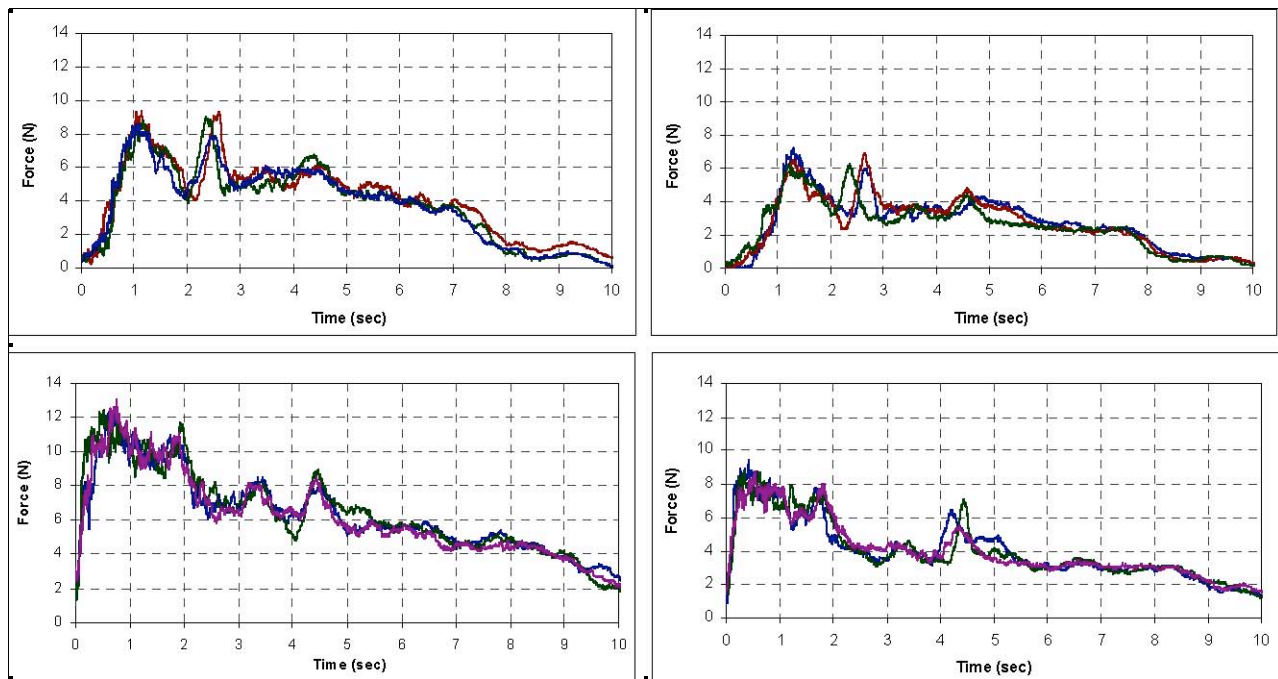


Figure 5 Force time histories on the solid (left) and perforated (right) bridge decks at 65mm (top) and 80mm (bottom) nominal wave heights

4. CONCLUSIONS

The experimental results reveal that the maximum pressures at the bottom of the bridge pier are as high as 4.5 times the hydrostatic pressure for both bridge models with solid and perforated decks at 65mm and 80mm nominal wave heights. In addition, the maximum pressures at the front face of the mid-span of the front girder are about 2.2 to 3 times the hydrostatic pressure, depending on the

nominal wave height. The perforation in girders and parapets reduces the average peak forces by about the same rate of the reduction in vertical projection area of the deck. However, substantial reduction in the forces thereafter throughout the force-time history is found. Thus, less damage to the bridge is anticipated for the bridge deck with perforations in girders and parapets.

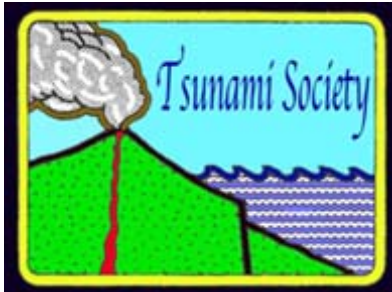
ACKNOWLEDGEMENTS

The authors would like to express sincere gratitude to the JICA AUN/SEED-Net for funding this research through the Collaborative Research Project. The partial support of the Department of Public Works and Town and City Planning, Ministry of Interior and The Royal Golden Jubilee project of the Thailand Research Fund is gratefully acknowledged. The appreciations are also extended to Assoc. Prof. Dr. Chaiyuth Chinnarasri, Assoc. Prof. Dr. Pennung Warnitchai, Mr. Pairoj Anantasetakul, Dr. Tayagorn Charuchaimontri, Mr. Nuttawut Thanasisathit, Mr. Surakai Banchuen and Mr. Ha Duyen Trung for their contributions in conducting the wave flume experiment. The service and facility provided at the Hydraulic Laboratory, Asian Institute of Technology (AIT) is highly appreciated.

REFERENCES

- Ballantyne, D. (2006). Sri Lanka lifelines after the December 2004 Great Sumatra Earthquake and Tsunami. *Earthquake Spectra* 22:S3, S545-559.
- Camfield, F. E. (1994). Tsunami effects on coastal structures. In *Coastal Hazards: Perception, Susceptibility and Mitigation*, Journal of Coastal Research Special Issue No. 12, 177-187.
- Iemura, H., Pradono, M. H., Yasuda, T. and Tada, T. (2007). Experiments of tsunami force acting on bridge models. *Journal of Earthquake Engineering* 29.
- JPHA (1999). Technical standards and commentaries of port and harbor facilities. Japan Port and Harbour Association (in Japanese).
- Kataoka, S., Kusakabe, T. and Nagaya, K. (2006). Wave forces acting on bridge girders struck by tsunami. *Proc. 12th Japan Earthquake Engineering Symposium* 154-157 (in Japanese).
- Lukkunaprasit, P. and Ruangrassamee, A. (2008). Buildings damage in Thailand in 2004 Indian Ocean tsunami and clues for tsunami-resistant design. *The Institution of Engineers Singapore Journal, Part A: Civil and Structural Engineering* 1:1, 17-30.
- Maheshwari, B. K., Sharma, M. L. and Narayan, J. P. (2006). Geotechnical and structural damage in Tamil Nadu, India, from the December 2004 Indian Ocean Tsunami. *Earthquake Spectra* 22:S3, S475-493.

- Scawthorn, C., Ono, T., Iemura, H., Ridha, M and Purwanto, B. (2006). Performance of lifelines in Banda Aceh, Indonesia, during the December 2004 Great Sumatra Earthquake and Tsunami. *Earthquake Spectra* 22(S3), S511-544.
- Shoji, G. and Mori, Y. (2006). Hydraulic model experiment to simulate the damage of a bridge deck subjected to tsunamis. *Annual Journal of Coastal Engineering* 53:2, 801-805 (in Japanese).
- Sheth, A., Sanyal, S., Jaiswal, A. and Gandhi, P. (2006). Effects of the December 2004 Indian Ocean Tsunami on the Indian Mainland. *Earthquake Spectra* 22:S3, S435-473.
- Unjoh, S. (2005). Damage to transportation facilities. The damage induced by Sumatra earthquake and associated tsunami of December 26, 2004, A report of the reconnaissance team of Japan Society of Civil Engineers, 66-76.



THE EARTHQUAKE AND TSUNAMI OF JULY 21, 365 AD IN THE EASTERN MEDITERRANEAN SEA - Review of Impact on the Ancient World - Assessment of Recurrence and Future Impact

George Pararas-Carayannis

Tsunami Society International, Honolulu, Hawaii, USA

postmaster@tsunamisociety.org ; drgeorgepc@yahoo.com

ABSTRACT

There is ample evidence indicating that on July 21, 365 AD a great earthquake near the west coast of the Island of Crete generated a mega-tsunami, which was responsible for extensive destruction throughout the Eastern Mediterranean, but particularly on Peloponnesus, the Greek Islands, Sicily, Libya, Cyprus, Palestine and Egypt. It is believed that the combined catastrophic impacts of the earthquake and tsunami were significant catalysts in furthering the declination of the Roman Empire and contributing to its subsequent final division between the East Roman and the West (Byzantine) empires in 395 A.D. In view of subsequent earthquakes and tsunamis in the region and the high probability that a similar great disaster will occur again, the present study reviews and summarizes the seismo-tectonic and kinematic characteristics of the Aegean and Anatolian micro-plates, their interaction with the African and Eurasian tectonic plates and examines and evaluates the historical records pertaining to this 4th Century AD disaster as to the destructive impact it had on the ancient world. Additionally, the study reconciles the impact described in historical and recent records with results obtained by numerical modeling studies, provides a rough estimate of the recurrence frequency of great tsunamigenic earthquakes in the Eastern Mediterranean region and assesses what the future impact may be in view of great increases in population densities along coastal areas.

Key words: tectonics; Eastern Mediterranean Sea; 365 AD earthquake; tsunami;

Science of Tsunami Hazards, Vol. 30, No. 4, page 253 (2011)

1. INTRODUCTION

Destructive earthquakes and tsunamis in the Eastern Mediterranean region have had significant impacts on the ancient world and even changed the course of history. One of the most destructive earthquakes on July 21, 365 AD along the western coast of the Island of Crete generated a mega-tsunami, which devastated the southern and eastern coasts of the Mediterranean and particularly impacted Peloponnesus, the Greek Islands, Sicily, Libya, Cyprus, Palestine and Egypt (Figure 1). According to historical records, it was a disaster of major proportions, which shocked the ancient world by destroying major cities and causing the deaths of thousands of people in coastal areas extending from present Croatia, to Greece and to the Nile Delta in Egypt. The combined catastrophic impacts of the earthquake and of the tsunami were significant catalysts in further decline of the Roman Empire and contributed to its subsequent final division between the Byzantine and West Roman empires in the year 395 A.D.



Figure 1. Approximate epicenter of the great 365 AD tsunamigenic earthquake.

In view of subsequent and more recent earthquakes and tsunamis in the same region and because of the high probability that such a major disaster will occur again in the future, many studies were conducted in recent years reviewing historical records and speculating on the source characteristics and impact of this great tsunamigenic earthquake of 365 AD. To clarify somewhat the ambiguities of the source characteristics of this great disaster, recent field studies and mathematical modeling were undertaken (Pararas-Carayannis & Mader, 2010) to further document and quantify crustal displacements at the tsunami origin source and to determine offshore tsunami heights along

Science of Tsunami Hazards, Vol. 30, No. 4, page 254 (2011)

coastlines of the Eastern Mediterranean Sea that could substantiate the degree of inundation of this great tsunami as described by ancient writings.

The present study re-examines and re-evaluates the historical records as well as the more recent accounts pertaining to the 4th Century AD disaster and the destructive impact it had on the ancient world. As background information, it provides a brief overview of the seismotectonic characteristics of the Aegean and Anatolian micro-plates and their interaction with the African and Eurasian tectonic plates. In spite of the rather limited historical data that prevents statistical analysis - an approximate estimate of the recurrence frequency of another great tsunamigenic earthquake is provided for the Eastern Mediterranean Basin region, based mainly on the kinematics of collision of tectonic plates. Finally, proper evaluation of future impact requires the development of risk assessment methodology that is based not only existing historical data but on research that can help predict the consequences of future events. For this reason and to reconcile the validity of historical records, the present study incorporates the results of the numerical modeling study undertaken in estimating the spatial and temporal characteristics of the 365 AD tsunami (Pararas-Carayannis & Mader, 2010).

2. EARLY HISTORICAL ACCOUNTS OF EARTHQUAKES AND TSUNAMIS IN THE EASTERN MEDITERRANEAN REGION

In the last three thousand years, numerous destructive earthquakes and tsunamis occurred in the Eastern Mediterranean region. Some of these events were documented with flowery narratives and unreasonable explanations in ancient writings. For example, Aristotle tried to explain earthquakes and the destructive waves they generate (tsunami) as being caused by winds entering the interior of the earth, heating up and blowing out. Also, Aristotle mentions this to be the mechanism for tsunami generation and gives as examples the destructive waves generated by the 373 BC earthquake at Ancient Elike and Vouros in the Gulf of Corinth.

Of all historical disasters in the Eastern Mediterranean region - perhaps because of its severe impact on the ancient world - the best documented by ancient historians was the one caused by the 365 AD great earthquake and tsunami. However, many Greek, Roman and Byzantine historians have documented many more earthquakes and tsunamis prior and after this 365 AD event.

According to historian Herodotus – considered to be the “Father of History” - the first recorded tsunami in the Eastern Mediterranean region occurred in 479 BC in Potidea of Halkidiki in the Northern Aegean Sea. The waves of this tsunami allegedly destroyed King Xerxes’ fleet during the second phase of the Persian wars. The citizens of Potidea attributed this event to the wrath of the tempestuous god Poseidon (Neptune), because the invading Persians had desecrated his statue.

Greek historian Thucydides (Θουκυδίδης) and historian/geographer Strabo (Στράβων) describe the effects of another sea wave (tsunami) from an earthquake in 426 BC in Fthiotida and the Gulf of Thermaikos in Central Greece. This tsunami was responsible for damage in the northern part of the Island of Evia, in Atalanta, coastal settlements on the island of Skopelos and for the destruction of Ancient Skarfia and other cities.

Historians/Geographers Strabo and Pausanias (Παυσανίας) refer to the aforementioned earthquake in the winter of 373/372 BC near Corinth (estimated magnitude up to 9 on the Richter scale) and the combined destruction of Ancient Elike (Ελίκη) - an important city in Ancient Achaia Province - in the Gulf of Corinth on northern Peloponnesus. Philosopher Aristotle (Αριστοτέλης) and

ancient Greek historian Diodorus Siculus (Diodorus of Sicily, Διόδωρος Σικελιώτης) and sophist Ailianos (Κλαύδιος Αιλιανός), indicated in their accounts that all animals left this area five days before this earthquake struck and headed towards the direction of Corinth. According to Pausanias, Elike and its inhabitants sunk into the Corinthian Gulf after the terrible earthquake. To this day the ancient city's exact location is not known but field investigation of coastal geomorphology and bathymetry (Pararas-Carayannis, 2007) indicate that large scale landslides – some of them generating tsunamis – have occurred in the past in this region east of the present city of Aegeion along a zone bounded by the rivers Selinounta (Σελινούντα), Kerinitis (Κερυνίτη) and Vouraikos (Βουραϊκος). Similarly the western port of Ancient Corinth known as Lechaio was destroyed by earthquakes and tsunamis.

The occurrence of a destructive tsunami in the harbor of Alexandria in Egypt is inferred by an account of historian Diodorus Siculus. Diodorus, in his highly allegorical narrative, likens the tsunami flooding of the city of Alexandria to a sea-monster sent by god Poseidon (Neptune) - believed to be the originator of earthquakes and tsunamis. Since the narrative refers to the Macedonian period of construction at the Alexandria harbor, we can conclude that this tsunami probably occurred between 331 BC and 325 BC.

As stated, the largest and best-documented disaster in the Eastern Mediterranean and Egypt in particular, resulted from the 365 AD great earthquake and tsunami. However, many of the ancient records are vague at best as to both the earthquake and tsunami impacts. Also, because of extensive cross-referencing of ancient records, misinterpretations and errors have been introduced in the scientific literature. For example, many of the ancient historical sources combine evidence of several earthquake and tsunami events during the fourth and fifth century into the single 365 AD event, while others assigned the destruction of important structures to subsequent and less intensive events. Also, based on their political or religious differences, ancient writers tended to describe the occurrence of natural disasters in terms of divine intervention or as warnings or consequences of unrelated events. Example of such misinterpretations are the opposing types of reporting by the Sophist Libanius (Λιβάνιος) and the church historian Sozomenus (Σωζομένος, «Εκκλ. Ιστορ.») as to the great earthquake of AD 365, presenting it as either a divine sorrow or as divine wrath for the death of Roman Emperor Julian, who had attempted to replace Christianity and reestablish paganism, two years before his death.

Also, Egypt had its share of destructive earthquakes and tsunamis in the last three thousand years. However, the historical records are not clear as to the origin of all the earthquakes. For example the ancient cities of Menotis and Heraclea were destroyed by an earthquake of unknown origin and no details are available (El-Sayed et al., 2004; Stanley et al. 2001, 2009). However, the historical record shows that many more earthquakes and tsunamis from distant and local sources, caused extensive destruction in the region after the 365 AD event, along the northern coast of Egypt. For example an earthquake in 746 AD – allegedly centered north of the Dead Sea - generated a tsunami, which sunk or destroyed many ships in Alexandria and elsewhere (Degg, 1990). Another tsunami in 746 AD, struck the coasts of Syria and Egypt. Alexandria was again struck by a tsunami in 811 or 881 AD but no details are available. Earthquakes in 950 and 956 AD caused damage to Alexandria's famous lighthouse but historic records do not mention if a tsunami struck. Also, no tsunami is known to have been generated by the Alexandria earthquake of 1201 AD, but a tsunami did strike the city after another earthquake in 1202. In 1303 AD, a large part of Alexandria was again destroyed by a tsunami

generated by an apparently great earthquake, which had its generating area south of the Island of Rhodes (Degg, 1990; Shaw et al., 2008). More earthquakes occurred again along the same northern area of Egypt in 1341 and 1375, but there are no records of tsunamis associated with these events. More recently, in 1870 and 1908, tsunamis struck again Alexandria.

3. OVERVIEW OF THE SEISMOTECTONICS OF THE EASTERN MEDITERRANEAN REGION

Before discussing further the historical accounts of the impact that the 365 AD earthquake and tsunami had on the ancient world, a brief discussion of the geological evolution and seismotectonics of the Eastern Mediterranean region is appropriate. Figure 2 illustrates the present features of geotectonic changes, following Post-Alpine Orogenesis.

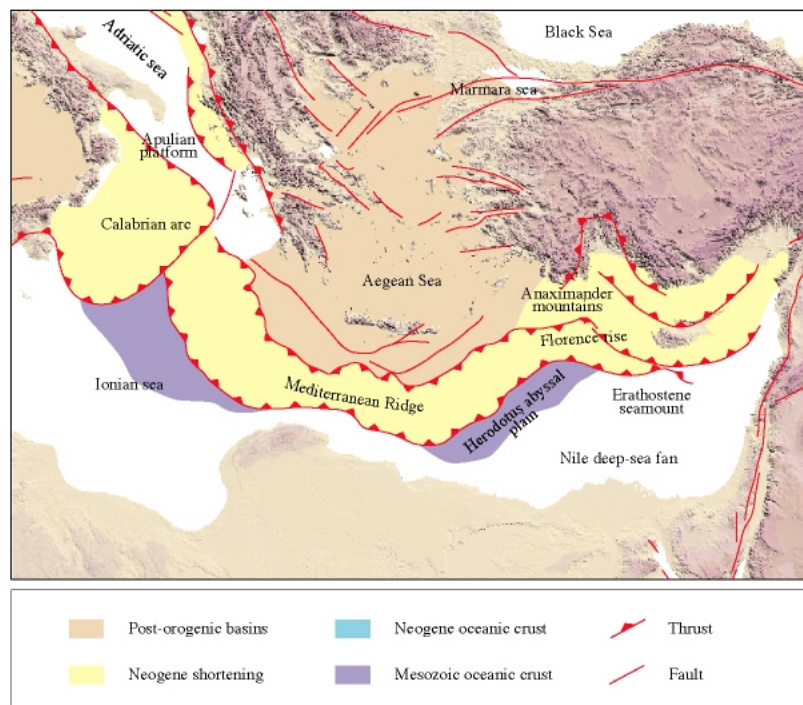


Figure 2. Simplified geotectonic map of the Eastern Mediterranean and Aegean Sea showing the subduction zone of the African plate with the Aegean, the Hellenic Arc, the orogenic belt and the volcanic arc in the southern Aegean Sea (*Dimitris Sakellariou, Hellenic Center for Marine Research*)

3.1 Alpine Orogenesis and Post-Orogenic Seismotectonic Changes

The seismotectonics of the Eastern Mediterranean region are dominated by the collision of Eurasia, Africa and Arabia plates and of two microplates - the Anatolian and the Aegean (McKenzie, 1972; Jackson & McKenzie, 1988; Jackson, 1994; Pararas-Carayannis & Mader, 2010). During the Cretaceous period (144 to 66.4 million years ago), continuing tectonic processes resulted in the Alpine Orogeny and the formation of the Alps. Stresses of the colliding tectonic plates lifted and folded the upper limestone layers, as well as the deeper metamorphic rock layers of the Eastern Mediterranean Basin. Eventually, big landmasses began to emerge from the sea, forming the Greek mainland and some of the islands of the present Aegean and Ionian Seas.

Tectonic collisions and Alpine Orogenesis resulted in further complex geotectonic deformations that created the Hellenic Orogenic Tectonic Belt, the long range of mountains that traverse the western side of the Aegean microplate. These tectonic processes continued to stress and fold the earth's upper crust in the region, thus forming more islands, more mainland mass and lifting the mountains of Greece to greater heights. The active tectonic interaction and collision of the converging African and Eurasian plates along the entire eastern Mediterranean margin resulted in multiple subduction zones, post-orogenic basins, accretionary margins, Neogenic crust shortening and extreme seismicity and volcanism - processes that continue to the present (Figure 4).



*Tectonic sketch of the Eastern Mediterranean
(adapted from Barrier, E., Chamot-Rooke, N. and Giordano, G., 2004,
Geodynamic Map of the Mediterranean, Commission for The Geological Map of the World, CCGM)*

Figure 4. Post-Alpine Orogeny - Seismotectonic Changes of the Eastern Mediterranean Basin (http://www.ifremer.fr/drogm_uk/Realisation/carto/Mediterranee/med-or.html)

3.2 Formation of the Hellenic Arc

As illustrated (Figs. 3 & 4), collision of the major tectonic plates in the Western Mediterranean region has formed broad boundaries of seismic and volcanic activity. The northern segment of the African plate south of the Adriatic Sea comprises of the Eastern Mediterranean oceanic lithosphere. Collision of the lighter-density oceanic eastern Mediterranean with the higher density continental lithosphere of Eurasia - part of which is the Aegean Sea microplate - has formed an arcuate zone of subduction along their boundary (Kokkalas et al. 2006). Thus, collision, convergence and subduction of the Africa plate beneath the southern Aegean Sea plate has formed the Hellenic Arc, an arcuate depression and a zone of active seismicity which extends along Western Peloponnesus and continues along the islands of Kythera and Antikythera to southern Crete, then eastward towards the island of Rhodes and Western Turkey. Paralleling the Hellenic Arc is the arcuate Volcanic Arc, which includes the volcanoes of Methana, Milos, Santorin, Colombo and Nisyros.

3.3 Rates of Convergence and Crustal Kinematics Along the Southern and Southwest Segments of the Hellenic Arc

The seismotectonics of Greece's southwestern and southern region are controlled primarily by the interaction of the Africa tectonic plate with the small Aegean Sea plate along the Hellenic Arc. The kinematics of Central Greece with respect to Europe and the implications for the tectonics of the eastern Mediterranean region have been determined with geodetic measurements (LePichon et al., 1995). Most of the earthquakes near the Hellenic Arc are shallow but further away from it, the focal depths are intermediate. The rate of subduction along the Hellenic Arc is estimated to be 35-40 mm/year (Reilinger et al, 1997). Most of the earthquakes that occur west and northwest of Crete near the Hellenic arc plate boundary are relatively shallow, with focal depths of less than 50 km (Pararas-Carayannis, 2006).

Differences in the rates of extension of two adjacent major segments of the external Western Hellenic Arc have created the Kythera Strait - a zone of complex, active, transform-extensional deformation and rotation (Lyberis et al., 1982). Oblique, en echelon, normal faulting indicates a pattern of dextral deformation. The seismic slip along the Kythera Strait is estimated at about 30 mm/yr (Papadopoulos 1989). With such high rate of seismic slip, the Kythera Strait can generate large, shallow and intermediate-depth earthquakes - with magnitudes of up to about 8.0 (Papazachos, 1996; Papazachos and Papazachou, 1997). A recent earthquake in January 8, 2006 along the Kythera Strait deformation zone had a focal depth of 48.4 km, which is close to the upper limit for intermediate earthquakes in this region. The focal depth was too deep for the generation of a tsunami (Pararas-Carayannis, 2006).

Most of the earthquakes in this particular region of the Greek Arc involve reverse as well as strike slip motion and some normal faulting motion. For example, the last major earthquake of January 8, 2006 in the Kythera Strait deformation zone, involved inverse but mostly lateral movement. As a consequence of this particular earthquake, it is estimated that the African plate moved in a northern direction by about 90 centimeters in relation to the Aegean Sea plate and to have subducted beneath it, while the Aegean plate continued its counterclockwise rotational movement

The long duration of the shaking (about 30 seconds) indicated a long rupture of perhaps as 50-60 km or even more (Pararas-Carayannis, 2006).

3.4 Seismicity and Tsunami Generation Along the Hellenic Tectonic and Volcanic Arcs

As stated, the Hellenic Arc in the southern Aegean Sea is created by the collision and convergence of the two great lithospheric plates of Africa and Eurasia with the Aegean microplate and is characterized by a zone of active seismicity which extends from the lower Ionian Sea islands and Western Peloponnesus, along the islands of Kythera and Antikythera to west side of southern Crete, where it changes to an eastward direction, continuing to Rhodes and Western Turkey. Different segments of this active boundary include the Hellenic Trough, the Strabo Trough, the Trough of Rhodes and the Pliny Trench. (Jackson, 1994; Westaway, 1994).

Thousands of earthquakes of all sizes have occurred in this region throughout recorded history (Pararas-Carayannis, 2001). Each segment of the Hellenic Arc is capable of producing major or even great earthquakes and destructive tsunamis. However, the crustal block that extends from the islands of Kythera/Antikythera islands to southwestern Crete appears to be the source region of great and very destructive earthquakes and tsunamis. This is the tectonic block where on July 21, 365 AD the great earthquake generated a mega tsunami in the Eastern Mediterranean. However, there have been many more historic earthquakes in the region and some have also generated destructive tsunamis. The following section reviews briefly the historical records and recent accounts of historical earthquakes and tsunamis in the region, but mainly in Greece.

3.5 Historical Earthquakes and Tsunamis in Greece and the Eastern Aegean Region

Of a total of 613 known historic earthquakes, at least 41 major events generated documented tsunamis that struck coastal areas of the Greek mainland and the Aegean islands. Sixteen of these earthquakes resulted in really damaging or disastrous tsunamis. Between 1801 and 1958, 482 earthquakes with intensity equal or greater than VI, and 170 with intensity greater than VIII occurred. Twenty of these earthquakes resulted in tsunamis and six of these tsunamis were particularly damaging or disastrous in the Aegean and the Eastern Mediterranean Sea (Galanopoulos, 1953, 1960). Thus, the occurrence of large tsunamis is quite usual for the Eastern Mediterranean and the Aegean Sea. Most of the large historical earthquakes are associated with the seismic zone of the convex side of the Hellenic arc (Hellenic Trench) (Papazachos et al., 1985, 1986). Also, extension and normal faulting within the Aegean plate are consistent with a NE-SW trending graben along which the Santorin volcanic field developed. Most of the larger destructive tsunamis in Greece in recent years have originated from this region of the volcanic arc, near the island of Santorin (see map, Fig. 2).

There is also substantial historical evidence that large earthquakes near the island of Crete were responsible for the destruction of the Minoan palaces on the island, including Knossos. The first major destruction of the Palace of Knossos by earthquakes occurred around 1720 BC. After the palace was rebuilt and restored to its original splendor, it was again destroyed by the earthquakes of the fourteenth century BC (Pararas-Carayannis, 1974, 2001). Subsequent earthquakes were responsible for further destruction.

A number of catastrophic tsunamis were generated from these early earthquakes and from the gradual collapse of the Santorin volcano over a period of time. The final explosion and collapse of the volcano of Santorin in 1625 BC generated a much larger tsunami, or a series of tsunamis, that inundated the coastal towns of Crete and acted as the catalyst in the declination of the Minoan civilization (Pararas-Carayannis, 1973). There is conclusive archaeological evidence that Minoan cities on the north and east coast of the island of Crete were also struck by huge tsunami waves (Marinatos, 1939). These included Amnisos, Malia, Niron Chani, Psira, Ghoumia, and Zakros.

Nothing is definitely known about the height of the Bronze Age tsunami on other Aegean Islands but estimates were made based on field-collected data. A rough estimate of the Santorin tsunami at Anaphi island, the closest to the origin, was extrapolated from the 7 m tsunami (corrected for eustatic change), as documented at Jaffa-Tel Aviv, 900 km away (Pararas-Carayannis, 1992). This estimate was based upon geometrical dispersion, neglecting effects of refraction, diffraction, or resonance, and resulted in an estimated height of 42 m, consistent with the 40-50 m elevation at which pumice deposits were found by Marinos and Melidonis (1959). The highest possible tsunami wave at the source could not have exceeded 50 meters (Pararas-Carayannis, 1992). Following the eruption and collapse of the volcano of Santorin many more tsunamis occurred in the Aegean Sea. For example and as discussed in detail in subsequent sections of this report, the 365 AD earthquake along western Crete generated the most destructive tsunami in the Eastern Mediterranean region. However, there were many more destructive tsunamis subsequently.

For example, on 26 September 1650, a destructive earthquake was accompanied by a submarine explosion from the Colombo Volcano, whose crater lies in the sea on the northeast of the island of Santorin. There was a devastating tsunami observed on the island of Ios, north of Santorin, and waves of up to 16 m were reported. In 1672, the islands of the Cyclades, and particularly Santorin, were again shaken by an earthquake. The island of Kos, to the east, was reported to have been swallowed up presumably by the resulting tsunami.

The best documented and most recent tsunamigenic earthquake in the Aegean Sea is the one that occurred on 9 July 1956 near the southwest coast of the island of Amorgos, killing 53 people, injuring 100, and destroying hundreds of houses (Galanopoulos, 1957). The earthquake resulted in a region of Central Greece along the Aegean/Anatolian microplates, which is associated, a mixed type of contractional-extensional deformation along WNW-trending faults (Fig. 5). Crustal deformation in this region of the Aegean Sea appears to be controlled both by rollback of the subducting slab and by the lateral extrusion of the Anatolia plate (Kokkalas et al., 2006). Apparently, earthquakes along these WNW-trending faults in the Aegean Sea can generate unusually destructive tsunamis. The waves of the 1956 tsunami were particularly high on the south coast of Amorgos and on the north coast of the island of Astypalaea. At these two places the reported heights of the tsunami were 25 and 20 m, respectively (Galanopoulos, 1960).

These are only a few examples of earthquakes and tsunamis generated in Greece and the Eastern Mediterranean region. There have been many more on the Greek mainland as well as in the Aegean and Ionian Seas and the Gulf of Corinth. The latest destructive earthquake and tsunami in the Gulf of Corinth occurred on February 24, 1981 near the Alkyonides Islands.

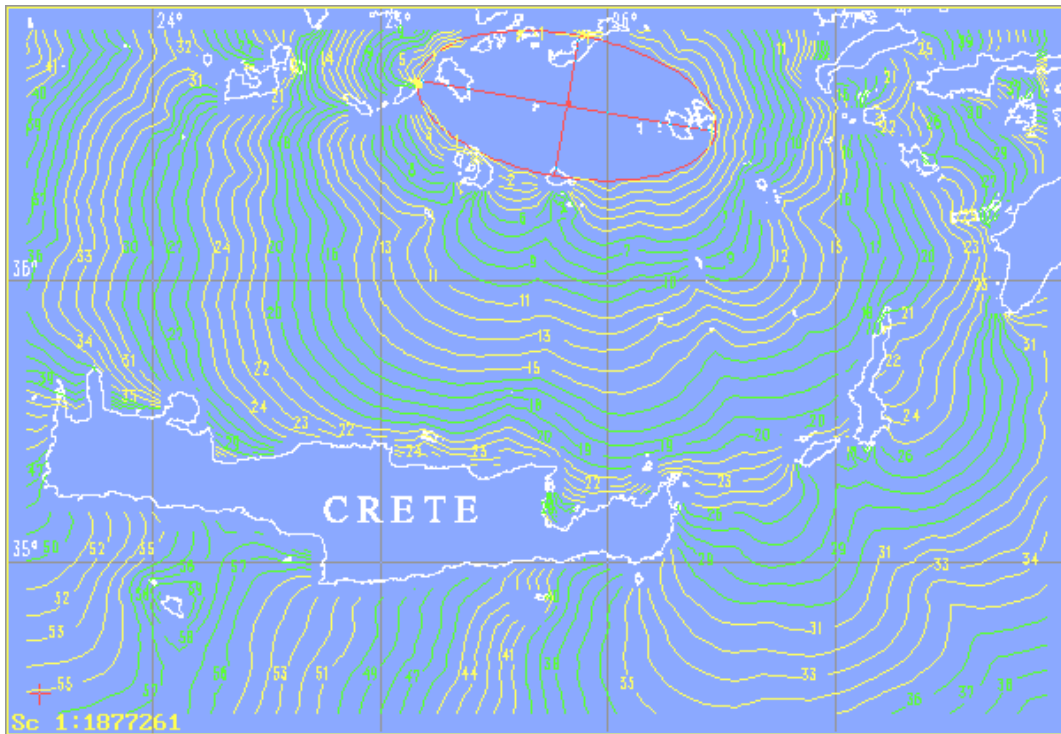


Figure 5. Generating area and travel time chart of the Tsunami of July 9, 1956 in the Aegean Sea near Amorgos Island (http://tsun.sccc.ru/MED/Med_tsu6.htm)

3.6 Earthquakes and Tsunamis along the southwestern segments of the Hellenic Arc.

The Kythera Strait is a zone of active deformation with particularly high seismic potential. The historic record indicates that many large earthquakes have occurred in this region in the past. Unfortunately, there is no adequate documentation for events prior to 1750. Some of the earliest known, large earthquakes occurred in 66 AD, in 365 AD, in 800 AD and in 1303 AD.

The occurrence of a large tsunamigenic earthquake in the year 800 AD remains questionable. It may have been confused with an earthquake, which occurred in 796 AD. It must be assumed that if indeed such earthquake occurred - whether in 796 or in 800 AD - it must have generated a destructive tsunami that struck Ancient Skandia (present Palaipolis) and other coastal settlements on the island of Kythera (Fig. 6) (Pararas-Carayannis, 2006).

In 1629 or 1630 AD an earthquake in the Kythera Strait generated a tsunami. Serious damage and some deaths occurred at Heraklion and elsewhere in Crete. No details are available on whether the damage and the deaths on Crete were caused by the tsunami or what the effects of the earthquake and of the tsunami were on Kythera Island. Another strong earthquake in the Kythera Strait on 6 February 1866 generated a tsunami. There was significant earthquake damage to Kythera Island. The tsunami reached a run-up height of 8 meters at Avlemonas on the eastern side of Kythera Island and caused damage to houses (Fuchs, 1886; Leonhard, 1899).



Figure 6. Massive coastal edifice failures on the east coast of Kythera Island, near the site of Ancient Scandia (present Palaiopolis), which was destroyed by tsunamis (photo: G. Pararas-Carayannis)

Also, a strong earthquake on 20 September 1867 with epicenter near Mani in south Peloponnesus generated a strong tsunami. There was heavy damage in Peloponnesus and slight damage at Kythera. The tsunami affected coastal areas at Kythera, Crete and Cyclades and reached islands in the Ionian and south Adriatic seas (Papazachos and Papazachou, 1997).

On 27 August 1886, a large destructive, earthquake in SW Peloponnesus generated a local tsunami (Papazachos and Papazachou, 1997). The quake was slightly felt at Kythera (Galanopoulos, 1953). No details about the tsunami are available. The previously mentioned 9 July 1956 tsunami generated near the southwest coast of the island of Amorgos, must have struck the island of Kythera but no details are available.

There is better documentation for the more recent events. At least ten strong earthquakes were documented for the period from 1750 to 1910 with magnitudes $M_s \geq 6.0$ or more. The mean recurrence was estimated to be of about 18 ± 18 years (Papadopoulos & Vassilopoulou 2001). Best known of the more recent events is the destructive Kythera earthquake of 11 August 1903. No details of a tsunami are available but it is believed that at least a local one occurred.

After 1910, when systematic instrumental seismic recording begun in Greece, the documentation of earthquakes in the region improved. Since 1910, the Institute of Geodynamics, National Observatory of Athens, recorded three strong earthquakes in the Kythera Strait - on March 18, 1937 ($M_s = 6.0$), on June 21, 1984 ($M_s = 6.2$), and November 21, 1992 ($M_s = 6.5$).

Recently, a historical data bank of earthquakes in the region was compiled from various sources in support of an experimental regional tsunami warning system for the Kythera Strait (Papadopoulos & Vassilopoulou 2001). The catalog of historical earthquakes for the region of Kythera Island that shows about 55 events. Some of these earthquakes generated tsunamis. Most noteworthy of the earthquakes that were destructive at Kythera are the following:

An earthquake on June 7, 1750 killed about 2,000 people at Kythera and caused considerable destruction on the island. As mentioned, a major earthquake (M_s about 7.9) on August 11, 1903 - with epicenter at sea south of Kythera - devastated the island. The shock was felt throughout Greece and as far away north as Trieste, as well as in South Italy, Egypt and Turkey. The quake killed four people, injured another ten and inflicted heavy damage on Kythera. Hardest hit on the island was the village of Mitata, which is located on ground consisting of alluvial deposits. A church and a school building collapsed and about 80 houses were damaged or destroyed. Also destroyed were the villages of Variadika and Kapsali. Many houses were destroyed in Avlemona (Papazachos and Papazachou 1997). Also, extensive damage occurred in Peloponnesus (Leonidio Kynourgia, Corinth), in the island of Santorin and as far away as Southern Italy and Sicily.

4. THE EARTHQUAKE OF 365 AD

The epicenter of the July 21, 365 AD earthquake main was near western Crete, close to the leading edge of the subduction boundary where the African tectonic plate pushes beneath the Aegean plate along the Hellenic Arc. The leading edge zone is close to the Ionian Sea islands of Kefalonia, Zakynthos, and Lefkas and to southern Peloponnesus, the islands of Kythera, Antikythera and Crete, where strong, frequent, destructive, shallow earthquakes have occurred throughout recorded history – most having focal depths usually varying from 0-60 km (Papazachos and Papazachou, 1997; Pararas-Carayannis, 2001).

Based on crustal displacements and intensities, the magnitude of the great earthquake has been estimated to be 8.3 and is believed to have been the strongest ever in the Eastern Mediterranean region. Peak accelerations in the epicentral region and along certain areas covered with alluvial deposits, may have been as much as 1g, which would be consistent with recorded peak accelerations of recent earthquakes elsewhere. Based on field studies on western Crete, the earthquake had an estimated minimum seismic intensity of XI on the Modified Mercalli scale in the immediate area. Although not reported in historical records, there must have been numerous aftershocks with magnitudes ranging from $M_s=6$ or more in the hours, days and months following the main shock.

4.1 Estimated Duration of Ground Motions

The historic records are unclear as to the duration of the strong ground motions and appear to group the main shock and subsequent strong aftershocks into one event. However, given the earthquake's estimated magnitude of 8.3, its shallow focal depth, its estimated length of rupture at almost 180 kms and a rupture rate estimated at 3.3 km per second, the overall duration of the main 365 AD quake could have been as long as 55 to 60 seconds or perhaps more, with possibly one or more brief interruptions (Pararas-Carayannis & Mader, 2010). The main event was probably followed by one or more separate sub-event ruptures on adjacent faults that could have been separated in time

by seconds or minutes, so the overall duration of ground motions would have seemed longer - as indeed reported in the ancient texts. Major aftershocks probably continued for hours, days, weeks and even months, before diminishing in strength.

4.2 Crustal Displacements

The main quake contributed to significant crustal uplift and subsequent aftershocks or separate earthquakes along adjacent fault zones contributed to significant subsidence. Recent satellite images (Fig. 7) indicate that indeed there was extensive gravitationally driven settling along southwestern Crete, following this 365 AD earthquake or perhaps other subsequent major earthquakes in the region.

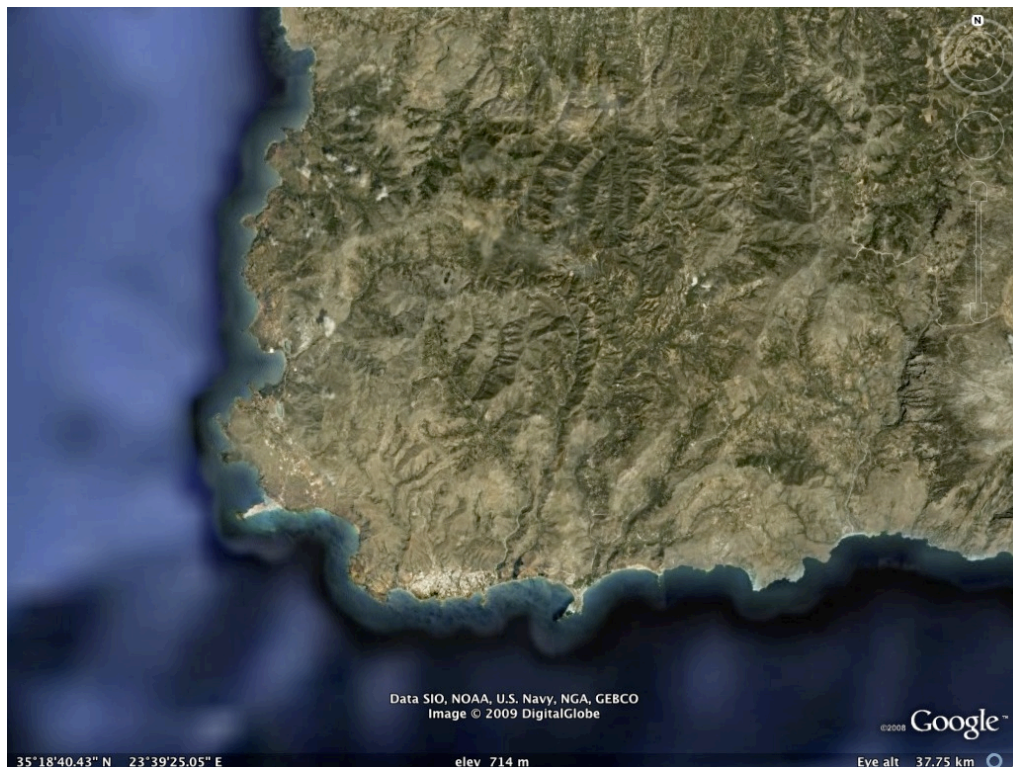


Figure 7. Google imagery of Southwestern Crete shows an arcuate subsidence of a large landmass on the southwestern end of the island.

Unfortunately, the historical writings do not provide any reliable data as to the chronology of events and the specific geomorphological changes associated with the 365 AD earthquake or the subsequent events. However, there have been numerous scientific and archaeological field investigations of raised shorelines and submerged ancient harbors of the Eastern Mediterranean that are indicative of major crustal displacements associated with significant earthquakes during the 4th, 5th and 6th Centuries AD (Thommeret *et al.* 1981, Flemming & Pirazzoli, 1981; 1996; 1999; Pologiorgi, 1985; Pirazzoli, 1999). For example, on the island of Antikythera there is evidence of crustal uplift that ranged between +1.0 and +2.7 m, estimated to have occurred sometime between 311 AD and 539 AD.

Science of Tsunami Hazards, Vol. 30, No. 4, page 265 (2011)

The 365 AD earthquake may have been a major contributing event to this uplift. The quake resulted in considerable upward crustal movement on the extreme western area of the island of Crete (Fig. 8).

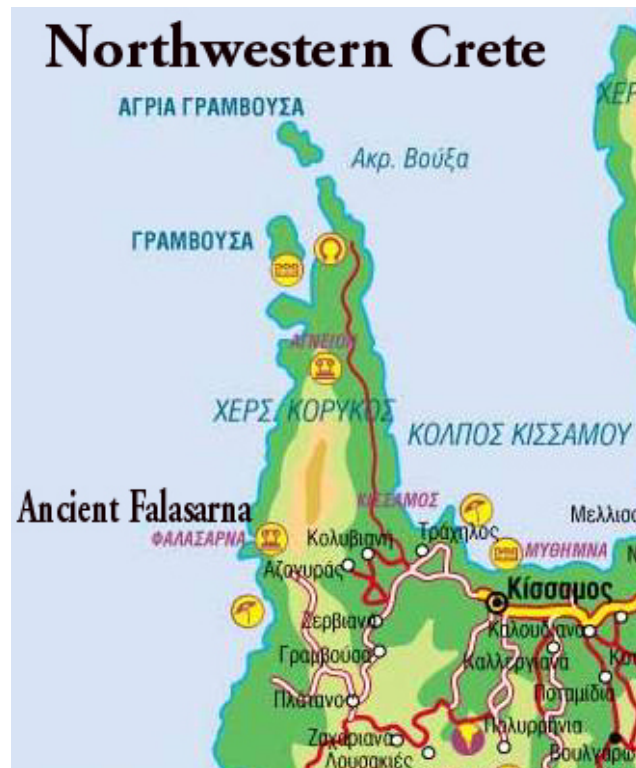


Figure 8. Ancient Falasarna on the Gramsvoussa Peninsula of Western Crete where maximum crustal displacements were determined.

Field studies of salt deposition and of erosional features indicate that the upward crustal displacements raised the land by as much as 6.66 meters on the average above the ancient sea level (corrected for eustatic sea level variation). Maximum uplift in one area was as much as 9.9 meters which would correspond to a seismic moment of about 10^{29} dyne-cm – a rather unlikely high energy release for earthquakes in the region. Whether the total uplift occurred as a result of the 365 AD earthquake seems improbable. Additional radiocarbon dating, geomorphology of shorelines along southwest Crete and GPS measurements support that substantial crustal displacements resulted from the 365 AD earthquake and subsequent large earthquakes within a 10 year period after this event. Furthermore, based on surveys of sediment distributions, the horizontal crustal displacements are believed to have ranged from 1m to as much as 20 m on certain areas. As mentioned earlier, satellite imagery shows also that subsidence of a large land mass along the southwestern region of Crete, but possibly at different times.

The crustal displacements caused by the 365 AD earthquake are examined in greater detail in subsequent sections pertaining to the quake impact on Western Crete and displayed graphically in the section pertaining to the tsunami generation area and its estimated dimensions.

4.3 Early Byzantine Tectonic Paroxysm - Stress Transference and Seismic Clustering

The 365 AD earthquake was an exceptional episode of sudden strain release over a very wide area along the Hellenic Arc. Apparently, it resulted in significant stress transference to other segments near the western and southern boundaries of the Anatolian–Aegean plate, which were activated and subsequently triggered other destructive earthquakes. There was unusually high seismic activity and clustering in Greece and the entire eastern Mediterranean region during the 4th, 5th and 6th centuries AD (Stiros, 2001), characterized as the "Early Byzantine Tectonic Paroxysm" (Pirazzoli, 1996; Pirazzoli et al. 1990).

5. IMPACT OF THE 365 AD EARTHQUAKE ON THE ANCIENT WORLD

Swarms of strong earthquakes appear to have occurred even earlier in the Eastern Mediterranean region at different periods of time and had great impact on ancient civilizations. For example, swarms of earthquakes and tsunamis in the 17th Century BC near Crete destroyed the Minoan palaces at Knossos, Agia Triada and Phaestos and the port facilities (Pararas-Carayannis, 1973, 1974, 1992, 2001). The palaces were rebuilt after the 17th Century destruction, but were partially destroyed once again by the tsunamis generated by the 1625 BC explosion/collapse of Santorin (Thera) volcano and its subsequent massive flank failures. It is believed that the 365 AD earthquake and tsunami caused further destruction to the remnants of the ancient Minoan palaces on Crete.

According to historic records, the 365 AD earthquake along the western side of Crete was felt throughout Eastern and Western Mediterranean and as far away as the eastern coast of Spain, particularly in the area where present Malaga is located. However, some of the records and subsequent references to them amalgamated and grouped all events together during that period as being caused by the 365 AD – thus clarifications are needed. For example, some of the historic records indicate great destruction along Eastern Sicily, the islands of Aioulou and in Calabria. In reality, however, destruction at these locations was caused by a strong earthquake, which had its epicenter near Aspromonte. However, coastal areas at these locations were struck by the 365 AD tsunami, which caused great destruction. Similarly, some of the ancient writings report erroneously that the destruction of the Greek colony of Cyrene (in present Libya) was also caused by the 365 AD earthquake, when in reality it was caused by an earthquake, which occurred shortly after 365 AD. Similarly, earthquake destruction in Ancient Nicomedia and Ancient Vithinia on Asia Minor was caused by local earthquakes in 358 AD and 362 AD. Also, destruction in Ancient Nikaia and in Constantinoupolis resulted from local earthquakes in 368 AD. In Palestine, a destructive earthquake occurred in 363 AD near Jerusalem. Finally, Ancient Pafos and Ancient Courion on Cyprus, were destroyed by a several earthquakes near the island in 365 AD, but not by the July 21, 365 AD earthquake near Crete.

The combined impact of the earthquake and tsunami were described by historian Ammianus Marcellinus (Roman History, Book XXIII, 6:32-36) as the “destruction of all the world”. Other historians referred to this event as a disaster of biblical proportions. More importantly, this disaster occurred at a very critical time in history when the Roman Empire was slowly hemorrhaging with

wars and political conflicts. Thus, the great devastation caused throughout the region by the combined effects of the earthquake and the tsunami, were major factors in the declination and eventual collapse of the Roman Empire. Many of the cities that were destroyed were never rebuilt. Some of the less-impacted cities did not adequately recover. Thirty years later, in 395 AD, the Roman Empire split between the East and the West (the Byzantine Empire), thus losing considerable influence and power grip in the region.

As stated there is ample historical information about the impact of the 365 AD earthquake as having occurred "everywhere" (Theofanis). Reportedly, strong ground motions were felt as far away as Dalmatia, Sicily, Libya, Cyprus and parts of Egypt and Palestine. The quake's greatest intensities occurred on Crete, Peloponnesus and many other regions of Greece, where many cities were destroyed, with the exception of Athens and other cities in Attica which were spared - allegedly because at the time celebrations in honor of hero Achilles were being held (Zosimus of Panopolis).

5.1 Earthquake Impact on Peloponnesus

Closer to the epicentral region, the ground motions were reported to be extremely intense. The earthquake destroyed the city of Patras (Triantafillos, 1959). There was extensive destruction of Ancient Gortyna on Peloponnesus and ten other cities (Perrey, 1848; Sieberg, 1932; Παπαζάχος Β. & Παπαζάχος Κ, 1989).

5.1.1 Earthquake impact on Ancient Olympia

Ample historical evidence confirms that strong earthquakes during this period greatly affected Ancient Olympia, the site where the Olympic games were held and where the famous Doric Temple of Zeus - erected in 456 BC. Accordingly, there was extensive destruction to many of the buildings, walls, supports and columns of buildings at the sacred city of Olympia and at the Doric temple of Zeus (Χιώτης, 1886,1887; Pararas-Carayannis, 2006). However, according to the historical records at the Museum of Ancient Olympia, earthquakes in 522 AD and 551 AD destroyed the temple, but no details are provided as to the specific damage caused by the 365 AD earthquake.

To help clarify ambiguities in the historic record as to the destruction of the Temple of Zeus and as to the 365 AD earthquake impact on other structures, a field investigation was undertaken. Its purpose was to determine to examine and map the directionality of failure of the temple's main columns and to estimate the ground accelerations that could have toppled the massive Doric columns (Fig. 9) (Pararas-Carayannis, 2007).

The orientation of the fallen columns indicated that the final toppling was caused not entirely by the 365 AD earthquake, as originally believed, but by a quake that had an east-west orientation. Thus, the earthquakes of 522 AD and 551 AD may have been partly the cause. These probably occurred near the Gulf of Corinth, to the north of Ancient Olympia, perhaps along the same fault zone that resulted in the destruction of Ancient Elike in the Gulf of Corinth by a great earthquake in 373 BC. The complete loss and disappearance of Elike was probably due to an associated coastal landslide triggered by such earthquakes, somewhere east of the present city of Aigion (Fig. 10). Although the 365 AD earthquake caused considerable destruction in Ancient Olympia, the quakes of 522 AD and 551 AD were closer and must have been responsible for most of the damage to the Temple of Zeus.

Further field investigation of the morphology of the coastline and of bathymetric charts indicated that many landslides have occurred in the past in the Gulf of Corinth – some without an associated earthquake - and in fact have generated destructive local tsunamis, in recent years (Pararas-Carayannis, 2007).



Figure 9. The directionality of failure of the Temple of Zeus massive Doric columns at Ancient Olympia provided clues as to intensity, maximum probable ground accelerations and source origin of the earthquake that caused their toppling (Photo G. Pararas-Carayannis).

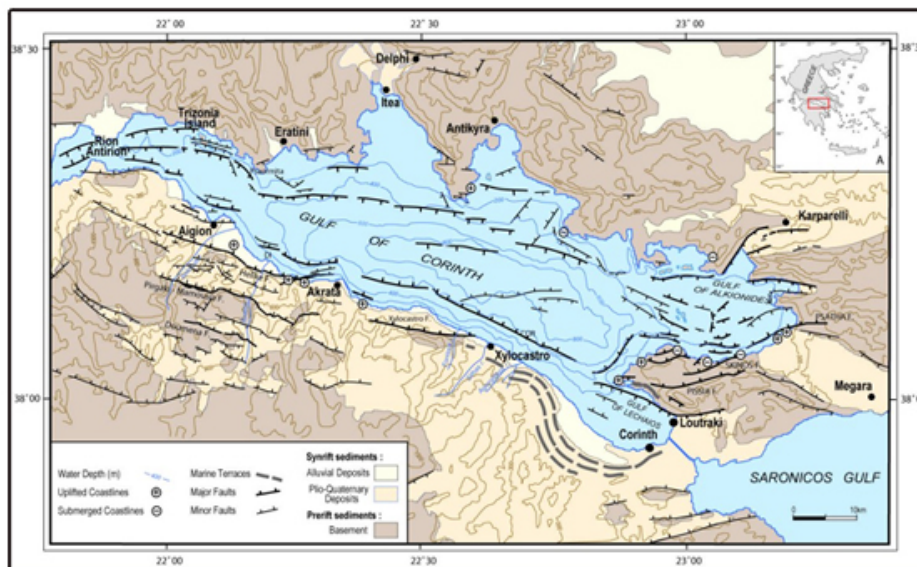


Figure 10. Major faults along the Gulf of Corinth. The lost Ancient Elike was east of the present city of Aigion, along a zone of parallel faults on land and at sea that have generated destructive local tsunamis.

Science of Tsunami Hazards, Vol. 30, No. 4, page 269 (2011)

5.1.2 Earthquake Impact on the Islands of Kythera and Antikythera

No documentation was found in any of the ancient records pertaining to the 365 AD earthquake's impact on the two islands. Although the historical record does not provide any information, because of the close proximity to the source region, both islands must have been greatly impacted. Ancient Scandia (present Palaiofoli) had been destroyed in the past by earthquakes and tsunamis and must have been devastated again by the 365 AD earthquake (Pararas-Carayannis, 2006). Similarly, Kapsali and other ancient settlements on Kythera Island must have sustained great destruction (Fig. 11).



Fig. 11. Map of Kythera Island. Ancient Scandia (present Paleopoli), Kapsali and other ancient settlements were destroyed by past earthquakes and tsunamis

5.1.3 Earthquake Impact on Crete

The impact of the great 365 AD earthquake on the island of Crete was described by the sophist Libanius, as “originating from beneath the seas and causing huge and devastating waves that swept over the island”. Knossos was practically leveled by the earthquake. Most of the destroyed cities on Crete were subsequently abandoned (Ξανθουλίδης, 1925). A history of Crete states that in the year 360 AD the ancient city of Pannona (now known as Boulismeni) was destroyed by a terrible earthquake (Κριάρης, 1930, 1937). Apparently the year given is wrong since this event occurred on July 21, 365 AD (Julian Calendar).

Western Crete and Ancient Falasarna - Crustal uplift rendered Ancient Falasarna on the western end of the Gramvousas Peninsula unusable as a port and thus the city declined in importance after the 365 AD earthquake (see Fig. 8) (Frost, 1989, 1997; Hadzidaki, 1988, 1996; Frost & Hadjidaki, 1990). Archaeological investigations (Flemming and Pirazzoli, 1981) of submerged ancient harbors identified an uplifted jetty of the port of Ancient Falasarna made of "unhewn blocks" (Fig. 12).



Figure 12. Uplifted jetty of "unhewn blocks" of the harbor of Ancient Falasarna, a stopover port used by ships sailing from Alexandria to Rome.

Remains of marine fauna on these blocks of Ancient Falasarna were found at heights of as much as 6.5 meters above sea level, inferring that this must have occurred since the second or third century AD, when this ancient town was flourishing and its harbor was still functional (Pologiorgi, 1985). A maximum uplift of about 9.9 meters over a smaller area near Ancient Falasarna has been dated to have occurred between 261 and 425 AD and attributed to probable co seismic movement accompanying the 365 AD earthquake (Pirazzoli et al., 1992). Also, uplift ranging between 0-9 meters

was observed along a distance of more than 100 km of the western part of the island of Crete. Radiometric data supported that it must have occurred around AD 370±52 (Thommeret *et al.* 1981, Pirazzoli *et al.* 1992). However, Western Crete was found to be clearly free of any isostatic or volcanic effects and, consequently, the possibility of any aseismic slip or of any non-tectonic effects have been ruled out (Stiros and Papageorgiou, 2001). The biological observations provided additional evidence that very rapid crustal movements had taken place during the 4th and 5th Centuries AD period (Laborel and Laborel-Deguen, 1994; Pirazzoli *et al.*, 1996). More than likely, these resulted from the 365 AD earthquake.

5.1.4 Earthquake Impact on Ancient Cyrenaia (Libya) and North Africa

Because of the great epicentral distance from the source region along western Crete, it is doubtful that Ancient Cyrenaia and other settlements of northern Africa were greatly affected by the 365 AD earthquake. Large parts of the Greek ancient city of Apollonia, in Cyrenaia (near the city of Susa in present Libya), could not have been greatly affected by the ground motions of this particular 365 AD earthquake – as claimed in historical records – because of the great distance from the source region. However, the city was impacted in the past by local earthquakes (Fig. 13) and coastal areas must have sustained destruction from the 365 AD tsunami.



Figure 13. Earthquake destruction of a theater in the ancient Greek city of Cyrene in Libya, by an earthquake that occurred shortly after the 365 AD earthquake. However Cyrene was severely damaged by the 365 AD tsunami.

5.1.5 Earthquake Impact on Cyprus

Destructive earthquakes have struck the Island of Cyprus over its long history and destroyed many of its towns and villages. However, the level seismic activity in the Cyprus region is significantly lower than that in Greece and Turkey. According to recent studies, there have been about 30 destructive earthquakes of intensity 8 or above on the Mercali scale from 1500 AD to the present time (Kythreoti and Pilakoutas, (?)). Most of the local earthquakes are concentrated along the south coast, along the tectonic zone known as the Cyprian Arc. However, the chronology of destructive earthquakes on Cyprus is not clear in historical records, although it is believed that the ancient cities of Pafos on the eastern coast and Courion on the southern coast of the island were severely impacted by earthquakes in the past (Fig. 14).



Figure 14. Map of the Island of Cyprus where Ancient Pafos and Ancient Courion (presently Episkopi) are located.

Ancient Pafos - Recent papers are unclear and state that Ancient Pafos was leveled by earthquakes in 365 AD, but without clarification as to whether it was the July 21, 365 AD earthquake near Crete that caused the destruction. Also, there is no mention of a tsunami in these records. However, because of the great epicentral distance of these two ancient cities on Cyprus from the source region of the July 365 AD earthquake along western Crete, the 365 AD earthquakes that

caused destruction on Cyprus, must have been separate events that either preceded or followed the great earthquake on Crete. Destruction at Pafos by an earthquake in 365 AD earthquake reduced the once big city into a small fishing village. It is very doubtful that the destruction was caused by the quake in Crete – as postulated. Patterns of column failure orientation could help determine directionality of maximum ground waves and the earthquake source responsible for the destruction of the city (Fig. 15).



Figure 15. Destruction of Ancient Pafos on the Island of Cyprus by local earthquakes.

Ancient Courion - Historic records show that five strong earthquakes during a period of eighty years destroyed Ancient Courion on the southern coast of Cyprus (presently town of Episkopi). A report published in a magazine (July 1988 issue of National Geographic) by an archaeologist claims that Ancient Courion was destroyed by the July 21, 365 AD earthquake. This is an erroneous report as the epicentral distance from Western Crete to Cyprus was too great to have caused the reported seismic destruction. However, as discussed in a subsequent section, the tsunami of July 21, 365 AD, which originated near Crete must have caused substantial destruction to the coastal area of the city.

5.1.6 Earthquake Impact on Egypt and the Nile Delta

The historic record is unclear as to what impact the 365 AD earthquake had on Egypt and the Nile Delta. The only known account is the one provided by the Roman historian Ammianus Marcellinus and is limited to a description of events in Alexandria. However, the historic record indicates that Egypt – and Alexandria specifically - has been affected by about twenty-five destructive earthquakes. Nine of these quakes originated from sources near the city, fourteen from distant locations along the Eastern Mediterranean – probably from the vicinity of the Hellenic Arc - and the rest from unspecified sources (Ambraseys et al., 1994; El-Sayed et al., 2000). Archaeological studies

indicate that the port of Alexandria at Faros Island had been partially submerged (Jondet, 1916), perhaps due to slippage and subsidence triggered by local earthquakes. Also, there are accounts stating that Alexandria and the Nile Delta have been affected by large, distant earthquakes originating in the Red Sea and the Gulf of Aqaba (Maamoun et al., 1984; Kebeasy, 1990).

The seismicity along the coastline of Egypt ranges from low to medium. Local earthquakes can have magnitudes up to $M_s=6.7$. Earthquakes near Egypt and the Nile Delta have caused extensive destruction in the past. Given the alluvial character of sediments in the region, ground motions are usually enhanced and also cause slippage along two prominent subterranean layers that contain high amounts of clay. Thus many antiquities from the Pharaonic and Hellenistic periods have slid into the sea. A rising sea level due to eustatic changes has also contributed to the submergence of ancient structures along the Nile Delta coast.

Alexandria – To what extent Alexandria was affected by the 365 AD earthquake is unclear. The city suffered great losses in the past due to earthquakes after its being founded by Alexander the Great in January 331 BC. Its vulnerability to earthquakes can be attributed to its location on sedimentary layers of the Nile Delta, which greatly enhance earthquake ground motions. The city was established on a narrow strip of land bounded to the north by the Mediterranean Sea and to the south by Lake Mareotis (Maryut), near the preexisting Egyptian settlement of Rakotis - a small port known since Homeric times and used for trade with the Phoenicians and Cretans (Tzalas, 2000). Homer, Herodotus, Thucydides and many other ancient writers had written about Rakotis. According to Plutarch's biography (Alex 26.4.1 - 26.8.1), Alexander the Great, having read their writings, was fascinated by Egypt and decided to establish a model city at this site of Rakotis (Favard-Meeks & Meeks, 2000). However the site turned out to be vulnerable to both earthquake and tsunami hazards.

The description below by the Roman historian Ammianus Marcellinus indicates that the 365 AD earthquake was strongly felt in Alexandria but he does not provide clear information as to any damage caused by the ground motions – if any – and does not indicate how much later after the ground motions were felt, the city was inundated by the tsunami. His account only states:

Slightly after daybreak, and heralded by a thick succession of fiercely shaken thunderbolts, the solidity of the whole earth was made to shake and shudder, and the sea was driven away, its waves were rolled back, and it disappeared, so that the abyss of the depths was uncovered and many-shaped varieties of sea-creatures were seen stuck in the slime.....”

Ammianus Marcellinus' description is vague and implies effects of a local earthquake in Alexandria, rather than effects caused by the 365 AD event, which originated along Western Crete. Given the great epicentral distance from Egypt, ground motions at Alexandria would not have been expected to be as strong as described, unless there was a separate concurrent or subsequent event. However, it is possible that strong ground motions were experienced in Alexandria, probably enhanced by the unconsolidated sediments.

Ammianus Marcellinus' makes no mention of earthquake damage – only of the tsunami impact on the city. Also, there is no mention in his or any other historical records of any damage from this earthquake to the famous Lighthouse of Alexandria on the island of Faros. Apparently, the Lighthouse

(Faros in Greek) - one of the seven wonders of the ancient world – was not affected by the 365 AD earthquake. However, there is historical record that an earthquake in 796 AD caused damage and the Lighthouse lost its 3rd floor. Also, a series of earthquakes between 950-956 AD contributed to further damage. Another earthquake in 1261 destroyed further the structure and the 1303 AD earthquake, destroyed it completely (Χαλαρή, 2007).

6. THE 365 AD TSUNAMI

6.1 Generating Region of the 365 AD Tsunami

Based on the well-documented uplift and distribution of crustal displacements on the island of Crete as described earlier, it was concluded that the rupture of the 365 AD event occurred along a major thrust fault with a strike of about N30°W and along two northern sub-faults that had a strike of about N50°E. Based on the recent rupture modeling study (Papadimitriou & Karakostas 2007), the overall rupture length for this event was re-estimated to have been as much as about 96 nautical miles (177.8 km) (Pararas-Carayannis & Mader, 2010). Furthermore, by projecting the field measurements of vertical crustal displacements on land from Crete and Antikythera Island into the sea, the area affected by the earthquake was estimated to have elliptical dimensions with major and minor axes of about 244 kms and 94 kms, respectively (Fig. 16). The total area affected was estimated to be about 72,019 km² (Pararas-Carayannis & Mader 2010).

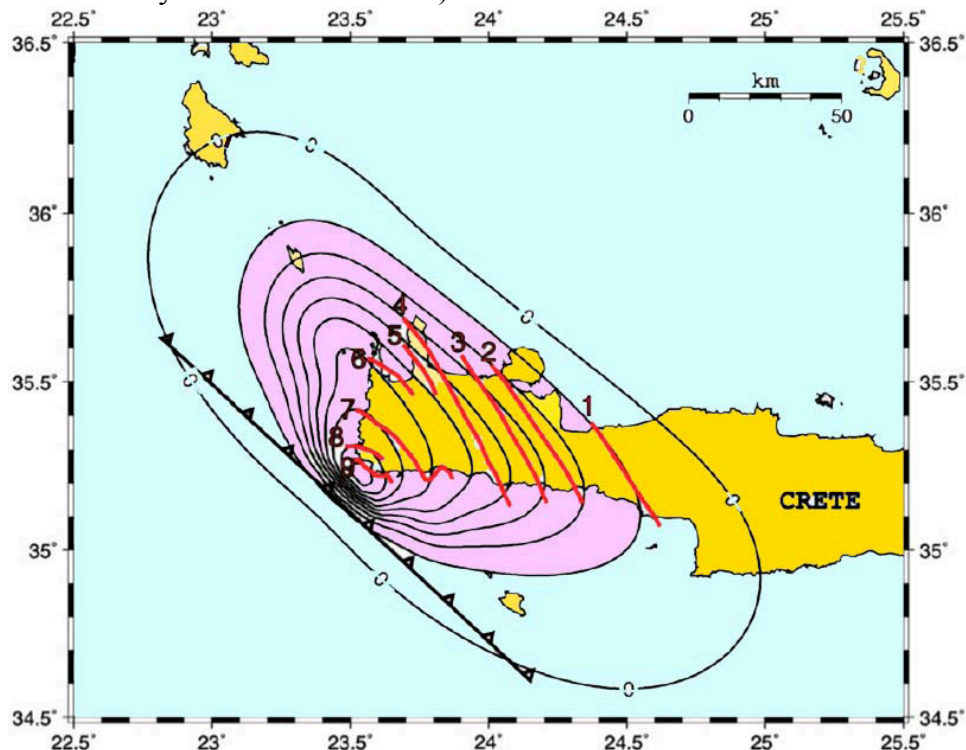


Figure 16. Crustal Displacements, Tsunami Generating Area (Pararas-Carayannis & Mader, 2010; mod. from Papadimitriou & Karakostas, 2007)

The tsunami source area was determined by deducting from the total area of 72,000 km², the land area affected by the earthquake on Crete and the islands - estimated at 4,710 km². Thus, the submerged portion that underwent vertical crustal changes was estimated to be at 67,290 km². This was the postulated 365 AD tsunami source region used for subsequent numerical modeling of tsunami height attenuation with distance and for estimating offshore tsunami heights near the coastlines in the Eastern Mediterranean region which were impacted by the tsunami (Pararas-Carayannis & Mader 2010).

The volume of displacements for that particular source area was used to estimate the portion of total earthquake energy that contributed to the generation of the tsunami. Since the total volume of displacements - the volume of the estimated isopach on land - was estimated to have been 6.63 km³ and the overall total volume of the earthquake displacements - total isopach - was estimated at 16.929 km³, the 365 AD tsunami was generated by ocean floor displacements of about 10.299 km³, which would be the vertically displaced volume of water.

6.2 Numerical Modeling of the 365 AD Tsunami

Using the above postulated source dimensions of the 365 AD tsunami, a numerical modeling study was conducted using the SWAN shallow-water numerical code which solves the long wave, shallow water, nonlinear equations of fluid flow (Mader 2004). The modeling was based on a 600 by 280 grid and four-minute travel time increments and provided tsunami travel times, wave height attenuation with distance and estimates of tsunami energy distribution. Figures 17 and 18 provide the propagation of the 365 AD tsunami along the Eastern Mediterranean Basin at different time increments after the earthquake. The numerical modeling study (Pararas-Carayannis & Mader, 2010) showed that no tsunami energy reached the Western Mediterranean Basin, the upper Adriatic Sea or the Northern Aegean above the latitude of the Sporades Islands. Figure 19 shows the locations and the tsunami heights in the open sea near the regions, which were impacted by the 365 tsunami, as documented by the historic records.

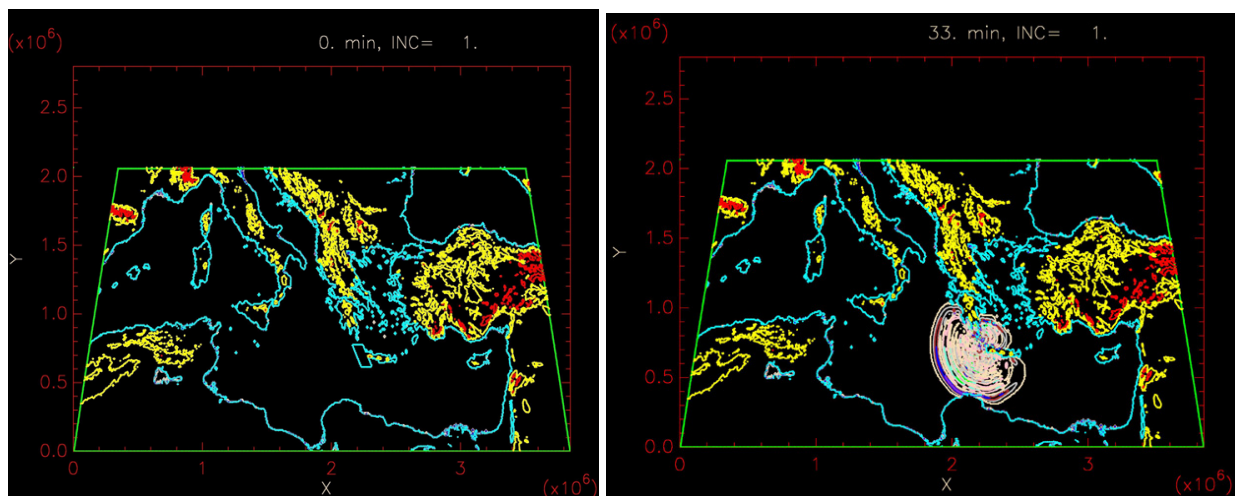


Figure 17. Propagation of the 365 AD tsunami along the Eastern Mediterranean Basin (33 min)

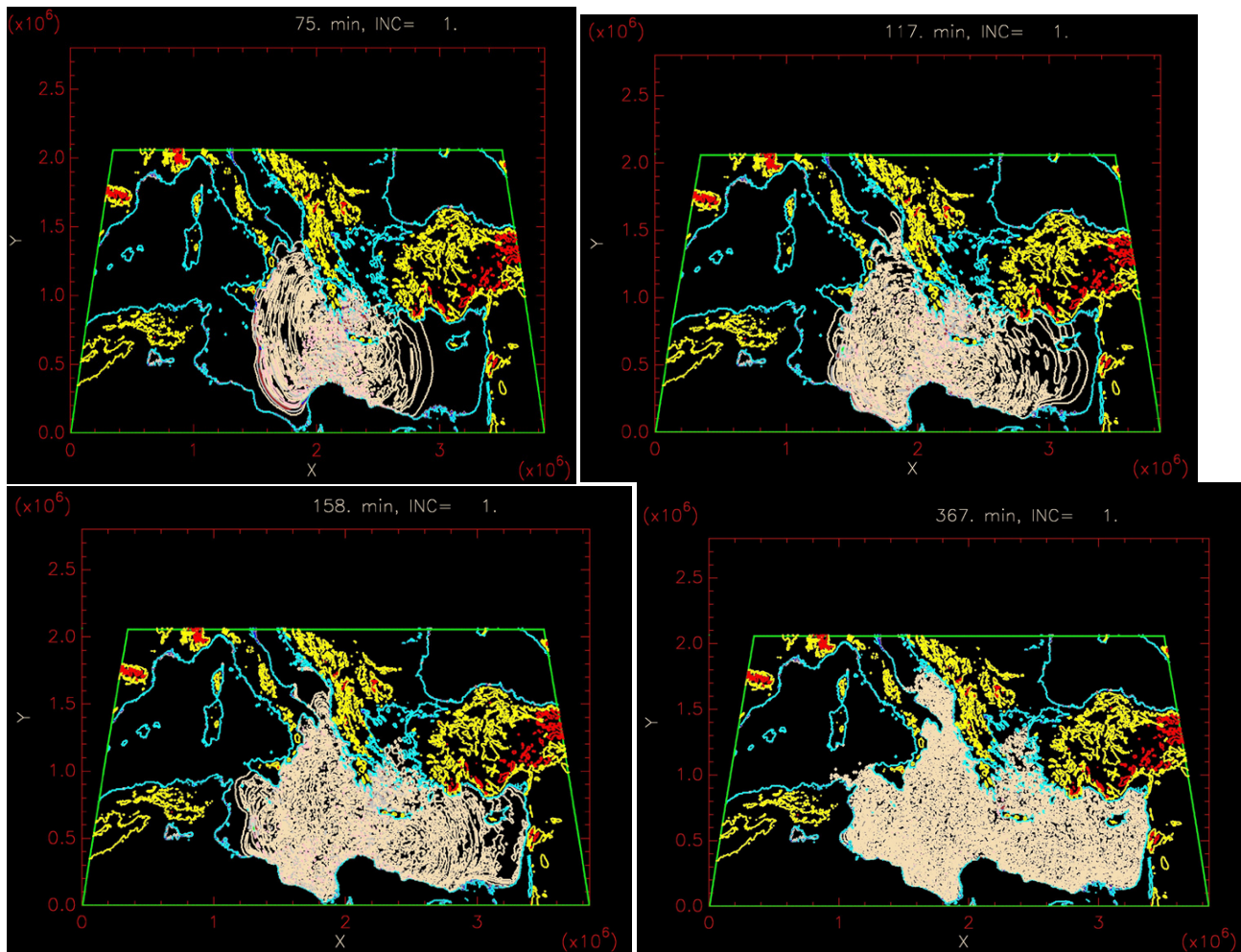


Figure 18. Propagation of the 365 AD tsunami in the Eastern Mediterranean Basin. Time increments 75, 117, 158 and 367 minutes after the earthquake. No tsunami energy reached the Western Mediterranean Basin, the upper Adriatic Sea or the Northern Aegean above the latitude of the Sporades Islands (Pararas-Carayannis & Mader, 2010).

7. IMPACT OF THE 365 AD TSUNAMI ON THE ANCIENT WORLD

The above-described numerical modeling studies (Pararas-Carayannis & Mader, 2010) indicate that the 365 AD tsunami did not affect the Western Mediterranean Basin, the upper Adriatic Sea or the Northern Aegean above the latitude of the Sporades Islands. However, coastal areas throughout the Eastern Mediterranean region were heavily impacted by the tsunami, thus validating historical accounts of extensive destruction to cities including Eastern Sicily, the islands of Aioulou and the coastline of Calabria. Also they validate that the tsunami must have caused destruction in Palestine, South Asia Minor, Cyprus, the Nile Delta, Careen, Apollonia and elsewhere along North Africa.

Indeed, as indicated by early historians, the tsunami affected the entire region. For example, historical accounts (Givonnas et al) state that the earthquake “transferred much of its energy into the sea”. From an excerpt of an ancient text it is also concluded that the tsunami affected both the southern Adriatic Sea and the southern and central Aegean Archipelago (Ζολώτας, 1902). Excerpts (Γεωργιάδης, 1904) from previous writers (Theofanis, Kedrinos and Zissimos) described both earthquake and tsunami effects. Several ancient texts tell of extensive destruction by the tsunami of coastal cities on Peloponnesus, Sicily and Egypt as well as Kyrini, Faistos, Gortyna and Pafos in Cyprus.

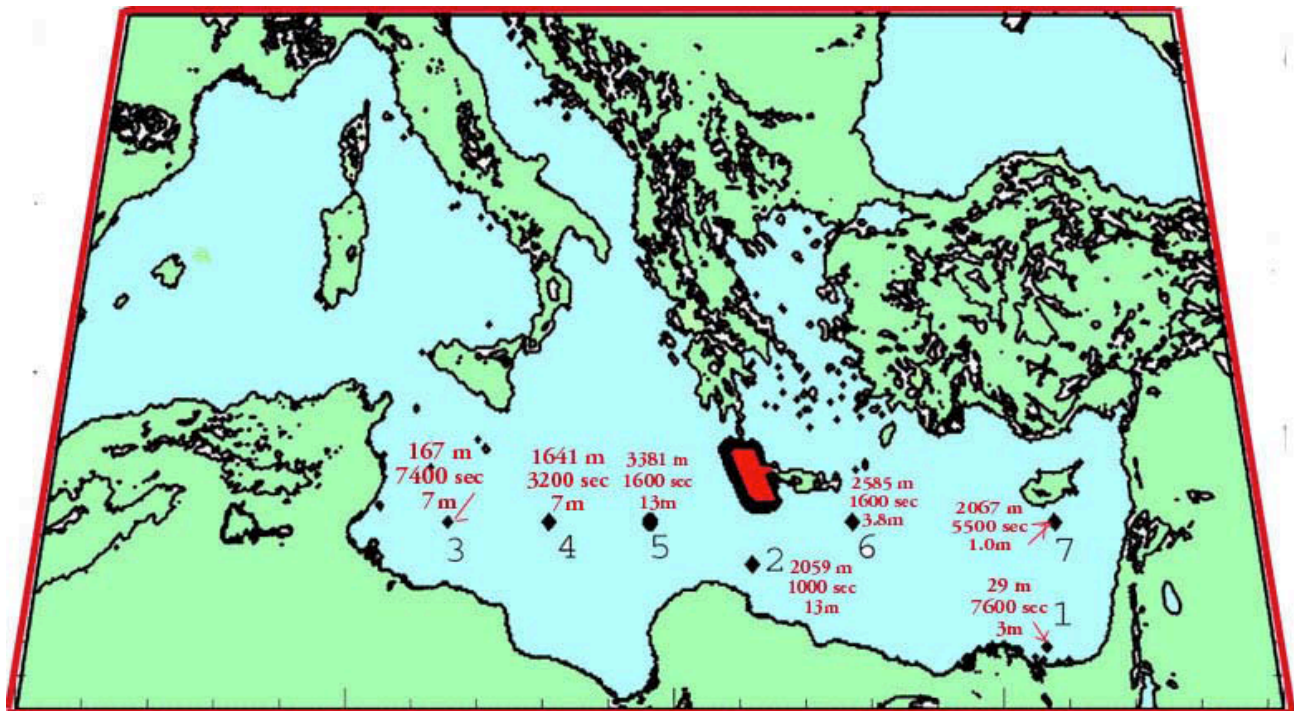


Figure 19. Tsunami travel time and height attenuation at selected locations in the Eastern Mediterranean Basin. Attenuated, offshore tsunami heights in meters and travel times in minutes (Postulated source displacement 50m) (After Pararas-Carayannis & Mader, 2010).

According to the historical accounts, the sea withdrew then returned, flooding everything and killing inhabitants of coastal areas in Dalmatia and Greece. There are accounts of sailors claiming that while somewhere in the Adriatic Sea, suddenly the water depth was reduced and their ship sat on the bottom and that a little later the water returned and refloated it. According to other historical accounts, many places in Crete, Achaia, Biotia, Epirus and Sicily were lost due to great waves. Reportedly, boats were thrown up on land and there was inundation of up to 100 stadia (18.5 km). However, such extensive inundation could only be possible in the flat areas of the Nile Delta interconnected with canals (Pararas-Carayannis, 2001).

7.1 Historical Accounts of Tsunami Impact in Peloponnesus, Kythera Straits, Crete, Cyrenaia (Libya), Alexandria, Cyprus, Palestine and Asia Minor.

Ammianus Marcellinus' accounts of overall earthquake and tsunami effects are perplexing and vague. Subsequent writers misinterpreted his description of events that preceded the tsunami as having occurred near Alexandria, when in fact occurred elsewhere. For example, Ammianus Marcellinus refers to the earthquake and the resulting tsunami in general and mentions that the waves in Alexandria hurled huge ships nearly two miles from the shore. He alludes to the location and occurrence of the disastrous events, by timing them with the first consulship of Roman Emperor Valentinian - who was in control of the Balkans and the eastern provinces of the Roman Empire at the time. Apparently his account refers to the general region and not necessarily to Alexandria. In view of such inconsistencies, there is a need for clarification. Figure 20 is a Greek map of the Mediterranean Sea showing primarily major ports that were either sunk (open circles) or elevated by earthquakes (black circles), as well as ports that were subsequently buried (square blocks).

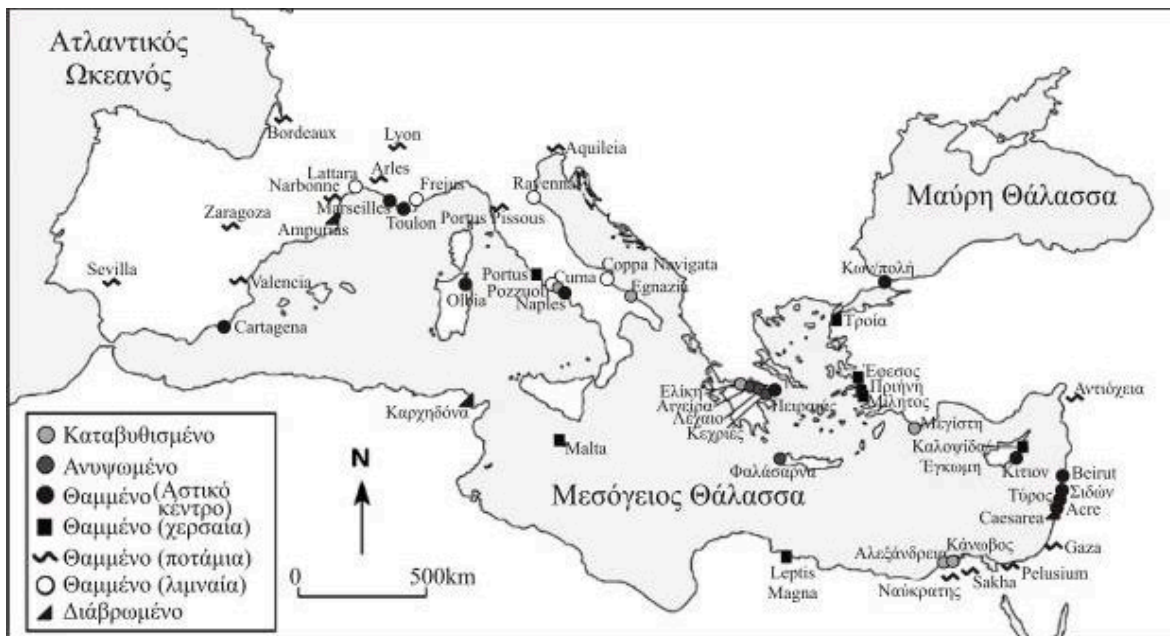


Figure 20. Map showing ancient ports of the Mediterranean Sea. Most of the exposed ports on the Eastern segment of the Basin are believed to have experienced the impact of the 365 AD tsunami. Some of the ports dating back to the Hellenistic period are given with Greek names (Map source: Χαλαρή, 2007, after Marriner & Morhange, 2007).

7.1.1 Tsunami Impact in Peloponnesus

Ancient Methone - Several ancient coastal cities on Peloponnesus were severely impacted. Ammianus Marcellinus specifically mentions in his description a Laconian vessel wreck near Methone on Southern Peloponnesus - apparently carried a great distance inland by the tsunami. Based

Science of Tsunami Hazards, Vol. 30, No. 4, page 280 (2011)

on the numerical modeling study, the maximum tsunami height at Ancient Methone is estimated to have been 10-12 meters.

Ancient Olympia - None of the historic accounts makes reference to either earthquake or tsunami damage at Ancient Olympia. However, a team of German geographers and Greek archaeologists studying paleotsunamis, postulate that the tsunami of 365 AD had an impact on the site and that it was buried by huge masses of marine sediment. Also the researchers cite as “clear evidence” of the marine origin of the sediments, the presence of mollusc and gastropod shells and the remains of abundant microorganisms such as foraminifera. Furthermore, in support of the tsunami impact hypothesis at Ancient Olympia, the researchers advocate that these marine sediments were transported inland at high velocity and high energy. Additionally, they reject the possibility that the site was buried by sediments of the nearby flowing Kladeos River, since its flow is presently weak. The scenario postulates that in 365 AD Ancient Olympia was about 8 kilometers from the sea and that the tsunami rushed into the narrow Alpheios River valley - into which the Kladeos River flows - thus flooding the site and burying with “marine” sediments.

This hypothesis of the 365 AD tsunami impact on Ancient Olympia is flawed and inaccurate for many reasons and a complete rebuttal is under preparation. It will suffice to state that until its excavation about 250 years ago, Ancient Olympia was indeed buried by flood deposits that were several meters thick. Indeed these sediments contained mollusc and gastropod shells as well as remains of abundant marine microorganisms. However, the construction of many of the structures of lesser importance at Ancient Olympia, used columns and building blocks that contained marine mollusc and gastropod shells and remains of micro-organisms such as foraminifera. These building materials were probably mixed conglomerates mined and transported to Olympia from distant locations – which were perhaps close to the sea. It is also true that the Kladeos River is now a stream carrying little volume of water. However, it should be pointed out that Ancient Olympia is located at a present elevation of about 33 meters above present sea level and that it is about 22 km from the shoreline. The 365 AD tsunami generation area was far away from the Alpheios River valley on Peloponnesus and because of its orientation, waves reaching it would not be expected to be high. Furthermore, the Alpheios River valley is narrow, the depth of the river is shallow and most of the energy of a tsunami would dissipate rapidly. Also, there has been a significant climate change in Greece in the last two thousand years and River Alpheios had more substantial flow in the past. The site of Ancient Olympia was covered by sediments, which were probably deposited by flash flooding. The 365 AD earthquake did cause destruction at Ancient Olympia but the tsunami did not affect the site, as postulated. The site of Ancient Olympia was covered by sediments many centuries after the 4th Century.

7.1.2 Tsunami Impact at Kythera and Antikythera Islands

There are no historic accounts on the impact of the 365 AD tsunami at Kythera and Antikythera Islands. However the earthquake was particularly damaging and completely changed the geomorphology of the area where the ancient port of Skandia was located (present Palaiopolis). In all probability the port was completely destroyed by tsunami wave action. A recent field investigation found evidence of coastal failures and subsidence near Palaiopolis. Also, there was evidence of

tsunami inundation at Agia Pelagia, Kastri and Avlemonas, on the east side of the Island of Kythera and at Kapsali on its southern coast (Pararas-Carayannis, 2006). Based on the numerical modeling study, the maximum tsunami height of the 365 AD tsunami at Kapsali is estimated to have been 10-12 meters.

7.1.3 Tsunami Impact in Crete

Other than some generic comments, the historical records provide little information as to the extent of damage in Crete. However, as mentioned in discussing crustal movements on western Crete, the combined effects of the earthquake and tsunami resulted in the destruction of Ancient Falasarna – a city founded in the 6th Century BC and an intermediate port for vessels sailing from Egypt to Rome. Since the 365 AD earthquake raised the land by 6.66 m above sea level near the ancient city, its harbor was rendered completely obsolete. Recent field studies and sedimentary analysis of the embankments of the harbor channel at Ancient Falasarna, found evidence of intense seismic activity and two tsunami deposits (Pirazzoli et al., 1992). The deposits correlate with earthquakes at circa 46-66 AD and 365 AD respectively, which according to historical accounts were associated with tsunamis (Guidoboni et al. 1994, Ambraseys et al. 1994). Because of the extensive crustal upthrust in this region, it is estimated that the tsunami run-up did not exceed 9 meters in height.

7.1.4 Tsunami Impact on Cyrenaia (Libya) and North Africa

Again, the historic record does not provide any information on the 365 AD tsunami impact on the coastal areas of Northern Africa. However the numerical modeling studies indicate that there must have been maximum impact at Cyrenaia and that of the tsunami must have reached as much as 15 meters at Ancient Apollonia, near the town of Susa (present Libya) and at other North Africa settlements.



Figure 21. Ruins of earthquake and tsunami destruction at Ancient Apollonia

7.1.5 Tsunami Impact at the Nile Delta and Alexandria

Undoubtedly, the 365 AD tsunami had a severe impact across the entire Nile Delta coastal zone - which extend for 240 km from Alexandria to Aboukir to Port Said. The region includes several lagoons, canals and the lakes Idku, Burullus and Manzala, which are separated by the sea by barrier islands and dunes (Fig. 22) (Χαλαρη, 2007; Wiegel, 2009).

Alexandria - An account by Kedrinus states that boats at the harbor of Alexandria suddenly sat on dry land. His account probably is derived from ancient historian Ammianus Marcellinus, who also stated that “when the curious crowd run to see the spectacle, the wave returned, drowning 5,000 people”. According to this historic account the “sea wave” was so high in Alexandria that it reached tall structures, overtopped walls, flooded gardens and homes.

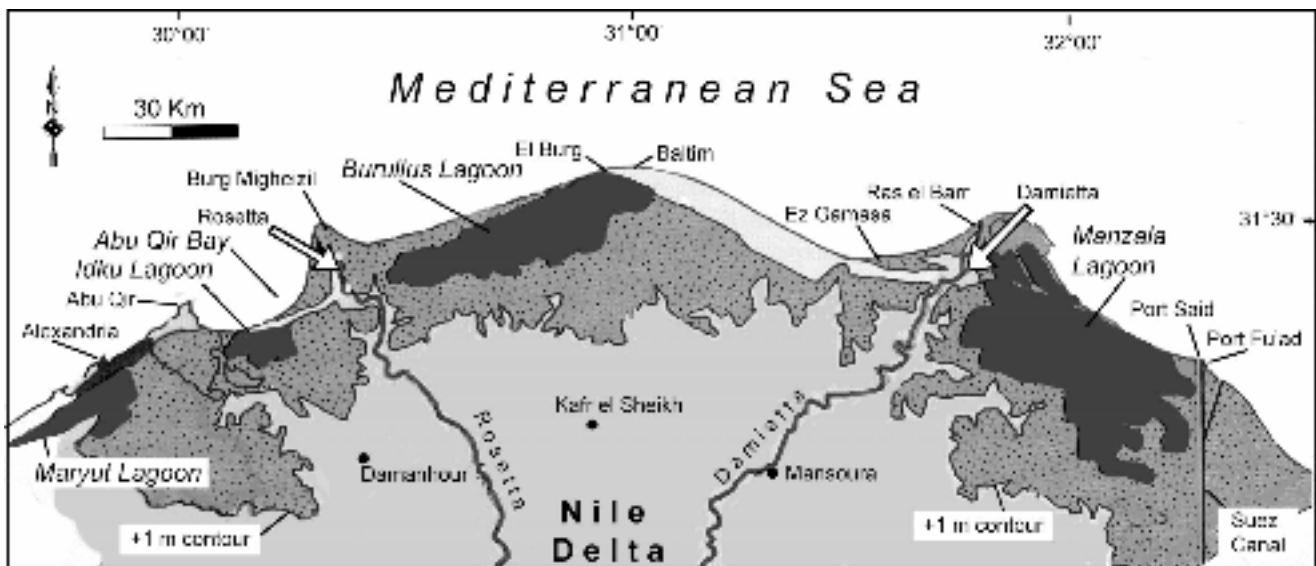


Figure 22. The entire Nile Delta coastal region was probably flooded by the tsunami of 365 AD.

The historic record indicates that Alexandria has been impacted by several earthquakes and tsunamis in the last three thousand years. However, various archaeological sources (Ammianus Marcellinus, 26.10.15-19; Sozomenus, Hist. Eccl.6.2) refer to the destruction of Alexandria by the 365 AD tsunami as the "day of horror" (Stiros, 2001). Also reported was that a large portion of the Nile Delta was flooded. As stated, Ammianus Marcellinus documented fairly well the impact of the tsunami in Alexandria but his description is vague as to how long after the earthquake was felt, the first tsunami wave arrived and whether the destruction begun with this or from subsequent larger waves. In his description of the 365 AD event, he stated:

On the 21st of July (365 AD), in the first consulship of Valentinian and his brother, fearful dangers suddenly overspread the whole world, such as are related in no ancient fables or histories.

For a little before sunrise there was a terrible earthquake, preceded by incessant and furious lightning. The sea was driven backwards, so as to recede from the land, and the very depths were uncovered, so that many marine animals were left sticking in the mud. And the depths of its valleys and the recesses of the hills, which from the very first origin of all things had been lying beneath the boundless waters, now beheld the beams of the sun.

Many ships were stranded on the dry shore, while people straggling about the shoal water picked up fishes and things of that kind in their hands. In another quarter the waves, as if raging against the violence with which they had been driven back, rose, and swelling over the boiling shallows, beat upon the islands and the extended coasts of the mainland, leveling cities and houses wherever they encountered them. All the elements were in furious discord, and the whole face of the world seemed turned upside down, revealing the most extraordinary sights.

For the vast waves subsided when it was least expected, and thus drowned many thousand men. Even ships were swallowed up in the furious currents of the returning tide, and were seen to sink when the fury of the sea was exhausted; and the bodies of those who perished by shipwreck floated about on their backs or faces.

Other vessels of great size were driven on shore by the violence of the wind, and cast upon the house-tops, as happened at Alexandria; and some were even driven two miles inland, of which we ourselves saw one in Laconia, near the town of Methone, which was lying and rotting where it had been driven.

The description does not mention the time lapse between the described strong earthquake ground motions and the arrival of the destructive waves in Alexandria. Furthermore the town of Methone in Laconia was located on Southern Peloponnesus, far from Egypt.

The waves of the 365 AD tsunami arrived on the Alexandrian coast from a northwest direction, so the island of Faros did not provide much protection to the city. The island had been given the name “Faros” which in Greek means lighthouse – a term adopted worldwide for such beacons of navigation. The entire Eptastadion area was flooded (Shaw et al., 2008). The Eptastadion was the causeway built to connect the city to the island of Faros where the famous Lighthouse was located. Alexander the Great’s architect Dinokratus, was responsible for its design and construction as well as of the city of Alexandria. The name Eptastadion was derived from its length of seven steps, each of its seven steps being 187 meters long. Its height above sea level is not known but apparently the tsunami waves overtopped it completely. Sediments accumulated subsequently on both sides of the Eptastadion formed a wider tombolo, which divided the city’s port into the East Harbor – also known as the “Grand Harbor “- and West Harbor, also known as “Evnostos” (Χαλαρή, 2007).

Although not mentioned in the ancient texts, because of the low topographical relief and the many canals and river branches of the Nile (Jondet, 1921), it would be reasonable to conclude that the tsunami more than likely flooded the wells, the 700 subterranean storage cisterns and the major canal from a Nile tributary that provided Alexandria with its fresh water supply. Although not reported in historical records, lack of fresh water probably contributed to more deaths due to epidemics in the following weeks and months after the tsunami struck. Based on the numerical modeling study, the maximum height of the tsunami in Alexandria was estimated at about 12 meters.

Also there is no record that the 365 AD earthquake or tsunami caused any destruction to the famous Lighthouse of Alexandria – one of the seven miracles of the ancient world and the symbol of the city – which according to ancient writers was located on the east side of the island of Faros (Faros of Alexandria) monument of Alexandria (Fig. 23).

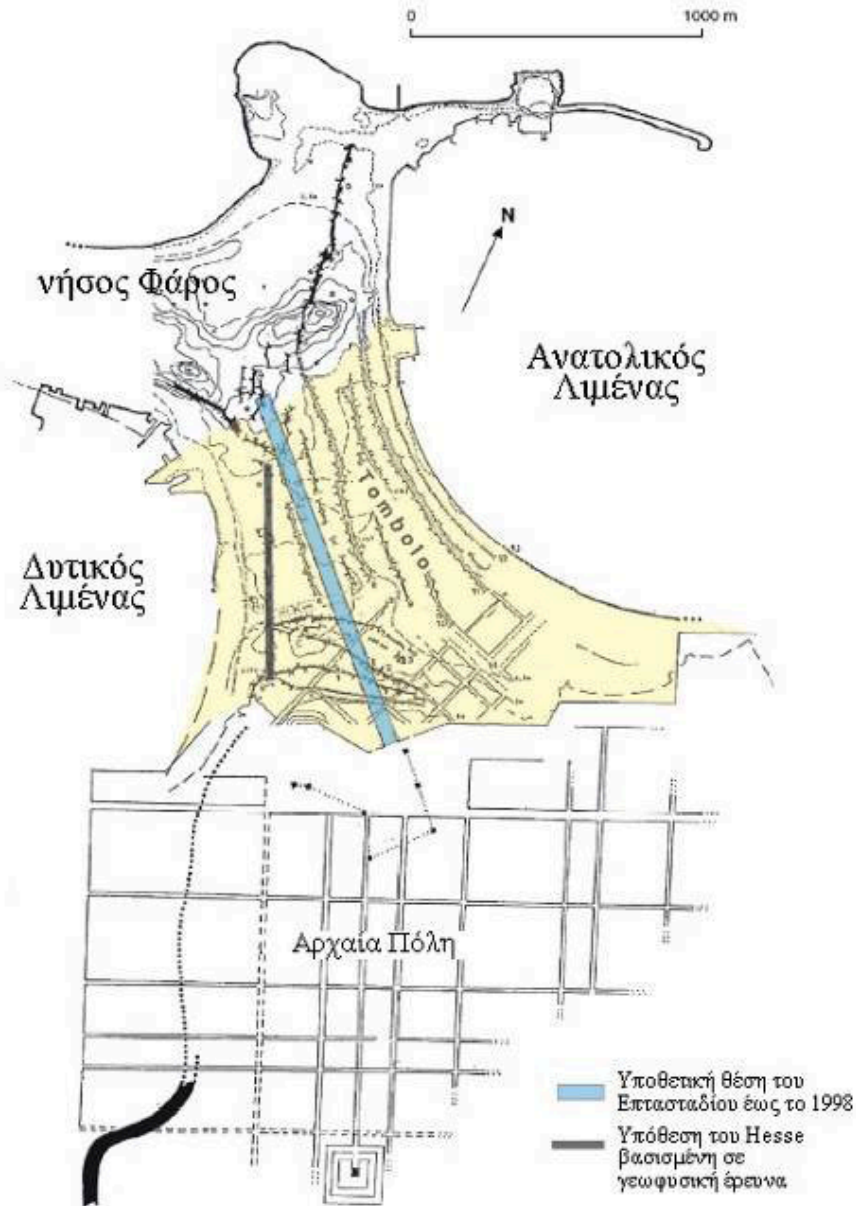


Figure 23. Map showing the Ancient City of Alexandria, The East and West Harbor and the most likely location of Eptastadion - the causeway (blue band) connecting Ancient Alexandria to the island of Faros where the famous Lighthouse was located. (source: Χαλαρή, 2007).

7.1.6 Tsunami Impact at Cyprus and Palestine

There is no historical account of the tsunami impact on Cyprus and, as stated, the alleged earthquake impact on the ancient coastal cities of Pafos and Courion must have been caused by other 365 AD local earthquakes and not by the one on Crete. However, both cities must have been greatly impacted by the tsunami generated near Crete and a great deal of destruction must have occurred to numerous other settlements, mainly along the western and southern coast of Cyprus. Numerical modeling studies indicate that the tsunami along these coasts was as much as 8 meters in height. Similarly coastal settlements on Palestine were struck by maximum tsunami waves estimated at 6-7 meters in height.

8. RECCURRENCE FREQUENCY OF GREAT EARTHQUAKES AND TSUNAMIS IN THE EASTERN MEDITERRANEAN REGION

There is no sufficient record of historical data to conduct a meaningful statistical analysis of the recurrence frequency of great earthquakes in the Eastern Mediterranean region. After the 365 AD event, the last known great earthquake in the region occurred in 1303 AD, but this event is poorly documented by historical records. However, based on these two events, the kinematics of collision of the tectonic plates in the region and the large uplift and subsidence that occurred along western Crete, it is estimated that such great tsunamigenic earthquakes occur approximately once every 800 years along the Hellenic Tectonic Arc. Thus, another great earthquake and destructive tsunami similar in severity as those of 365 and 1303 AD, is statistically long overdue. Given the increases of population densities along coastal areas of the Eastern Mediterranean region, a tsunami generated by another such great earthquake along the Hellenic Arc will be extremely destructive.

9. CONCLUSIONS

The present study reviews and comments on the validity of historical records and incorporates the results of a numerical modeling study in estimating the spatial and temporal characteristics of the 365 AD tsunami. Although major earthquakes are frequent in the Eastern Mediterranean region, great earthquakes and tsunamis as those of 365 AD are rare. There is no sufficient historical data, thus the statistical recurrence frequency of such great disasters is difficult to estimate. Also, there are many uncertainties about the relative motions between the tectonic plates of Africa and Eurasia and of the crucial role the Aegean--Anatolian microplates play in the tectonic evolution of the Eastern Mediterranean region. As stated, this evolution results from continuous continental collision, subduction and crustal shortening processes. Given the seismotectonic history and estimated rates of tectonic plate collisions, it is very likely that another destructive earthquake and tsunami similar to the 365 AD and 1303 AD events is statistically long overdue and very likely will occur again in the region. Such great tsunamigenic earthquakes can be expected to occur every 800 years or so. A similar disaster will have a devastating impact in the entire Eastern Mediterranean region. However, the numerical modeling study indicates that such a tsunami will not be significant in the Western Mediterranean Basin, the upper Adriatic Sea or the Northern Aegean above the latitude of the Sporades

Islands (Pararas-Carayannis & Mader, 2010). In view of the great demographic changes and increase of population in coastal areas, further research is needed for proper evaluation of the future impact that a great tsunami will have in the region. Also, needed is the development of risk assessment methodology that is based not only on the scant historical data, but also on assessing the present vulnerabilities of coastal communities in the Eastern Mediterranean Basin.

REFERENCES

Ambraseys, N., C. Melville, and R. Adams, 1994, *The Seismicity of Egypt, Arabia and the Red Sea*, Cambridge University Press, Cambridge.

Ammianus Marcellinus, *Roman History*. London: Bohn (1862) Book 26. pp. 405-434.
The Complete Online Library of Ancient Sources.

<http://www.thedyinggod.com/chaldeanmagi/sources/ammianus.html>

Degg, M.R., 1990: 'A Database of Historical Earthquake Activity in the Middle East'.
Transactions of the Institute of British Geographers, New Series, 15 (3): 294-307.

Diodorus of Sicily, *Bibliotheca historica*, Book I, The Complete Online Library of Ancient Sources.
<http://www.thedyinggod.com/chaldeanmagi/sources/diodorus.html>

El-Sayed, A., Korrat, I., Hussein, H.M., 2004. 'Seismicity and Seismic Hazard in Alexandria (Egypt) and its Surroundings'. *Pure and Applied Geophysics*, 161: 1003–1019

Flemming, N.C., and P.A. Pirazzoli, 1981, *Archéologie des côtes de la Crète, Histoire et Archéologie, Dossiers* 50, 66-81.

Frost, F.J. 1989, "The last days of Phalasarna" *Ancient History Bulletin* 3, pp 15-17.

Frost, F.J. 1997, "Tectonics and History at Phalasarna", in, Swiny, *et. al.* (eds.), pp 107-115.

Frost, F.J., Hadjidaki, E. 1990, "Excavations at the Harbour of Phalasarna in Crete" *Hesperia* 59, pp 513-27

Fuchs, C. W., 1886. Statistik der Erdbeben von 1865 his 1885, Silzungsberichte der Mathemat. Naturwissenschaftlirhen Classe der Kaiserlirhen Akademie der Wissenschaften. 92, Wien.

Galanopoulos, A. G., 1953. Katalog der Erdbeben in Griechenland fur die Zeit von 1879 bis 1892. *Ann. Geol. Pays Helleniques*, 5, Athens.

- Galanopoulos, A. G., 1957. The seismic sea wave of July 9, 1956, *Prakt. Acad. Athenes* 32, 90-101.
- Galanopoulos, A. G.: 1960. Tsunamis observed on the coasts of Greece from antiquity to present time, *Annali de Geofisica* X111, - 4), Rome, 371-386.
- Guidoboni, E., A. Comastri, and G. Traina, 1994. *Catalogue of Ancient Earthquakes in the Mediterranean Area up to 10th Century*, Istituto Nazionale di Geofisica, Roma, 504 pp.
- Hadjidaki, E. 1988, "Preliminary Report of Excavation at the Harbour of Phalasarna in West Crete" *American Journal of Archaeology* 92, pp 463-79.
- Hadjidaki, E. 1996, "The Hellenistic Harbour of Phalasarna in Western Crete: A Comparison with the Hellenistic Inner Harbour of Sraton's Tower", In Raban & Holum (eds.), p 53-64
- Herodotus, *The Histories*, George Rawlinson (Translation) and Hugh Bowden (Introduction), Everyman's Library, IM. Dent & Sons, Ltd., London, 1992, 748 pp.
- Jackson, J., McKenzie, D., 1988. The relationship between plate motions and seismic moment tensors, and the rates of active deformation in the Mediterranean and Middle East. - *Geophysical Journal* 93, 45-73.
- Jackson, J. , 1994), Active tectonics of the Aegean region, *Annu. Rev. Earth Planet. Sci.* **22**, 239-271.
- Jondet, Gaston, 1916. "Les Ports Submerges de l'Ancienne Ile de Pharos," *Memoires de l'Institut Egyptien*, Tome ix, 1916, 101 pp.
- Kebeasy, R.M., 1990: 'Seismicity'. In: SAID, R., (ed.), *The Geology of Egypt*, Rotterdam: A.A. Balkema: 51-59.
- Kythreoti, S. and K. Pilakoutas, (?) Earthquake Risk Assessment Case Study: Cyprus Report of Dept. of Civil and Structural Engineering, University of Sheffield, Sheffield, UK
- Laborel, J., and F. Laborel-Deguen, 1994. Biological indicators of Holocene sea-level variations and of co-seismic displacement in the Mediterranean area, *J. Coast. Res.* **10**, 395-415.
- Leonhard, R., 1899. Die Insel Kythera - Eine geographische Monographie, Library of Historical Studies, 182, Athens, 47pp.

LePichon, X., Chamot-Rooke, N., Lallemand, S., Noomen, R., Veis, G. 1995. Geodetic determination of the kinematics of Central Greece with respect to Europe: implication of eastern Mediterranean tectonics. - *J. Geophys. Res*, 100, 12675-12690.

Maamoun, M., Megahed, A., & Allam, A., 1984: *Seismicity of Egypt*, HIAG Bull. 4: 109–160.

Mader L. Charles, 2004, Numerical Modeling of Water Waves - Second Edition. CRC Press (2004) book, ISBN - 0-8493-2311-8

Marriner, N., Morhange, C., 2007: 'Geoscience of ancient Mediterranean harbours', *Earth-Science Reviews*, 80: 137-194.

McKenzie, D.P. 1972. Plate Tectonics of the Mediterranean region. - *Nature* 226, 239-243.

Papadimitriou E. & V. Karakostas, 2007. Rupture model of the great AD 365 Crete earthquake in the southwestern part of the Hellenic, Arc. *Acta Geophysica* vol. 56, no. 2, pp. 293-312, 2007

Papadopoulos G.A. and A Vassilopoulou, 2001 HISTORICAL AND ARCHAEOLOGICAL EVIDENCE OF EARTHQUAKES AND TSUNAMIS FELT IN THE KYTHIRA STRAIT, GREECE Institute of Geodynamics, National Observatory of Athens, 11810 Athens, Greece.

Papazachos, B. C. and K. Papazachou, 1997. The Earthquakes of Greece, Ziti Editions, Thessaloniki, 304 pp (in Greek).

Papazachos, C. B., Koutitas, C. H., Hatzidimitriou, M. P., Karacostas, G. B., and Papaioannou, A. Ch. 1985. Source and short-distance propagation of the July 9, 1956 southern Aegean tsunami, letter section, *Marine Geol.* 65, 343-351.

Papazachos, C. B., Koutitas, C. H., Hatzidimitriou, M. P., Karacostas, G. B., and Papaioannou, A. Ch: 1986. Tsunami hazard in Greece and the surrounding area, *Ann. Geophys.* 4 (B1), 79-90.

Pararas-Carayannis, G., 1973. The waves that destroyed the Minoan empire, *Sea Frontiers* 19(2), 94-106.

Pararas-Carayannis, G., 1974. The waves that destroyed the Minoan empire, Revised for Grolier Encyclopedia, Science Supplement, Man and His World, pp. 314-321.

Pararas-Carayannis, G., 1992. The Tsunami Generated from the Eruption of the Volcano of Santorin in the Bronze Age *Natural Hazards* 5::115-123,1992. 1992 Kluwer Academic Publishers (Netherlands.)

Pararas-Carayannis, G., 2001. The Potential for Tsunami Generation in the Eastern Mediterranean Basin and in the Aegean and Ionian Seas in Greece.

<http://www.drgeorgepc.com/TsunamiPotentialGreece.html>

Pararas-Carayannis, G., 2006/ The Earthquake of January 8, 2006 in Southern Greece.

<http://www.drgeorgepc.com/Earthquake2006Greece.html>

Pararas-Carayannis, G., 2007. The Destruction of the Temple of Zeus in Ancient Olympia by the 4th, 5th and 6th Century Earthquakes (Pending publication)

Pararas-Carayannis, G. & Mader Charles L. 2010. "The Earthquake and Tsunami of 365 AD in the Eastern Mediterranean Sea". Proceedings of the 9th U.S. National and 10th Canadian Conference on Earthquake Engineering; Compte Rendu de la 9ième Conférence Nationale Américaine et 10ième Conférence Canadienne de Génie Parasismique, July 25-29, 2010, Toronto, Ontario, Canada • Paper No 1846

Perrey, A., 1848 Memoir sur les tremblements de terre ressentis dans la peninsula Turco-Hellenique et en Syrie. "Academie Royale de Belgique", 1-73, 1848.

Pirazzoli H.A. et. al. 1992. "Historical Environmental Changes at Phalasarna Harbour, West Crete" *Geoarchaeology* 7, p 371-92.

Pirazzoli, P.A., 1996. *Sea-level Changes. The Last 20,000 Years*, Wiley, New York, 211 pp.

Pirazzoli, P.A., 1999. Les ports antiques soulevés de la Méditerranée orientale. In: V.M. Plag, H.-P., Ambrosius, B., Baker, T., Beutler, G., Bianco, G., Blewitt, G., Boucher, C., Davis, J., Degnana, J., Johansson, J., Kahle, H.-G., Kumkova, I., Marson, I., Mueller, S., Pavlis, E., Pearlman, M., Richter, B., Spakman, W., Tatevian, S., Tomasi, P., Wilson, P., Zerbini, S. 1998. Scientific objectives of current and future WEGENER activities. - *Tectonophysics* 294, 177-223.

Pirazzoli, P.A., J. Laborel, and S. C. Stiros, 1996. Earthquake clustering in the eastern Mediterranean during historical times, *J. Geophys. Res.* **101**, 6083-6097.

Pologiorgi, M., 1985. Kisamos, the topography of an ancient town of western Crete, *Archaeologika Analekta ex Athinon* **18**, 65-80 (in Greek).

Reilinger, R., McClusky, S., Oral, M., King, R., Toskoz, M., Barka, A., Kinik, I., Lenk, O., Sanli, I. 1997. GPS measurements of present-day crustal movements in the Arabia-Africa-Eurasia plate collision zone. - *J. Geophys. Res.*, 102, B5, 9983-9999.

Shaw, B., Ambraseys, N.N., England, P.C., Floyd, M.A., Gorman, G.J., Higham, T.F.G., Jackson, J.A., Nocquet, J.-M., Pain, C.C., Piggott, M.D., 2008: 'Eastren Mediterranean tectonics and tsunami hazard inferred from the AD 365 earthquake.' *Nature Geoscience*, Nature Publishing Group, doi:10.1038/ngeo151.

Sieberg, A., 1932. Untersuchungen über erbeben und bruchschollenbau im östlichen Mittelmeergebiet. Verlag von Gustav Fisher, 163-273, Jena, 1932.

Stanley, Jean-Daniel, Andrew G. Warne, and Gerard Schnepf, 2001. "Nile Flooding Sank Two Ancient Cities," *Nature*, Vol. 412, 19 July 2001, pp 293-294

Stanley, Jean-Daniel and Toscano, M.A., 2009. Ancient archaeological sites buried and submerged along Egypt's Nile Delta coast: Gauges of Holocene delta margin subsidence. *Journal of Coastal Research*, 25(1), 158–170. West Palm Beach (Florida), ISSN 0749-0208.

Stiros, S., 2001. The AD 365 Crete earthquake and possible seismic clustering during the fourth to sixth centuries AD in the Eastern Mediterranean: a review of historical and archaeological data, *J. Struct. Geol.* **23**, 545-562.

Stiros, S.C., and S. Papageorgiou (2001), Seismicity of western Crete and the destruction of the town of Kissamos at AD 365: Archaeological evidence, *J. Seismology* **5**, 381-397.

Thommeret, Y., J. Laborel, L. Montaggioni, and P. Pirazzoli, 1981. Late Holocene shoreline changes and seismotectonic displacements in western Greece (Greece), *Z. Geomorph.Supl.* **40**, 127-149.

Wiegel, Robert L., 2009. THE NILE RIVER DELTA COAST AND ALEXANDRIA, EGYPT A BRIEF OVERVIEW OF HISTORY, PROBLEMS, AND MITIGATION, Dept. Civil & Environmental Engineering Report, University of California, Berkeley, CA

GREEK REFERENCES

Γεωργιάδης, Σ. Α. 1904, Περί σεισμών και κατασκευής αντισεισμικών οικοδομημάτων, 246 σελ., Αθήνα, 1904.

Givonnas ?, Not seen – quoted by Παπαζάχος Β. & Παπαζάχος Κ., 1989, Οι Σεισμοί της Ελλάδας, Σελ. 356. Εκδόσεις Ζήτη, Θεσσαλονίκη, 1989.

Ζολώτας, Ι. Γ. 1902, Ιστορία της Χίου. Τομ. Α, 87 - 95 Αθήνα, 1902.

Zolotas, 1921. Not seen – quoted by Παπαζάχος Β. & Παπαζάχος Κ., 1989, Οι Σεισμοί της Ελλάδας, Σελ. 356. Εκδόσεις Ζήτη, Θεσσαλονίκη, 1989.

Κριάρης, Π., 1930, 1937 Ιστορία της Κρήτης. Τομ. Α και Β, Αθήνα, 1930, 1937.

Παπαζάχος Β. & Παπαζάχος Κ., 1989, Οι Σεισμοί της Ελλάδας, Σελ. 356. Εκδόσεις Ζήτη, Θεσσαλονίκη, 1989.

Ξανθουλίδης, Στ., 1925. Ο σεισμός του 1856. ' ' Νεα Εφημερίς, 27.4.1925 ' ' Ηράκλειο, 1925.

Triantafillos, 1959. Not seen – quoted by Παπαζάχος Β. & Παπαζάχος Κ., 1989, Οι Σεισμοί της Ελλάδας, Σελ. 356. Εκδόσεις Ζήτη, Θεσσαλονίκη, 1989.

Χαλαρή, Α. 2007. Διδακτορική διατριβή, Geology Dept., University of Patras, Greece.

Χιώτης, Π., 1886, 1887, Ιστορική έποψη περί σεισμών εν Ελλάδι και ιδίως εν Ζακύνθω. Έφημερίς Κυψέλη ' ' , 256 - 259, 274 - 277, Αθήνα, 1886, 1887.

Zissimos (Zosimus of Panopolis), The Complete Online Library of Ancient Sources.
<http://www.thedyinggod.com/chaldeanmagi/sources/zosimus.html>

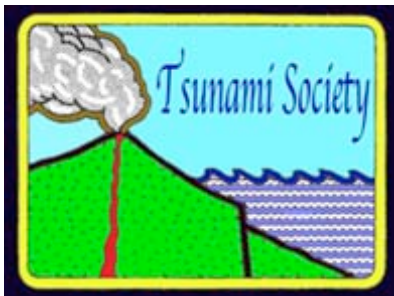
Sotirios Kokkalas, Paraskevas Xypolias, Ioannis Koukouvelas and Theodor Doutsos, 2006.
Postcollisional contractional and extensional deformation in the Aegean region. Geological Society of America Special Papers, 2006, 409, p. 97-123

Theofanis & Kedrinis, Not seen – quoted by Παπαζάχος Β. & Παπαζάχος Κ., 1989, Οι Σεισμοί της Ελλάδας, Σελ. 356. Εκδόσεις Ζήτη, Θεσσαλονίκη, 1989.

MAP

Marine Geosciences, Morpho-bathymétrie de la Méditerranée Méditerranée Orientale,
http://www.ifremer.fr/drogm_uk/Realisation/carto/Mediterranee/med-or.html

ISSN 8755-6839



SCIENCE OF TSUNAMI HAZARDS

Journal of Tsunami Society International

Volume 30

Number 4

2011

Copyright © 2011 - TSUNAMI SOCIETY INTERNATIONAL

TSUNAMI SOCIETY INTERNATIONAL, 1741 Ala Moana Blvd. #70, Honolulu, HI 96815, USA.

WWW.TSUNAMISOCIETY.ORG